ORGANIZATION AND STRUCTURE OF PRECIPITATING CLOUD SYSTEMS

ROBERT A. HOUZE, JR. AND PETER V. HOBBS

Department of Atmospheric Sciences
University of Washington
Seattle, Washington

1. INTRODUCTION

Precipitating clouds are important in the global circulation and climate because they interact strongly with large-scale motions through latent-heat release, cloud-scale vertical air motions, and in-cloud radiative transfer. From a local perspective, precipitation is important because it is often depended upon as a source of water and, at the same time, poses a forecasting problem because it may arrive in storms, which are sporadic, difficult to

ADVANCES IN GEOPHYSICS, VOLUME 24

ISBN 0-12-018824-4

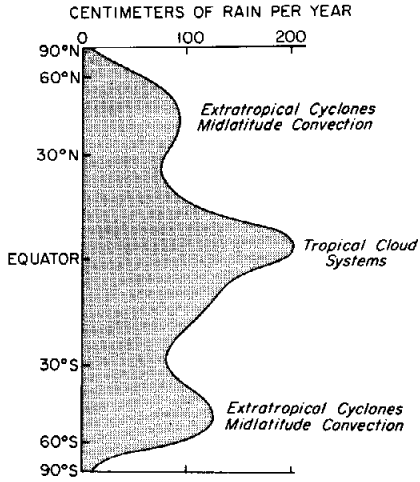

FIG. 1. Globally averaged annual precipitation. Types of cloud systems associated with peaks are indicated. Adapted from Sellers (1965).

predict, and sometimes violent. An understanding of the storms producing precipitation is therefore desired both for facilitating detailed local weather forecasts, on time scales of 1–10 hr, and for improving longer term regional and global climatic predictions through realistic parameterizations of the effects of storm clouds in large-scale models. Improvements in both types of forecasts should lead to better management of water as a resource.

Basic understanding of atmospheric precipitation processes has been elusive because the scales of phenomena involved in precipitation development cover a wide range, extending well below the minimum temporal and spatial scales resolvable with standard meteorological observations.[1] This fact necessitates the use of numerical models of clouds and the mounting of special field experiments in which meteorological radars and instrumented aircraft are deployed to observe the smaller scale processes. In the past 35 years, beginning with the Thunderstorm Project (Byers and Braham, 1949), many field experiments involving radar and aircraft have been conducted over diverse parts of the earth. During recent years, numerical modeling of clouds has also become quite sophisticated. As a result, considerable knowledge has been accumulated on the organization and structure of storms with which precipitation is associated.

[1] Hobbs (1981a) points out that the phenomena involved in the development of precipitation range from the nucleation of cloud particles to the scale of baroclinic waves. In terms of spatial scales this range involves fifteen orders of magnitude, which is the same as the range of scales involved in comparing the linear dimensions of the earth with that of the Milky Way!

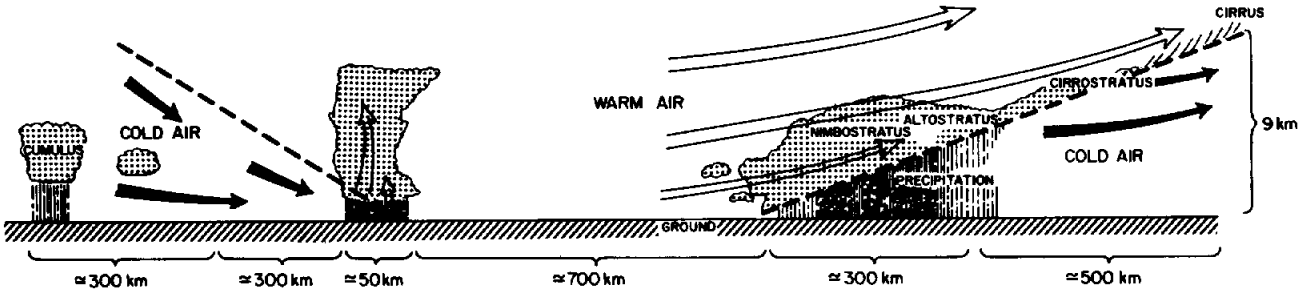

FIG. 2. Idealized vertical cross section through a midlatitude cyclone, according to the Norwegian model. (Note that the vertical scale is stretched by a factor of about thirty compared to the horizontal scale).

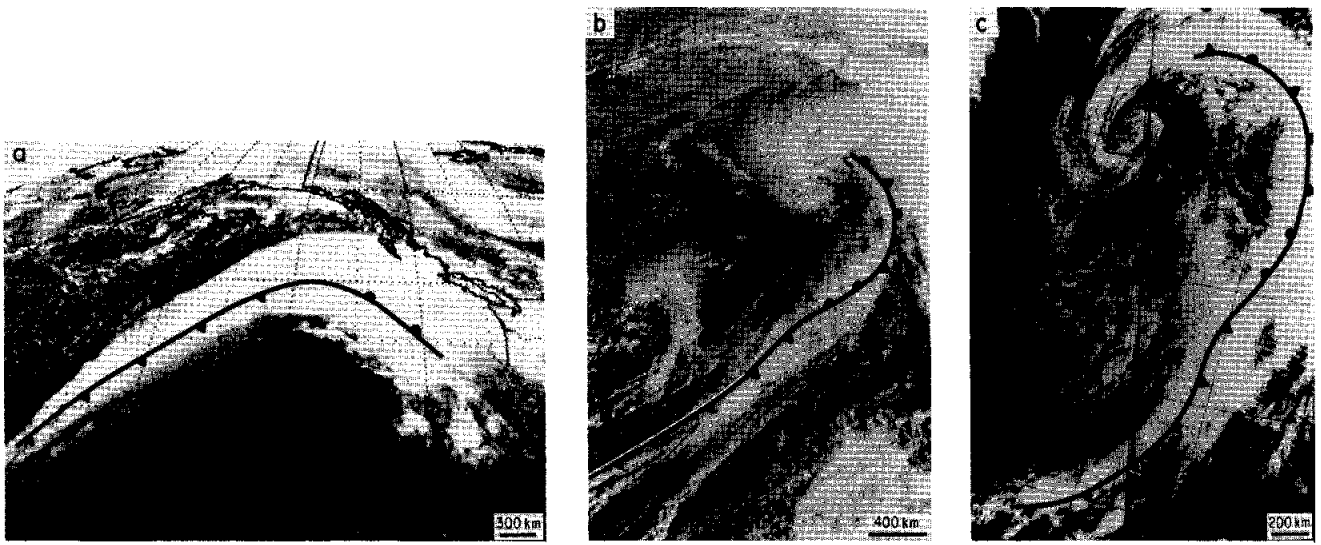

FIG. 3. Satellite photographs of cloud patterns associated with extratropical cyclones. (a) "Open wave" stage when the warm front (–●–●–), the cold front (–▲–▲–), and the warm sector (cloudless region between the warm and cold fronts) are distinct. (b) The larger cloud system to the right is typical of that associated with a cyclone in its occluded stage of development. The smaller cloud system, located just to the left of the center of the photograph, is a "polar vortex." (c) The spiral cloud system in the upper part of this photograph is typical of a cyclone in its mature stage of development.

In this article, we review this knowledge, emphasizing precipitating cloud "systems," which contribute the bulk of precipitation over the earth. Most precipitation occurs in storms that are 20–2000 km in horizontal dimension (the meso-β through meso-α scale ranges of Orlanski, 1975, and Hobbs, 1981a). Small showers may greatly outnumber larger precipitating cloud systems, but these do not contribute significantly to total precipitation (López, 1978; Simpson *et al.*, 1980; Houze and Betts, 1981). Therefore, the cloud systems that we consider in this article are all in the mesoscale size range. Besides implying large size, the term *system* is fitting because, as we shall see, the mesoscale storms accounting for most precipitation have complex internal structures. For example, meso-α frontal clouds contain meso-β rainbands, which in turn contain smaller structures, whereas meso-β thunderstorms group together to drive meso-α circulations, and so on.

Precipitation occurs over the globe in three major latitude belts (Fig. 1). The midlatitude maxima of the Northern and Southern Hemispheres are essentially mirror images of each other and are accounted for by cloud systems associated with extratropical frontal cyclones and midlatitude thunderstorms. The equatorial maximum is accounted for mainly by rainfall from tropical cloud clusters and, to some extent, by hurricanes and smaller scale convection. The remainder of this article is organized around the major precipitating cloud systems of each latitude belt. Extratropical cyclones are described in Section 2, midlatitude convective systems in Section 3, and tropical cloud systems in Section 4.

2. Extratropical Cyclones

2.1. Introductory Comments and Historical Perspective

As noted in Section 1, many of the distinctive cloud patterns seen in satellite photographs of the earth are associated with extratropical cyclones ("cyclones," for short). Cyclones dominate the weather in midlatitudes and are the familiar systems followed on daily weather maps. They are characterized by "fronts" that curve outward for thousands of kilometers from the low-pressure centers of the storms. Upward air motions associated with these fronts (Fig. 2), and the clouds and precipitation that form in response to these air motions, coincide in broad outline with the patterns of the fronts (Fig. 3).

The regular occurrence of different types of clouds, precipitation, and other weather in various regions of cyclones has been recognized since the earliest days of synoptic meteorology (see, for example, the work of Abercromby, 1887). The classical picture of the large-scale structure and life

cycle of cyclones was developed by the Bergen school in the early 1900s (e.g., Godske *et al.*, 1957), and their models are still widely accepted. The Bergen school introduced the concepts of "warm," "cold," and "occluded" fronts. In this model (Fig. 2) the clouds and precipitation associated with warm fronts are depicted as being essentially uniform and produced by the slow, widespread uplifting of the warm-sector air as it rides up over denser, colder air. Precipitation diminishes appreciably, and may be absent, in the warm sector which follows the passage of the warm front. At the cold front, the undercutting of the warm-sector air by denser air of polar origin can produce heavy, convective precipitation. Behind the cold front, the weather is bright with scattered convective showers. The classical model depicts an occluded front as resulting from the cold front's "catching up" and merging with parts of the warm front. The reader is referred to Palmén and Newton (1969) for detailed descriptions of the larger scale aspects of cyclones.

The organization of clouds and precipitation on the mesoscale, and the meso- and microphenomena that lead to precipitation in cyclones, are not discussed in detail in the classical Bergen model. This is not surprising, since at the time this model was being developed observational facilities suitable for detailed studies of subsynoptic features were not available. Before turning to a description of our current understanding of the mesoscale and microscale structure of cyclones and the mechanisms leading to the production of precipitation in these storms, we will give a brief review of earlier work that has provided the foundation for recent progress in understanding.

An important advance in understanding the microphysical processes leading to the formation of precipitation in cyclones was made by Bergeron (1935), who proposed that most (if not all) precipitation particles in these storms originate as ice crystals in clouds. According to this hypothesis, ice crystals are nucleated in a much larger population of supercooled droplets at temperatures below about $-10°C$. Since the saturation vapor pressure in a mixed cloud which is dominated by supercooled droplets is significantly in excess of ice saturation, the ice crystals grow rapidly by deposition from the vapor phase and may reach sufficient size to fall out as precipitation.

Another major advance in the study of clouds and precipitation processes in cyclones occurred in the early 1950s as a result of the increasing use of radars in meteorological studies. The common occurrence in cyclones of radar "bright bands" just below the melting level (produced by snow melting to rain) confirmed the importance of ice particles in the production of precipitation. As the resolving powers of radars were improved, increasingly finer details became apparent in the precipitation patterns. First, the precipitation was observed to be nonuniform, particularly aloft, even ahead of warm fronts. Second, "mare's tails," or streamers of snow, produced by the continuous formation of snow crystals in "generating cells" aloft, were

often observed in radar displays. The reader is referred to the work of Marshall and Gordon (1957) for a review of these early radar studies.

One of the earliest coordinated aircraft-radar studies of cyclones was carried out by Cunningham (1951), who made several flights through a deep cyclone in Massachusetts. The structure of the clouds was found to be quite heterogeneous, even in the warm-frontal region where, according to the Norwegian model, the slow, uniform ascent of air should have produced fairly uniform cloud layers. In addition to the growth of ice particles in upper-level generating cells, growth of ice particles by coagulation at lower levels and the growth of raindrops by coalescence below the melting level were found to be important in different regions of the cyclone.

In the 1960s and early 1970s, attention was focused on studies (mainly involving radar and/or serial rawinsondes) of the organization of precipitation on the mesoscale in cyclones. Nagle and Serebreny (1962) identified the basic pattern of rainbands in frontal systems approaching the West Coast of the United States. Elliott and Hovind (1964), in studies of fronts off the coast of California, identified organized bands of convective precipitation, some 35–70 km wide and 55–100 km apart, embedded within general frontal precipitation. From rawinsonde data, Elliott and Hovind (1965) also deduced that the frontal structure included several important subsynoptic features. The warm-frontal region consisted of alternating tongues of warm, moist air and cold, dry air. The wavelength of this alternating pattern was about 200–300 km, and the bands of prefrontal convection generally occurred within the warm, moist tongue closest to the occluded front. Potential instability in the frontal lifting zone was maintained by cold advection aloft.

Kreitzberg (1964) studied Pacific cyclones entering Washington State by combining the use of serial rawinsondes and a vertically pointing radar. He concluded that the vertical motions are much more complex than is suggested by the Bergen model, that certain recurring mesoscale features are observable, and that on the mesoscale the frontal zones (particularly the warm front) are composed of multiple subzones. Kreitzberg noted that in occlusions[2] air of lower moist static energy arrives in a series of pulses (called "prefrontal surges") ahead of the occlusion. Associated with each prefrontal surge is a region of vertical air motions and associated precipitation. Kreitz-

[2] Frontal systems entering the West Coast of the United States often are presented on analyzed weather maps as occlusions, and their structures bear some resemblance to classical occluded fronts. Often, however, these frontal systems do not evolve by the classical occlusion process postulated by the Bergen school. Instead, they may form discontinuously as so-called instant occlusions. This process is not well understood. In this paper we are not concerned with the process by which an "occlusion" forms, but rather with the structure and organization of precipitation processes once the larger storm has developed. We use the term *occlusion* loosely, to refer to these frontal systems regardless of their origin.

berg and Brown (1970) found that most of the widespread precipitation associated with cyclones in New England occurs in mesoscale bands and groups of showers. A subsynoptic core of cold, dry air in the middle troposphere, ahead of a surface occlusion, was found to suppress widespread cloudiness in the upper regions of the cyclone but to furnish potential instability lower down.

Nozumi and Arakawa (1968) made an extensive study, using radar, of cyclones in Japan. In 82% of the cyclones studied, one or more mesoscale bands of precipitation were detected in the warm sector.

Austin and Houze (1972) used quantitative radar measurements and a network of precipitation gauges to study the organization of precipitation in cyclones in New England. They found that the precipitation patterns consistently displayed a hierarchical organization, in which small (~ 10–10^2 km^2) and large ($\sim 10^3$–10^4 km^2) mesoscale precipitation areas, each containing convective cells, were embedded in the general cyclonic rain shield.

The studies outlined above showed that considerable substructure exists within the basic frontal precipitation patterns associated with cyclones, and that "mesoscale rainbands" are a major feature of this substructure. Detailed studies of rainbands in cyclones have been carried out in the British Isles by K. A. Browning and his co-workers and in the Pacific Northwest by P. V. Hobbs and his co-workers. The results of these studies, which we will now summarize, have synthesized much of the early work on the mesostructure of cyclones and provided new insights into cloud and precipitation processes.

2.2. *Classification of Rainbands in Cyclones*

The principal types of rainbands (or "bands," for short) observed in cyclones, and their positions in relations to fronts, are shown in Fig. 4. The types are:

Type 1. *Warm-frontal bands.* These bands occur within the leading portion of the frontal system, where warm advection occurs through a deep layer, and they have orientations similar to that of the warm front. These bands are typically about 50 km wide. They may be located ahead of the warm front (Type 1a), coincide with a surface warm front (Type 1b), or simply have an orientation similar to that of a warm front even though no well-defined warm front can be seen in standard thermodynamic or wind data.

Type 2. *Warm-sector bands.* These bands are in the warm sector and are oriented parallel to the surface cold front. They are typically up to about 50 km wide.

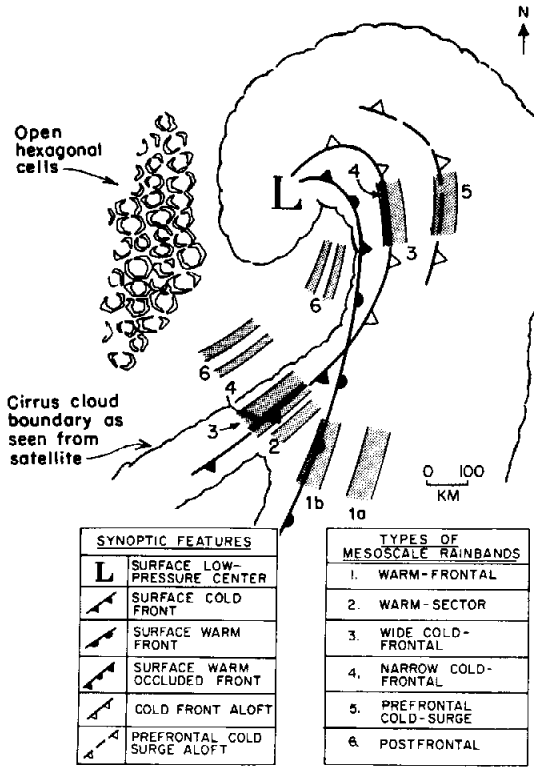

FIG. 4. Schematic depiction of the types of rainbands (numbers 1–6) observed in extratropical cyclones. From Hobbs (1981b).

Type 3. *Wide cold-frontal bands.* These bands are oriented parallel to the cold front. They are about 50 km wide and either straddle or are behind the surface cold front. In the case of occlusions, they are associated with the cold front aloft.

Type 4. *The narrow cold-frontal band.* This type of band differs markedly from the other types of bands. It is very narrow (~5 km) and coincides with the position of the cold front at the surface.

Type 5. *Prefrontal, cold-surge bands.* These bands are associated with the surges of cold air ahead of the cold front, of the type described by Kreitzberg (1964). Otherwise these bands are essentially the same type of feature as the wide cold-frontal bands.

Type 6. *Postfrontal bands.* These bands are lines of convective clouds that form well behind and generally parallel to the cold front.

In addition to the above are smaller, *wavelike rainbands* that occasionally

are superimposed with the other rainbands (Houze *et al.*, 1976b; Matejka *et al.*, 1980; Parsons and Hobbs, 1982b). Unbanded mesoscale patterns of convective clouds, sometimes organized into roughly hexagonal-shaped cells, occur in the maritime polar air well behind the cold front.

Although the full classification of rainbands described above is based on observations in the Pacific Northwest (Houze *et al.*, 1976b; Hobbs, 1978; Matejka *et al.*, 1980), it is consistent with observations of rainbands in the United Kingdom (Browning and Harrold, 1969, 1970; Browning *et al.*, 1973, 1974; Harrold, 1973; Browning and Pardoe, 1973; Harrold and Austin, 1974), and in the northeastern United States (Cunningham, 1951; Boucher, 1959; Austin and Houze, 1972). It is also consistent with observations made in subtropical oceanic cyclones near Japan (Nozumi and Arakawa, 1968). There is, therefore, good reason to believe that the picture in Fig. 4 is representative of the inherent mesoscale organization of precipitation in extratropical cyclones.

It should be noted that not all of the rainbands shown in Fig. 4 are necessarily present in any one cyclone. Note also that the observed sequence of bands will be dependent on the location of the observer with respect to the large-scale features of the cyclone.

In the following sections we describe, in more detail, what is known about the mesoscale features depicted in Fig. 4. In each case we present information, insofar as it is available, on the air motions within the rainband, the substructure of the rainband, the precipitation-producing mechanisms, and the dynamic processes responsible for the formation of the band.

2.3. Warm-Frontal Rainbands

Warm-frontal rainbands arise when precipitation becomes enhanced in mesoscale regions embedded within the large area of cloudiness and stratiform precipitation produced by the widespread lifting associated with warm advection in the leading portion of the cyclonic system. Shown in Fig. 5 is a schematic which summarizes information on the structure of warm-frontal rainbands and the processes by which precipitation is formed in these rainbands. There is considerable observational evidence that the precipitation within these rainbands involves "seeding" from above by ice particles (Cunningham, 1951; Plank *et al.*, 1955; Browning and Harrold, 1969; Houze *et al.*, 1976a, 1981b; Hobbs and Locatelli, 1978; Herzegh and Hobbs, 1980; Matejka *et al.*, 1980). The ice particles are nucleated in groups of generating cells aloft, where they grow to precipitable size, probably by a combination of vapor deposition and riming (i.e., collecting supercooled water droplets). They then fall through stratiform cloud below, where they continue to increase in mass by deposition, aggregation, and riming. In this

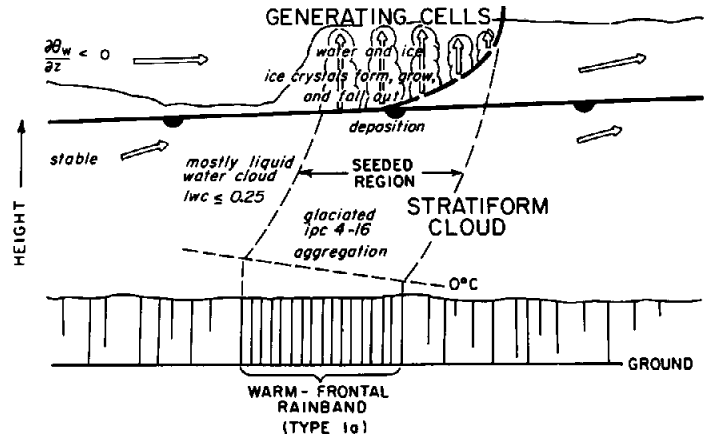

FIG. 5. Model of a warm-frontal rainband shown in vertical cross section. The structure of the clouds and the predominant mechanisms for precipitation growth are indicated. Vertical hatching below cloud bases represents precipitation: the density of the hatching corresponds qualitatively to the precipitation rate. The heavy broken line branching out from the front is a warm-frontal zone with convective ascent in the generating cells. Ice particle concentrations (ipc) are given in numbers per liter; cloud liquid water contents (lwc) are in g m^{-3}. The motion of the rainband in the figure is from left to right. From Hobbs (1978) and Matejka *et al.* (1980).

type of rainband, riming growth is usually small, whereas growth by deposition can be very important. It should be noted that whereas aggregation (which may be particularly important near the melting level) can have an appreciable effect on particle fall speeds, it can not change precipitation rates. The streamers of ice originating from individual generating cells give rise to enhanced precipitation rates over small mesoscale regions within each warm-frontal rainband. These regions account for the small mesoscale areas and cells identified in these rainbands by Austin and Houze (1972) and Hobbs and Locatelli (1978).

Although seeding from above appears to play a crucial role in enhancing precipitation in warm-frontal rainbands, typically only 20–35% of the total mass of precipitation reaching the ground originates from the "seeder" zone. The remaining 65–80% originates in the "feeder" clouds below, although the ice particles from above are needed to collect this mass (Cunningham, 1951; Herzegh and Hobbs, 1980; Houze *et al.*, 1981b). There is also evidence that in some cases the feeder clouds are enhanced by nonconvective mesoscale lifting and that on occasion this lifting is sufficient to increase precipitation rates through liquid-phase processes alone (Herzegh and Hobbs, 1980; Houze *et al.*, 1981b). The "seeder–feeder" process in warm-frontal rainbands has been quantitatively reproduced in a numerical model described by Rutledge and Hobbs (1982).

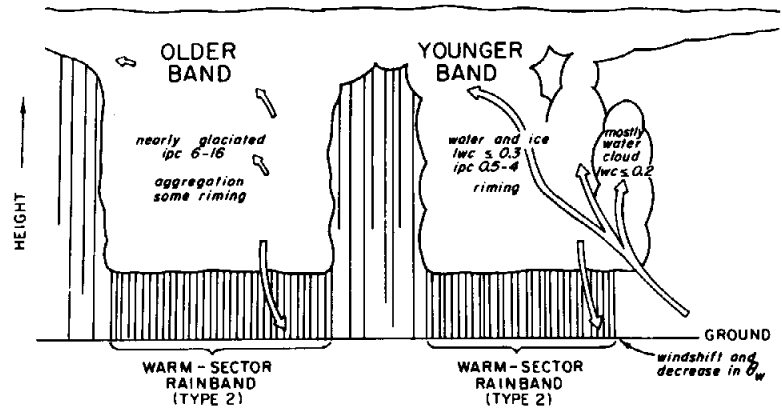

FIG. 6. Model of two warm-sector rainbands shown in vertical cross section. The structure of the clouds and the predominant mechanisms for precipitation growth are indicated. Vertical hatching below cloud bases represents precipitation: the density of the hatching corresponds qualitatively to the precipitation rate. Open arrows depict airflow relative to the rainbands; θ_w is wet-bulb potential temperature. Ice particle concentrations (ipc) are given in numbers per liter; cloud liquid water contents (lwc) are in g m^{-3}. The motion of the rainbands in the figure is from left to right. From Hobbs (1978) and Matejka *et al.* (1980).

Since the generating cells associated with warm-frontal rainbands are often located in potentially unstable layers, it is evident that they are produced by the lifting of these layers to release their instability. Potentially unstable air above warm fronts tends to arrive behind tongues of warm, moist air that branch out from the warm front (Kreitzberg, 1964), and it has been noted (Kreitzberg and Brown, 1970; Matejka *et al.*, 1980) that warm-frontal rainbands are associated with such branches (Fig. 5).

Questions remain about the source of the potential instability and the mechanism for its release. Air-trajectory analysis indicates that layers of potential instability above warm fronts in extratropical cyclones may sometimes originate in the potential instability of the subtropical air mass (Houze *et al.*, 1976a). Alternatively, the potential instability may be generated by differential advection in the middle troposphere (Elliott and Hovind, 1964; Harrold, 1973). A third possibility that has been suggested is that the generating cells form when a layer of moist tropospheric air overrun by dry stratospheric air is lifted and becomes saturated (Wexler and Atlas, 1959).

Lindzen and Tung (1976) have investigated the ducting of gravity waves in a statically stable layer that is bounded above by an unstable or neutral layer. They find that mesoscale gravity waves can propagate under these conditions, and they propose that vertical motions associated with these waves may initiate warm-frontal rainbands. These vertical motions could

produce rainbands either by promoting the release of instability in the potentially unstable layer above the duct (i.e., by producing a mesoscale seeder zone with a high concentration of generating cells) or by creating a denser feeder cloud at lower levels as a result of the increased lifting and condensation on the mesoscale. This mechanism has appeal because the stratification required by the theory is similar to that observed and the theoretical wavelengths and phase speeds are similar to those measured for warm-frontal rainbands (Parsons and Hobbs, 1982b). To prevent undue dispersion of the energy of the waves, it is necessary that the wind at some altitude within the unstable or neutral region be about equal to the velocity of the wave. The latter requirement implies a "steering level" for rainbands, at an altitude which also agrees with observations (Hobbs and Locatelli, 1978).

Symmetric instability is another possible mechanism for lifting in baroclinic zones where rainbands occur (Bennetts and Hoskins, 1979). The alignment of rainbands along the direction of the thermal wind, their spacing, and the stable lifting needed to release potential instability, indicate that symmetric instability, modified by moisture, could be responsible for the generation of warm-frontal rainbands.

2.4. Warm-Sector Rainbands

The vigor and intensity of warm-sector rainbands varies considerably. In their most vigorous form, they may take the form of prefrontal squall lines. The less vigorous warm-sector rainbands often show similarities to squall lines; more work is needed to distinguish clearly the weaker and stronger cases. In the present discussion we will describe the weaker warm-sector bands. Midlatitude squall lines are treated in Section 3.5.

Figure 6 summarizes some of the dominant features of the weaker type of warm-sector rainbands. In contrast to the warm-frontal bands, which are primarily stratiform, with shallow embedded convective cells aloft, the warm-sector bands can contain deep convective cells, extending vertically through the full depth of the rainband. These bands are fed by boundary-layer convergence concentrated at a surface gust front, similar to those of squall lines.

As depicted in this figure, rainbands often occur in series, with the younger, more vigorous bands preceding the older bands. The clouds of younger rainbands are strongly convective, containing relatively high concentrations of supercooled cloud water, but low concentrations of ice. Growth of ice particles by riming is an important feature of these bands. However, the older, less intense bands are dominated by ice particles, which continue to

grow by aggregation. The heavy riming (including graupel formation and growth) that occurs in the young active warm-sector bands is in marked contrast to the slight riming and predominance of vapor deposition and aggregation in the more stratiform warm-frontal bands.

In some warm-sector bands, seeder–feeder processes can be involved in the growth of the precipitation. In one case, 10–20% of the mass of precipitation from the rainband originated in the seeder zone, and 80–90% in distinct regions below the seeder zone. One of these regions was a zone of deep, vigorous convection in which 50–60% of the mass of precipitation developed. The other region consisted of stratiform cloud, which served as a feeder zone, in which 30–40% of the total mass of precipitation developed. The precipitation efficiencies in the convective and stratiform regions were ~40 and ~80%, respectively (Hobbs *et al.*, 1980). More work is needed to understand the difference between this type of warm-sector band and the deep convective type.

Warm-sector rainbands may be associated with internal gravity waves that propagate away from the cold front. During their initial stages of formation, positive feedbacks involving moisture may be important (Parsons and Hobbs, 1982b). Possible mechanisms for formation of the gravity waves are geostrophic adjustment (Ley and Peltier, 1978) and frontal convection (Ross and Orlanski, 1978). At large distances from the cold front, ducting of internal gravity waves (Lindzen and Tung, 1976) is possible and may explain the maintenance of warm-sector rainbands. Other possible mechanisms for maintaining warm-sector rainbands include wave-CISK (Lindzen, 1974; Raymond, 1975), forced symmetric instability (Bennetts and Hoskins, 1979), and the release of potential instability (Kreitzberg and Perkey, 1976, 1977).

2.5. *Wide Cold-Frontal Rainbands*

Wide cold-frontal rainbands occur when lifting over the cold-frontal surface is enhanced by several tens of centimeters per second over horizontal distances of several tens of kilometers. Structurally they resemble warm-frontal rainbands. Release of potential instability in the form of generating cells occurs aloft. Ice crystals that form in these cells grow as they fall through lower cloud layers to give rise to rainbands (Hobbs, 1978; Matejka *et al.*, 1980; Hobbs *et al.*, 1980), as depicted schematically in Fig. 7. Since the steering level of these rainbands is located at the height of the generating cells, they can move faster than the surface cold front.

As in the case of warm-sector rainbands, those wide cold-frontal rainbands in which a seeder–feeder mechanism operates have a high (~100%) precipitation efficiency (Hobbs and Matejka, 1980).

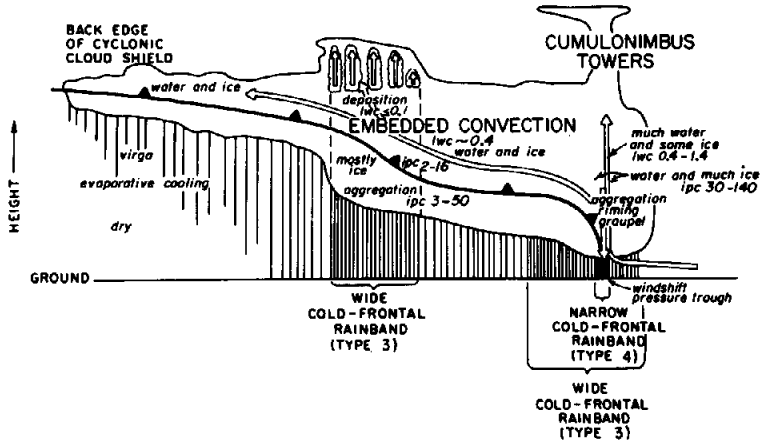

FIG. 7. Model of the clouds associated with a cold front showing narrow and wide cold-frontal rainbands in vertical cross section. The structure of the clouds and the predominant mechanisms for precipitation growth are indicated. Vertical hatching below cloud bases represents precipitation: the density of the hatching corresponds qualitatively to the precipitation rate. Open arrows depict airflow relative to the front: a strong convective updraft and downdraft above the surface front and pressure trough, and broader ascent over the cold front aloft. Ice particle concentrations (ipc) are given in numbers per liter; cloud liquid water contents (lwc) are in g m^{-3}. The motion of the rainband in the figure is from left to right. Horizontal and vertical scales are approximate, but typical of aircraft and radar observations in specific cases. From Hobbs (1978) and Matejka *et al.* (1980).

Symmetric instability (Bennetts and Hoskins, 1979) is a likely mechanism for the formation of wide cold-frontal rainbands. The predictions of this theory, with respect to the location, movement, and spacing of rainbands, are in good agreement with observations (Parsons and Hobbs, 1982b).

2.6. The Narrow Cold-Frontal Rainband

The narrow cold-frontal rainband occurs at the leading edge of a cold front, where converging air produces a narrow (~5 km wide) updraft. Air may ascend in this updraft at a velocity of a few meters per second directly above the windshift at the surface when the cold front reaches the ground, or above the cold-frontal passage aloft in a warm-type occlusion (see Figs. 4 and 7). The cloud towers associated with the updraft may penetrate the larger cloud shield associated with the cold front (as shown in Fig. 7), but more commonly they do not. The source of moisture in the updraft is a low-level, southerly jet situated just ahead of the cold front, onto which the easterly moving cold front continually encroaches (Browning and Harrold,

1970; Hobbs *et al.*, 1980). The updraft typically forms a coupled system with a downdraft, the latter coinciding with the heavy precipitation ($\sim$100 mm hr^{-1}) associated with the narrow cold-frontal rainband (Fig. 7).

The cloud band associated with the updraft in the narrow cold-frontal rainband contains large amounts of liquid water, but relatively low ice-particle concentrations. Consequently, the ice particles grow primarily by riming. The particle concentrations are high ($\sim$100 $liter^{-1}$) in the downdraft. Precipitation aloft consists of rimed aggregates of ice particles. Graupel and hail may form in these bands.

The heaviest precipitation in the narrow cold-frontal rainbands is organized, on the small mesoscale, into ellipsoidal areas oriented at angles of 30–35° to the synoptic-scale cold front (Hobbs, 1978; James and Browning, 1979; Hobbs and Biswas, 1979; Hobbs and Persson, 1982). Hobbs and Biswas refer to these areas as "precipitation cores," and we will use this term here. A schematic of the structure of a cold front on the small mesoscale is shown in Fig. 8, where it can be seen that the precipitation cores are located in regions of high surface convergence. The precipitation cores are separated by "gap" regions where the mesoscale cold front "kinks," resulting in reduced convergence and therefore lower precipitation rates.

The relationship between the passage of a precipitation core and variations in wind, pressure, temperature, and rainfall on the surface are indicated schematically in Fig. 8. Both windshifts and pressure checks occur $\sim$5 min before a peak in rainfall rate, and temperature drops occur at the time of, or shortly after, the heavy rain associated with the downdraft of a precipitation core (James and Browning, 1979; Hobbs and Persson, 1982). The sequence of events on the surface during the passage of a gap region depends on whether or not small, convective precipitation areas within the windshift zone pass over the ground station. If they do not, the pressure check and windshift occur slightly before or at the same time as the fall in temperature, and the rainfall rate does not peak (James and Browning, 1979). If a convective precipitation area does pass over the station, a distinct peak occurs in the rain rate, followed by a pressure check, windshift, and temperature drop. The last three parameters may change simultaneously, or the pressure check and windshift may occur just prior to the temperature drop (Hobbs and Persson, 1982).

In many respects, the passage of a precipitation core associated with a narrow cold-frontal rainband resembles a squall-line gust front. Although the outflow of cold air from a squall line is generally not accompanied by precipitation, a pressure jump and a shift in the wind generally occur 5–10 min ahead of a drop in temperature.

The circulation of the air at low levels in the vicinity of the northeastern tip of a precipitation core (i.e., near one of the "kinks" in the temperature

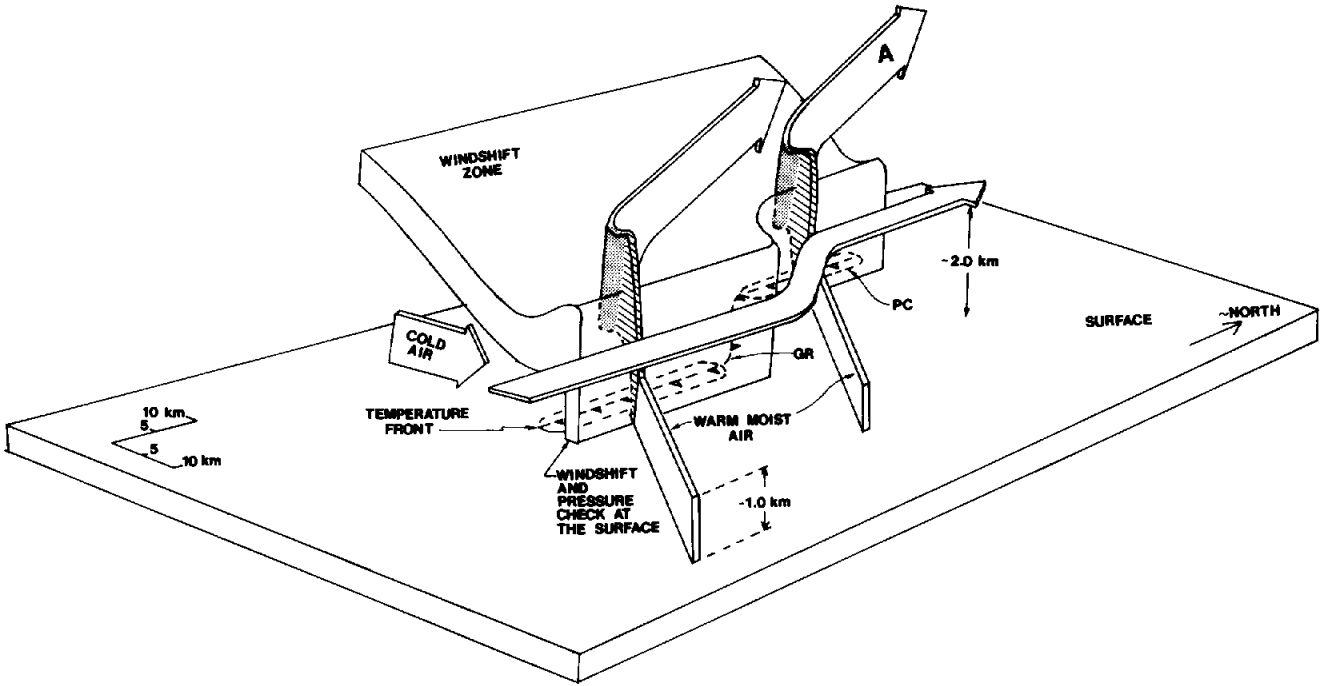

FIG. 8. Schematic summarizing the small-mesoscale structure of a cold front. The areas of the precipitation cores (PC) on the ground are outlined by the elongated ovals along the temperature front (_ ▲ _ ▲ _) and they are separated by gap regions (GR) where the temperature front jags. The large arrows represent the airflow relative to the motion of the precipitation cores. The hatched areas are the areas of strong updrafts, and the stippled areas are the areas of weak downdrafts. Adapted from Hobbs and Persson (1982).

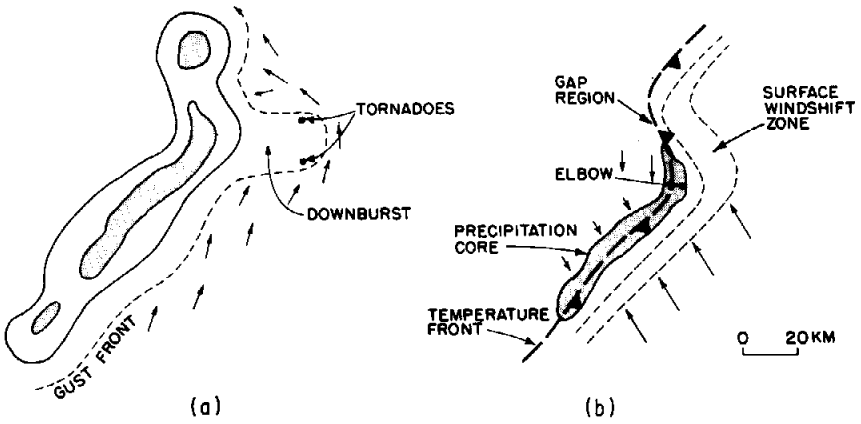

FIG. 9. Schematics of: (a) the "bow" echo that Fujita (1981) associates with mesoscale downbursts and tornadoes; (b) the "boomerang" echoes that Hobbs and Biswas (1979) associate with narrow cold-frontal rainbands.

front) is such as to induce cyclonic rotation of the winds; this forms a "mesolow" in which there is strong wind shear (Hobbs and Persson, 1982). Carbone (1982) has documented a case where a moderate tornado developed from such a mesolow in northern California.

Fujita (1981) has pointed out that in the central United States mesoscale downbursts (i.e., localized currents of rapidly sinking air, which induce an outward burst of damaging winds on or near the ground—see Section 3.6) and tornadoes are often associated with radar echoes that have a "bow" shape (Fig. 9a). The radar echoes associated with the mesolows of cold fronts have a similar shape (Fig. 9b), called "boomerang" echoes by Hobbs and Biswas (1979). It appears therefore that Fujita's bow echo represents an extreme example of the more common boomerang echo associated with cold fronts.

Gravity-current models, such as that described by Benjamin (1968), which simulate the dynamics of a high-density fluid overtaking a lower density fluid, provide reasonable predictions for the speeds of propagation of cold fronts (Carbone, 1982; Hobbs and Persson, 1982) as well as gust fronts associated with thunderstorms (Charba, 1974). Moreover, the breakup of the narrow cold-frontal rainband into precipitation cores and gap regions resembles the pattern seen when gravity currents are produced in laboratory tank experiments (Simpson, 1972). Another possible mechanism for the formation of precipitation cores and gap regions is through instabilities produced across the cold front by the strong horizontal shear of the component of the wind parallel to the front (Matejka, 1980; Hobbs and Persson, 1982).

2.7. *Prefrontal Cold Surge*

In an occlusion, the cold air advances over the warm front in a series of pulses. The strongest pulse is generally analyzed as the cold front itself; the weaker pulses are referred to as prefrontal cold surges (Kreitzberg, 1964; Kreitzberg and Brown, 1970; Browning *et al.*, 1973; Matejka *et al.*, 1980). A surge is marked at the surface by a temporary slight rise in pressure or a decreasing fall in pressure (Fig. 10).

Behind the prefrontal cold surge aloft is a core of low moist static energy air that tends to suppress upper cloud layers but enhances potential instability below. A deep band of cloud and precipitation precedes, or straddles, the leading edge of the prefrontal cold surge. This prefrontal-cold-surge (or "surge," for short) rainband is similar in structure to the wide cold-frontal and warm-frontal rainbands. The mechanisms responsible for the formation of surge rainbands are probably the same as those that form wide cold-frontal bands (Parsons and Hobbs, 1982b).

2.8. *Postfrontal Rainbands*

Postfrontal rainbands (Type 6 in Fig. 4) are lines of convection that form in cold air masses behind zones of strong subsidence, immediately following

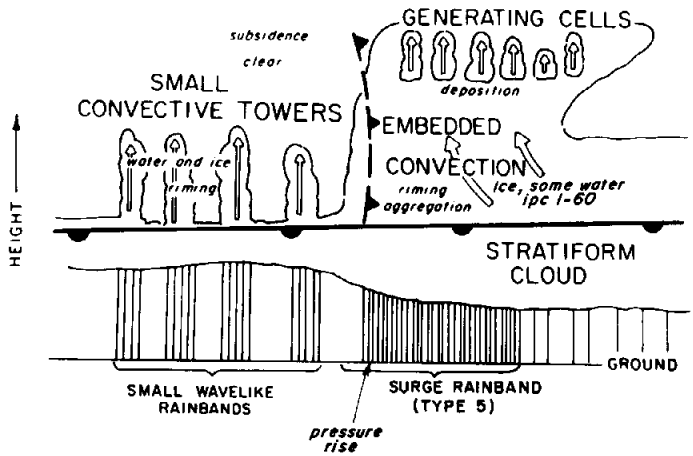

FIG. 10. Model of rainbands associated with a prefrontal surge of cold air aloft, ahead of an occluded front. The broken cold-front symbol indicates the leading edge of the surge. (The primary cold front is off the figure to the left.) The structure of the clouds and the predominant mechanisms for precipitation growth are indicated. Vertical hatching below cloud bases represents precipitation: the density of the hatching corresponds qualitatively to the precipitation rate. Open arrows depict airflow relative to the cold surge and convective ascent. Ice particle concentrations (ipc) are given in numbers per liter. The motion of the cold surge and the rainbands in the figure is from left to right. From Hobbs (1978) and Matejka *et al.* (1980).

the passage of a cold front. Since postfrontal bands are not usually obscured by upper-level clouds or embedded in widespread layer clouds, they may often be observed visually from the ground and in satellite photographs. On the small mesoscale, postfrontal rainbands comprise groups of convective clouds occupying horizontal areas ranging from ~ 50 to $\sim 10^3$ km^2. Sometimes new lines of convection form immediately ahead of an existing line of decaying cells, suggesting that in these areas they behave as organized convective systems such as squall lines (Houze *et al.*, 1976b). In this respect they resemble warm-sector rainbands.

As in warm-sector bands, the microphysical structures of postfrontal rainbands depend strongly on the age of the convective cells being sampled. In young cells containing relatively large quantities of supercooled water, ice crystals grow by riming; showers of graupel are common in such situations. In older cells, which tend to be glaciated, particle growth is primarily by aggregation.

The unstable conditions associated with postfrontal rainbands suggest that a wave-CISK mechanism, incorporating horizontal temperature gradients and vertical shear, is a possible mechanism for their formation (Parsons and Hobbs, 1982b).

Following the passage of postfrontal rainbands, large areas behind the cyclone are often covered by regions of convective clouds. In many respects those clouds are similar to those of postfrontal rainbands, in that they originate in unstable layers and are convective in nature. However, they are organized into hexagonal cells ~ 40 km across and are separated by clear regions ~ 20–50 km across. The centers of cells are often cloud-free, in which case they are referred to as "open hexagonal cells" (Krishnamurti, 1975a). The heights of the radar echo tops of these cells are similar to those of the postfrontal bands, and they move with the wind at about the level of free convection. The convection model proposed by Krishnamurti (1975a,b,c) provides a reasonable explanation for open hexagonal cells. However, despite the fact that this theory provides accurate predictions of the location of hexagonal cells and some of their characteristics (e.g., movement, cloudy or cloud-free centers), it often underestimates the spacing of cells by up to an order of magnitude (Krishnamurti, 1975c; Parsons and Hobbs, 1982b).

2.9. Some Interactions between Rainbands

Narrow and wide cold-frontal rainbands exhibit the most obvious interactions (Parsons and Hobbs, 1981). The observed interactions can be divided into three categories (Fig. 11). In the first, a wide cold-frontal band moves over and ahead of a narrow cold-frontal band. This modifies the

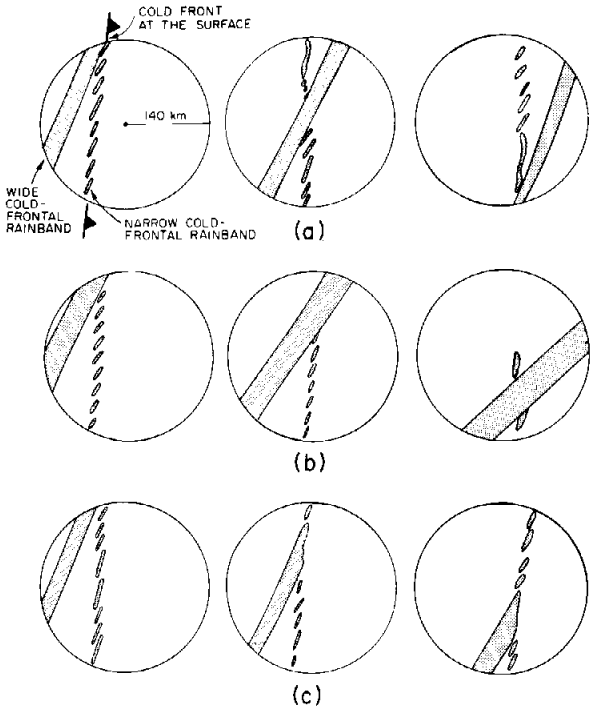

FIG. 11. Schematic showing three modes of interaction of a wide cold-frontal rainband with a narrow cold-frontal rainband. (a) The wide cold-frontal rainband overtakes the narrow cold-frontal rainband. The narrow cold-frontal rainband is disturbed but re-forms after the wide cold-frontal rainband moves on. (b) The wide cold-frontal rainband overtakes the narrow cold-frontal rainband and the latter dissipates. (c) The wide cold-frontal rainband reaches, but does not move ahead of, the narrow cold-frontal rainband. From Parsons and Hobbs (1981).

narrow cold-frontal band, though it continues to exist (Fig. 11a). The modification to the narrow cold-frontal band begins when the wide cold-frontal band is located over the surface cold front. At this stage, it may be difficult to locate the narrow cold-frontal band. The passage of the wide band over the narrow may cause some decrease in the frontal convergence in the boundary layer, which is necessary for the maintenance of the narrow cold-frontal band (Hobbs and Persson, 1982). As the wide cold-frontal band moves ahead of the surface front, the narrow cold-frontal band begins to re-form as an irregular line containing precipitation cores, although the latter may be without distinct alignment. Later the cores align at their usual angle of 30–35° to the front. The time scale for the re-formation of the precipitation cores ranges from 10 to 75 min.

In the second category of interaction, a wide cold-frontal band moves

over and then ahead of the narrow cold-frontal band but the latter does not re-form (Fig. 11b). After the wide cold-frontal band moves ahead of the surface front, the narrow cold-frontal band dissipates and the frontal windshift is greatly weakened.

The third category of interaction that has been observed occurs when the wide cold-frontal band moves over the surface front but then dissipates (Fig. 11c). In this case, the narrow cold-frontal band and the precipitation cores are particularly well defined, while the wide cold-frontal band aloft is rather weak.

2.10. Orographic Effects

Orography can have a profound influence on rainbands. In the case of small (~50 m high), isolated hills, precipitation may be increased on the windward slopes as enhanced condensation produces a feeder cloud that is scavenged by precipitation falling from higher level seeder clouds (Bergeron, 1935). The seeder–feeder process leads to the strong correlation between elevation and precipitation amounts reaching the ground. This situation has been modeled quite well by Storebø (1976), Bader and Roach (1977), and Gocho (1978).

Lifting of the air by topographic features can produce convection in the mid-troposphere and perhaps initiate rainbands (Browning *et al.*, 1974). However, high terrain (e.g., mountain ranges $\geq$ 1 km in height) may lead to downward motion on the lee slopes (Fraser *et al.*, 1973) or it may, on the windward slopes, block the low-level flows necessary for the maintenance of rainbands (Hobbs *et al.*, 1975).

In a recent study, Parsons and Hobbs (1982a) observed that warm-frontal and wide cold-frontal rainbands are generally only interrupted by descent in the lee of large orographic features. Since precipitation is produced mainly by the seeder–feeder mechanism in these two types of rainbands, any condensate produced by orographic lifting enhances the precipitation from the rainbands. Similarly, orographic lifting enhances the precipitation from those warm-sector rainbands in which the seeder–feeder mechanism plays an important role in the production of precipitation. There is a tendency for rainbands to be generated over hills when the atmosphere is unstable either in the lower layers (e.g., in postfrontal conditions) or aloft (e.g., in the warm sector). When the airflow in the lower layers is stable and parallel to a range of mountains, channeling of the flow by the mountains can cause dissipation of rainbands. The precipitation associated with narrow cold-frontal rainbands is generally unaffected by orography, although high mountains can change the orientation of the bands.

2.11. Vortices in Polar Air Masses

In Fig. 3b the clouds just to the left of the center of the picture, and to the west of the trailing front, are associated with a small vortex in the polar air mass. In Europe such vortices are referred to as "polar lows," while in North America they are called "comma clouds" (Reed, 1979). These vortices exhibit many similarities to cyclones, although they are smaller in scale, and they can give rise to significant weather. For example, in California they account for a fairly large proportion (20–50%) of the precipitation (Monteverdi, 1976).

Locatelli *et al.* (1982) documented three case studies of vortices that contained mesoscale rainbands of the types described above, and features which, in the case of cyclones, would have been analyzed as fronts. Locatelli *et al.* also point out that in the cases they studied, the vortices played key roles in forming so-called instant occlusions.

3. Midlatitude Convective Systems

3.1. Thunderstorms

During the warmer half of the year, precipitation over midlatitude land masses is dominated by deep convective events, collectively referred to as thunderstorms, which stand in contrast to the large-scale cyclonic storms described in the preceding section. The "Glossary of Meteorology" (Huschke, 1959) defines a thunderstorm as ". . . a local storm invariably produced by a cumulonimbus cloud, and always accompanied by lightning and thunder, usually with strong gusts of wind, heavy rain, and sometimes with hail." In addition, it defines a tornado as "a violently rotating column of air, pendant from a cumulonimbus cloud and nearly always observable as a funnel cloud. . . . On a local scale it is the most destructive of all atmospheric phenomena." The term "severe thunderstorm" is usually reserved to describe thunderstorms that are accompanied by tornadoes, very large damaging hail, especially strong nontornadic winds associated with storm downdrafts (including "gust fronts" and the type of sudden downdraft referred to by Fujita, 1981, as a "downburst"), or some combination of these phenomena.

Thunderstorms may occur either in isolation or grouped together in mesoscale complexes or squall lines. These groups of storms are quite significant and the subject of much recent research. In Sections 3.2 and 3.3, we consider the structure of individual thunderstorms. Then in Sections 3.4 and 3.5 we discuss mesoscale complexes of storms and squall lines.

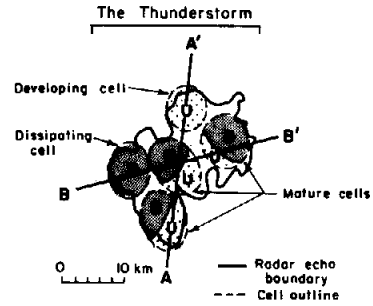
The Thunderstorm
A'
Developing cell
Dissipating cell
B'
B
Mature cells
A
0 10 km
Radar echo boundary
Cell outline

(a)

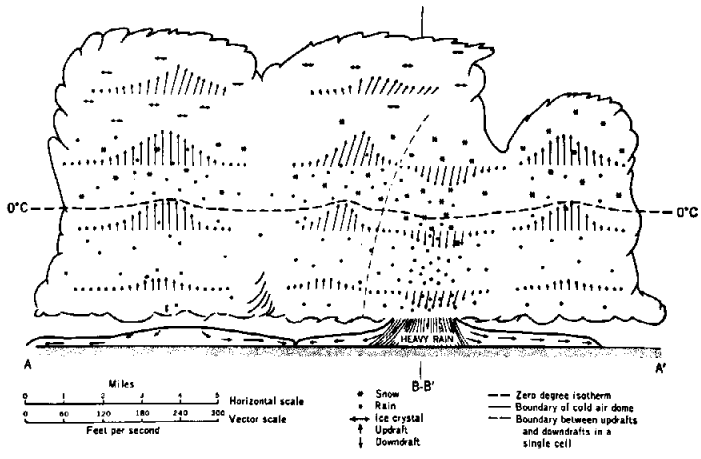
0°C
0°C
A
A'
HEAVY RAIN
B-B'
Miles
Horizontal scale
Vector scale
Feet per second
Snow
Rain
Ice crystal
Updraft
Downdraft
Zero degree isotherm
Boundary of cold air dome
Boundary between updrafts and downdrafts in a single cell

(b)

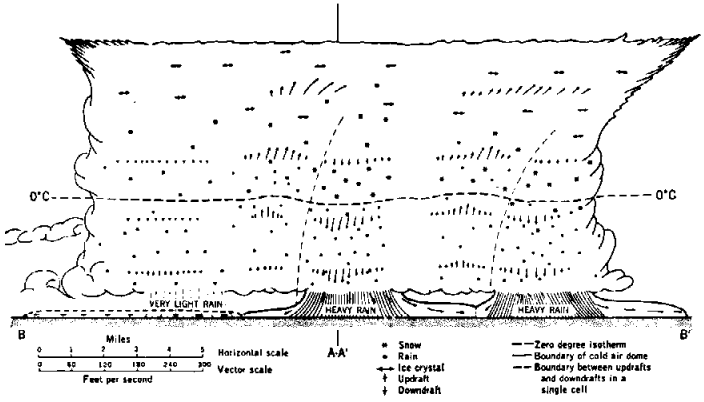
0°C
0°C
VERY LIGHT RAIN
HEAVY RAIN
HEAVY RAIN
B
B'
A-A'
Miles
Horizontal scale
Vector scale
Feet per second
Snow
Rain
Ice crystal
Updraft
Downdraft
Zero degree isotherm
Boundary of cold air dome
Boundary between updrafts and downdrafts in a single cell

(c)

As elsewhere in this article, we focus our discussion on the internal air-motion and precipitation structures of storms. We do not treat thunderstorm forecasting or the electrical activity of the storms.

3.2. Multicell Storms

The internal structure of thunderstorms was first investigated as a specific observational objective in the Thunderstorm Project (Byers and Braham, 1949). This project was the first coordinated use of instrumented aircraft and radars together with intensive soundings and surface observations to explore the structure of a particular type of storm. The storms investigated were the common summertime thunderstorms of Florida and Ohio. These thunderstorms typically occur in widespread convectively unstable air masses characterized by low-level warm, humid air and little vertical wind shear. This type of storm has come to be referred to as the "air mass" thunderstorm. In the Thunderstorm Project, the internal structure of the storm was found to consist of a generally random pattern of "cells" (Fig. 12). The term "thunderstorm" is used to refer to the overall aggregate of cells, and its lifetime (several hours in the case of air mass storms) considerably exceeds that of an individual cell ($\sim$1 hr). Thus, the pattern of cells within the air mass thunderstorm is continually changing.

A special case occurs when only a single cell develops, matures, and dissipates, but no adjacent or subsequent cells develop to form a larger storm complex. Chisholm and Renick (1972) assert that such "single-cell storms" are the most common type of thunderstorm. This is probably true, if every towering cumulus that reaches considerable height and precipitates is considered to be a thunderstorm. However, the significance of single-cell storms in terms of precipitation (Simpson *et al.*, 1980) or storm damage (see Chisholm and Renick's Fig. 1) is practically negligible. Hence, we focus here on thunderstorms consisting of more than one cell.

In the Thunderstorm Project, it was deduced that each cell within a thunderstorm undergoes a life cycle with characteristic stages. The life cycle of a single cell within a thunderstorm has since been simulated quantitatively in numerous cloud models. For example, Ogura and Takahashi (1971) used a simple model that computes the areal averages of in-cloud properties at

FIG. 12. (a) Plan view of an example of an air mass thunderstorm observed in Ohio during the Thunderstorm Project. Developing cells contained updrafts (U); mature cells, both updrafts and downdrafts (D); and dissipating cells, only downdrafts. In (b) and (c) vertical cross sections along B–B′ and A–A′ are shown. Adapted from Byers (1959).

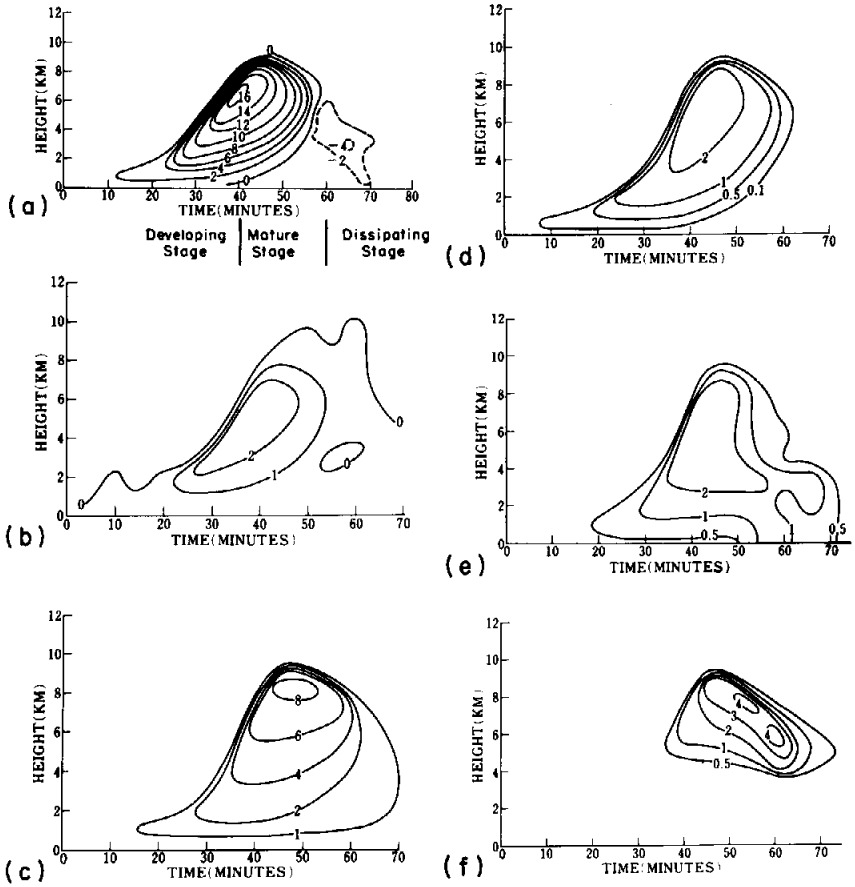

FIG. 13. Time–height cross sections of (a) vertical velocity (m/sec), (b) excess temperature (°C), (c) liquid and solid water content (g/kg), (d) content of cloud droplets (g/kg), (e) content of raindrops (g/kg), and (f) content of ice crystals (g/kg) for a thunderstorm cell simulated by a one-dimensional, time-dependent cloud model. From Ogura and Takahasi (1971).

a series of heights in a cylindrical cell. Their results illustrate the stages in the life cycle of a thunderstorm cell (Fig. 13).

The developing stage (called the "cumulus" stage by Byers and Braham, 1949) is characterized by a growing cloud pushing its way up toward its maximum height (Fig. 13d). The interior of the cell at this stage is filled with buoyant air (Fig. 13b) moving upward (Fig. 13a). Precipitation particles begin developing early and near cloud base but do not yet reach the ground (Fig. 13e). The tendency of the precipitation particles to fall is offset in this early stage by the strong updraft.

Eventually, the weight of the precipitation particles becomes considerable and their drag on the air initiates a negatively buoyant downdraft in the lower portion of the cell. The appearance of this downdraft (at 40 min in Fig. 13) marks the beginning of the "mature" stage of the cell, in which updraft and downdraft coexist. Losing their supporting upward motion, the precipitation particles begin reaching the ground (50 min in Fig. 13).

The disappearance of the updraft (after 60 min) defines the beginning of the "dissipating" stage of the cell. During this stage, a weak downdraft persists until the remainder of the precipitation falls out as light rain.

The cells making up the air mass thunderstorm depicted in Fig. 12 were in various stages of their life cycles. Those with updraft only were in their developing stages, those with both updraft and downdraft were in their mature stages, while those with downdraft only were in their dissipating stages. The formation of new cells in such storms is favored where the cold downdraft spreading out at low levels from an older cell helps to lift ambient air to its level of free convection (e.g., the new cell near A′ in the cross section of Fig. 12b). New cells are thus formed in the vicinity of old cells, especially between cells, where two downdraft outflows collide (Byers and Braham, 1949; Simpson *et al.*, 1980). It is largely by this process that the multicellular cluster comprising the thunderstorm is developed and maintained. While emphasizing the importance of this regeneration mechanism for cells, Byers (1959; see also Byers and Braham, 1949, pp. 77–79) also noted that:

> In many cases the time interval between the beginning of the outflow and the appearance of the new cell on the radarscope is too short to permit explanation of the new one as a result of the underrunning cold air or a similar time-consuming process. There are cases, as indicated by the radar echoes, in which one new cell or a cluster comes into existence almost simultaneously with the initial or parent cell; this suggests that a preferred region of convergence and ascent favors the development of several cells.

Such a region of convergence can occur along an "arc cloud line," which marks the boundary of a downdraft outflow emanating from a distant older thunderstorm or storm complex (see Section 3.6.2 for further discussion), or be produced by some other highly localized forcing (e.g., sea-breeze convergence; see Simpson *et al.*, 1980).

The air mass thunderstorm, described by the Thunderstorm Project, is a member of a broader class of storms referred to generally as "multicell" thunderstorms. Another type of multicell thunderstorm, which we shall call the "organized" multicell storm, differs from the air mass storm in that it occurs in an environment of substantial wind shear and, as a result, the cells form and move through the storm in a systematic rather than a random fashion. This process is illustrated in Fig. 14, which is a vertical cross section along the direction of motion of a multicell thunderstorm that produced

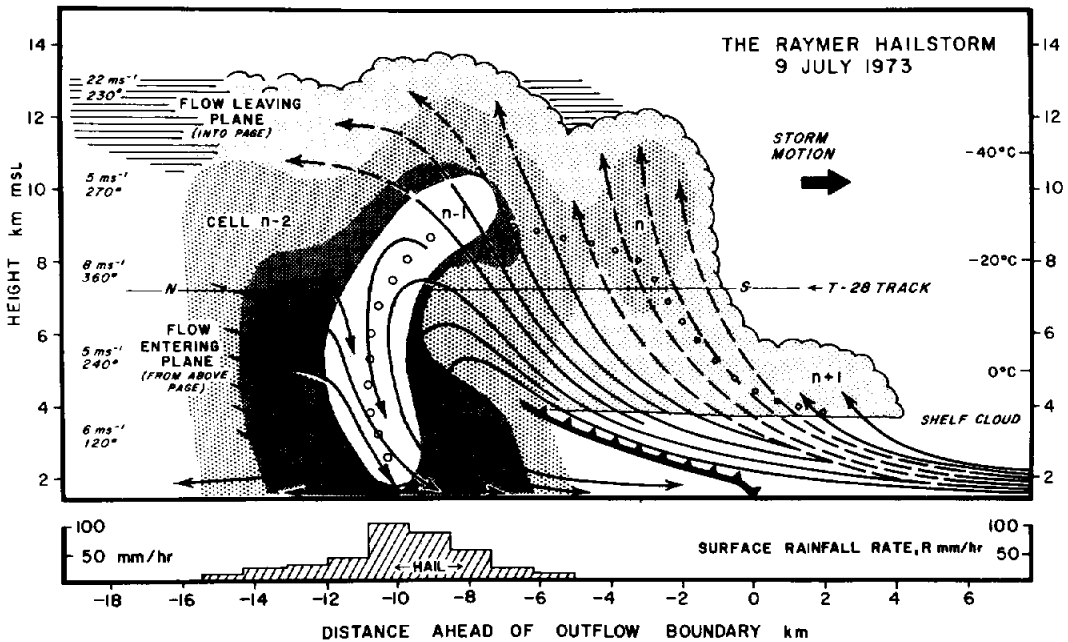

FIG. 14. Schematic model of a multicell hailstorm observed near Raymer, Colorado. It shows a vertical section along the storm's north to south (N–S) direction of travel, through a series of evolving cells. The solid lines are streamlines of flow relative to the moving system; they are shown broken on the left side of the figure to represent flow into and out of the plane and on the right side of the figure to represent flow remaining within a plane a few kilometers closer to the reader. The chain of open circles represents the trajectory of a hailstone during its growth from a small particle at cloud base. Lightly stippled shading represents the extent of cloud and the three darker grades of stippled shading represent radar reflectivities of 35, 45, and 50 dBZ. Environmental winds (m/sec, deg) relative to the storm are shown on the left-hand side of the figure. From Browning *et al.* (1976).

hail in eastern Colorado. The figure can be thought of either as an instantaneous picture of the storm, with cells in various stages of development, or as a sequence of stages in the life of one cell as it moved, in a relative sense, through the storm. New cells (at $n+1$ in Fig. 14) formed on or just ahead of the leading edge of the storm. As cells moved through the storm, they underwent life cycles very similar to the life cycle of a cell in an air mass thunderstorm. At $n+1$ and n, the cells were in the developing stage, with updraft air filling the cells and precipitation particles developing aloft but not yet falling to the ground. Precipitation particles were initiated near cloud base $n+1$ and grew by collection of supercooled cloud water. Above the 0°C level, the collectors were primarily ice particles, whose growth, after their formative stages, was dominated by the accumulation of rime ice, which formed as cloud liquid water was accreted. Continuation of this riming built up graupel particles and hailstones, which eventually became big enough to fall relative to the ground (Dye *et al.*, 1974). The schematic hail trajectory in Fig. 14 was based on an assumption that the particle, once initiated, remained within the same cell throughout its lifetime. Heymsfield *et al.* (1980) present evidence that optimal hail production in a multicell storm occurs by the initiation of graupel particles and hailstones in smaller cells and their subsequent advection into the updraft of the most intense cell of the storm. Other studies note still finer scale patterns of vertical velocity (Battan, 1975, 1980), radar reflectivity (Barge *et al.*, 1976), and surface hailfall (Goyer, 1977), which indicate that further variability in hail growth is superimposed on the basic cellular pattern of the storm.

The cell at $n-1$ was the most intense in the storm depicted in Fig. 14. It had the characteristics of a mature thunderstorm cell: its maximum height had been attained; the updraft in its upper regions coexisted with a strong downdraft at lower levels; and heavy precipitation, including hail, was reaching the ground. By $n-2$, the cell had the characteristics of a dissipating cell: the updraft had disappeared; weak downdraft existed throughout the cell; and precipitation, though still falling, was considerably weakened.

Chalon *et al.* (1976) showed that the motion of the organized multicell thunderstorm in Fig. 14 was the result of two components: one was the result of the movement of individual cells ($\mathbf{V}_c$ in Fig. 15a) along the direction of the middle-level winds and slightly to the left of the overall storm movement, while another ($\mathbf{V}_p$) was the result of the periodic and discrete propagation by new cell formation on the right forward flank of the storm. Thus, the new cell formation always occurred on the storm's leading edge. Other organized multicell thunderstorms frequently exhibit new cell formation on their right rear flanks, with cell dissipation on the left forward flanks (Brooks, 1946; Browning, 1962; Chisholm and Renick, 1972; Newton and Fankhauser, 1975). In such cases, the discrete propagation retards the motion

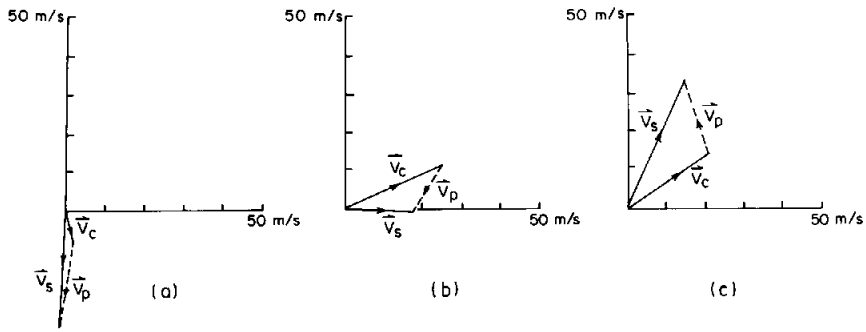

FIG. 15. Organized multicell thunderstorm motion ($\mathbf{V}_s$) as the sum of individual cell motion ($\mathbf{V}_c$) and discrete propagation by new cell formation ($\mathbf{V}_p$) for (a) forward-moving, (b) right-moving, and (c) left-moving storms. Case (a) is from Chalon *et al.* (1976). Cases (b) and (c) are described by Newton and Fankhauser (1975).

of the storm and makes it deviate to the right of the individual cell motion (Fig. 15b). Since individual cell motions are typically within ±30° of the mean wind in the cloud layer,[3] the overall storm motion is also typically to the right of the mean wind. These rightward-deviating storms are quite common; however, organized multicell storms also occasionally deviate to the left of their individual cell motion (and hence to the left of the mean wind in the cloud layer) as a result of systematic cell formation on the left flank of the storm and dissipation on the right (Fig. 15c; see also Hammond, 1967; Newton and Fankhauser, 1975).

The ambient wind shear determines whether a multicell thunderstorm takes on the characteristics of an air mass storm, with random cell regeneration, or of an organized storm, with an orderly pattern of cell formation on a favored side of the storm. As in the air mass storm, new cell formation in the organized multicell storm tends to be triggered at the edge of downdraft outflow from an older cell. However, since the organized storm moves through an environment of substantial vertical wind shear, there is strong flow relative to the storm at various levels, including low levels. Thus the boundary layer becomes an inflow layer feeding into a particular side of the thunderstorm, and new cell generation is highly favored where this strong low-level inflow meets the downdraft outflow of the mature cell. At this point (the zero horizontal coordinate in Fig. 14), maximum and highly

[3] These departures from the mean wind are to the left for smaller cells, to the right for larger cells, and are greater when the environmental winds are strongly veered (Newton and Fankhauser, 1964, 1975).

concentrated velocity convergence leads to new cell formation. As long as the relative flow pattern remains intact, the tendency to form cells on this side of the overall storm is maintained. The orientation of the ambient shear vector, and hence the low-level flow vector, determines on which flank of the storm cells regenerate. In the case of air mass thunderstorms with little shear in the environment, there is little flow relative to the storm at any level. A horizontal inflow layer cannot become firmly established, and no side of the storm is strongly favored for cell development. However, even in air mass storms with slight shear, Byers and Braham (1949) noted a tendency for new development on the low-level upwind side of downdraft outflows (see their pp. 77–79).

When the relative flow in the organized multicell storm is examined at all levels, it is seen that the cells constituting the storm are either superimposed on a circulation pattern on the scale of the thunderstorm itself, or the cells together constitute such a pattern. It can be seen from Fig. 14 that the circulation pattern is characterized by general ingestion and upward flow of warm moist air entering the storm in the low-level inflow layer. The rising air encompasses the updrafts of the developing and mature cells. It exits in an anvil on the upper-level downwind side of the storm. Dry midtropospheric air enters on the middle-level upwind side, is cooled as precipitation particles evaporate into it and sinks in a broad downdraft, which occupies nearly the whole lower portion of the storm and contains the downdrafts of all the mature and dissipating cells. As the downdraft air generally spreads out at the surface, part of it goes against the environmental low-level flow. This portion of the overall storm downdraft region is associated with the downdraft of the mature cell, the leading edge of which runs under the inflowing updraft air in the region of new cell formation. Another portion of the downdraft air flows out of the storm on its low-level downwind side.

Whether the larger storm-scale updraft–downdraft pair of the organized multicell thunderstorm really constitutes a circulation physically distinct from the individual cells, or is simply an agglomeration of the air motions of the cells closely spaced in order of their successive stages of development, is not clear. Whichever is the case, the continued low-level inflow of warm moist air and midlevel inflow of dry air maintained by the storm-scale flow allows the storm to last for a long time. In contrast, the lifetime of an air mass storm, which lacks an organized storm-scale flow, is limited, since it can draw only upon the boundary-layer air in its near environment. For this reason, the organized multicell storms are generally longer lived and more severe than air mass storms (Weickmann, 1953; Newton and Fankhauser, 1975).

3.3. Supercell Storms

The most severe thunderstorm is the so-called supercell thunderstorm. The name supercell (coined by Browning, 1964) refers to the fact that although this type of storm is about the same size as a multicell thunderstorm, its cloud structure, air motions, and precipitation processes are dominated by a single storm-scale circulation consisting of one giant updraft–downdraft pair. Smaller scale features in supercells have been noted by Barge *et al.* (1976), and Battan (1980) suggests that further structural details might be discernible from very high resolution radar observations. However, these superimposed finer scale structures do not appear to be separate thunderstorm cells, and the major aspects of supercell structure can be understood in terms of the storm-scale circulation alone. Advances in understanding the growth of large damaging hail and the formation of tornadoes have followed from recent numerical modeling and detailed observational documentation of the storm-scale circulation.

It has been recognized for a long time that supercell storms occur in environments of great potential instability and strong vertical wind shear (Newton, 1963). Recent numerical modeling studies confirm this fact and further show that multicell and supercell storms comprise two distinct classes of thunderstorms (Weisman and Klemp, 1981, 1982). The multicell storms occur in weak to moderate shear. Weaker shear allows the downdraft gust front at low levels to move ahead of its parent cell; the warm inflow to the original updraft is cut off, and a new cell is triggered along the outflow boundary (Thorpe and Miller, 1978; Weisman and Klemp, 1981; Wilhelmson and Chen, 1982). Supercell storms occur in moderate to strong shear, which allows the updraft and downdraft to adopt a configuration in which they propagate together. A detailed discussion of supercell organization and structure is given in the following subsections.

3.3.1. Visual Appearance of the Supercell Storm. The visual appearance of a supercell thunderstorm viewed from the side is shown in Fig. 16 in the form that is usually taught to ground-based tornado spotters. The tornado vortex is visible as a funnel-shaped cloud pendant from a rotating wall cloud extending downward from cloud base. Usually, the rotation in the tornado and wall cloud is cyclonic and is also suggested by striations of the primary cumulonimbus cloud base. A tail cloud is sometimes seen streaming cyclonically into the west side of the wall cloud from the region of cool air and heavy precipitation. The tornado usually occurs near the peak of a wedge of low-level warm air entering the region of the storm typically from the east or southeast. This warm air rises over the gust front to form the updraft of the storm-scale circulation. Cold downdraft air deposited by the

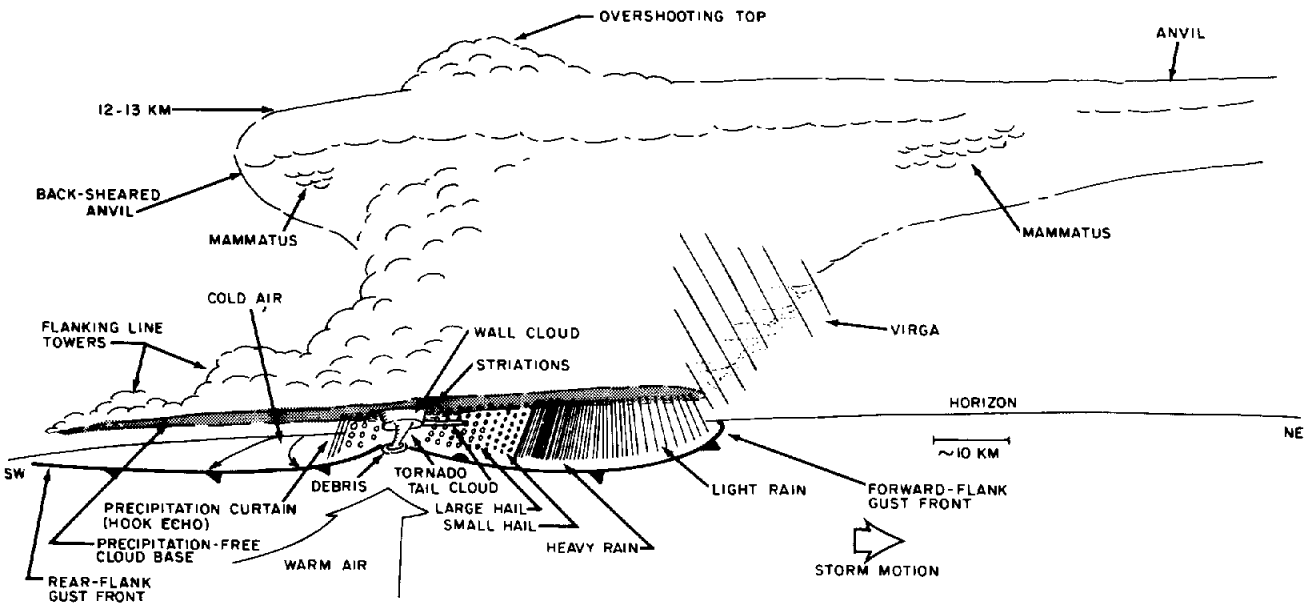

FIG. 16. Schematic visual appearance of a supercell thunderstorm. Based on National Severe Storms Laboratory publications and an unpublished manuscript of H. Bluestein.

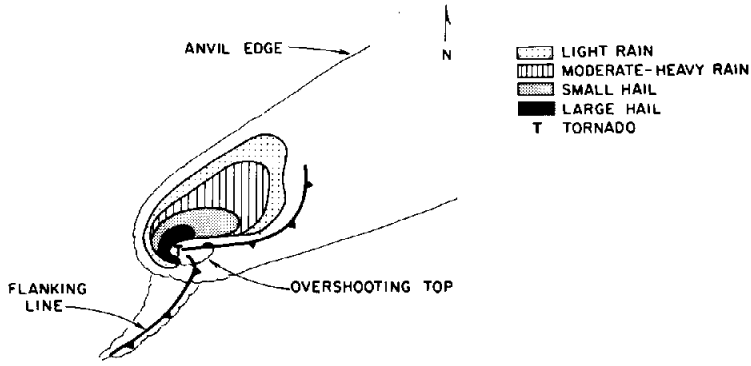

FIG. 17. Plan view of an idealized supercell thunderstorm as it would appear in a satellite picture and in the low-level precipitation pattern that would be detected by a horizontally scanning land-based radar. Cloud features seen by satellite include the flanking line, the edge of the anvil cloud, and the overshooting cloud top. Position of gust front (given by frontal symbols) and tornado are also shown. Based on National Severe Storms Laboratory publications.

storm at the surface spreads out behind the gust front. In Fig. 16, precipitation reaching the ground behind the gust front forms a curved backdrop for the tornado. Weaker tornadoes can occur along the southwest (or rear-flank) gust front (Bates, 1968; Davies-Jones and Kessler, 1974; Forbes and Wakimoto, 1982) or along the lateral boundaries of "downbursts" (see Section 3.3.7). We will concern ourselves here with the predominant type of tornado found at the peak of the wedge of warm air near the storm center.

Warm air rising along the rear-flank gust front or confluence line results in a "flanking line" of towering cumulus (Lemon, 1976). Lifting is most intense near the peak of the gust front, where the visibly active cumuliform growth is seen to extend up through the tropopause to form an overshooting cloud top. Divergence at the tropopause level gives rise to the anvil, which extends downwind to the east or northeast at upper levels. Mammatus structures are commonly seen at the base of the anvil; explanations for their occurrence have been suggested by Scorer (1972) and Emanuel (1981).

An orderly pattern is seen in the precipitation to the northeast of the tornado in Fig. 16. Closest to the tornado, large hail occurs, then, progressing northeastward, small hail, heavy rain, light rain, and virga. As will be shown in Section 3.3.4, this sorting is a result of the intense internal storm-scale air motions. Interestingly, two of the attributes of the storm that classify it as severe, namely, the large hail and the tornado (cf. Section 3.1), are found in close proximity near the center of the storm.

3.3.2. Appearance of the Storm in Satellite and Radar Imagery. An idealized horizontal projection of the cloud-top topography of a supercell,

as it would appear in a satellite picture, and the low-level precipitation pattern that would be detected by a horizontally scanning ground-based radar are shown superimposed in Fig. 17. The near coincidence of the tornado, the peak of the wedge of warm air, the overshooting cloud top, and the indentation in the horizontal precipitation area are evident. The horizontal distribution of the size-sorted precipitation particles produces a distinctive radar reflectivity pattern, since light rain, heavy rain, small hail, and large hail produce increasingly greater echo intensities. The large hail produces an extremely intense echo surrounding the notch in the precipitation pattern where the tornado is located. This radar reflectivity pattern is generally referred to as a "hook echo."

The radar reflectivity patterns vary significantly with height in the storm (Fig. 18). The notch in low-level horizontal echo pattern (1 km in Fig. 18a)

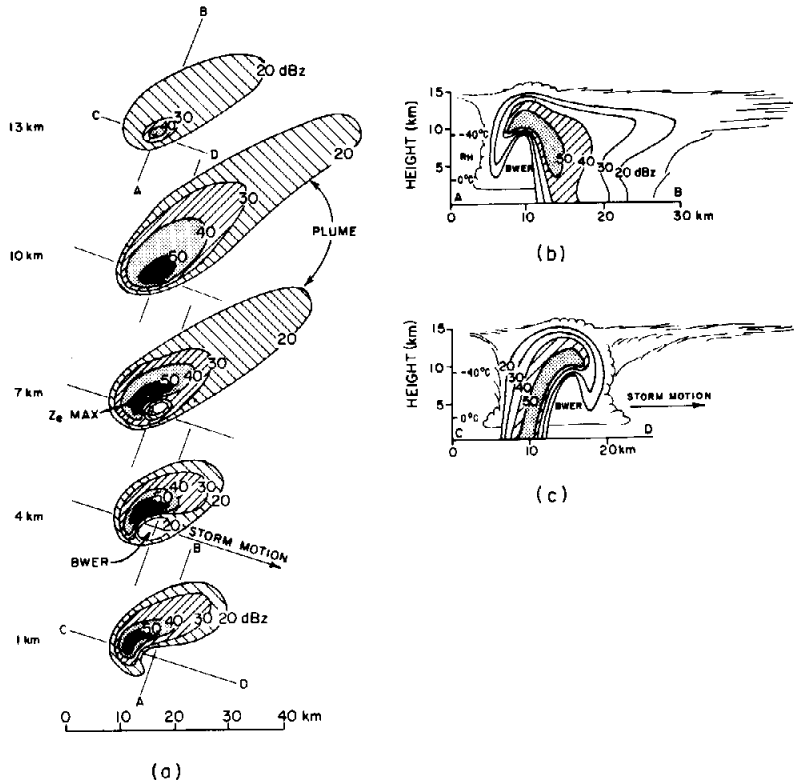

FIG. 18. Schematic illustration of supercell structure typically observed by radar in Alberta. Horizontal sections of reflectivity (Z_e, in units of dBZ) at various altitudes are shown in (a). Vertical sections are shown in (b) and (c). Cloud boundaries are sketched; BWER refers to the "bounded weak-echo region." From Chisholm and Renick (1972).

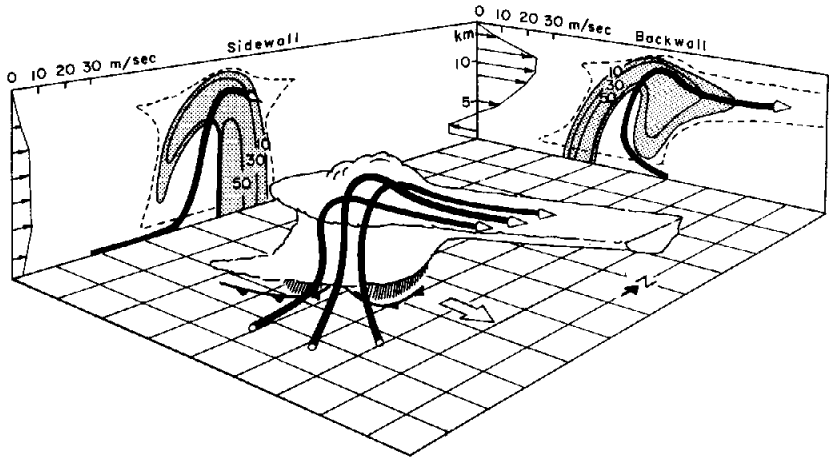

FIG. 19. Perspective view of an Alberta supercell storm. Storm-relative airflow, radar reflectivity (solid lines labeled in dBZ), cloud boundaries (sketched and dashed), and environmental wind profiles are indicated. Wide arrow indicates storm motion. Adapted from Chisholm and Renick (1972).

is associated with a "bounded weak-echo region" (BWER) or "echo-free vault" that extends upward toward the overshooting top of the storm (Fig. 18a, 4 and 7 km; Fig. 18b,c).

3.3.3. Environmental Wind Shear and Updraft Structure. The BWER seen in Fig. 18b,c is associated with the intense updraft of the storm-scale circulation (Fig. 19). At low levels, the wedge of warm air flowing toward the center of the storm rises over the gust front. It rises so rapidly that hydrometeors in the updraft do not grow to radar-detectable size until they reach great altitudes. Thus, the BWER coincides with the core of the updraft (see the vertical cross sections on the back and side walls of Fig. 19). Air reaching the top of the cloud turns and exits toward the east or northeast, in a direction consistent with the upper-level winds. The inpouring of air at low levels from the southeast is also consistent with the environmental winds. As will be further shown in Section 3.3.5, the strong wind shear in the environment (see back and side walls of Fig. 19) is crucial to the formation and maintenance of the storm-scale circulation of the supercell.

3.3.4. Hailfall Pattern of the Supercell. The extremely strong updraft in the supercell storm (~10–40 m/sec; Barnes, 1970; Marwitz, 1972; Davies-Jones, 1974; Klemp *et al.*, 1981) makes possible the growth of very large

hailstones. The growth process has been hypothesized to occur more or less as shown in Fig. 20. Various particle trajectories can ensue depending on the size and location of hail embryos when they first appear in the main updraft. Embryos may be initiated within the main updraft or introduced into the main updraft from feeder clouds located along the flanking line (Barge *et al.*, 1976; English *et al.*, 1982). Particles initially located in the core of the updraft and following trajectory 0 in Fig. 20b are carried aloft and into the storm's anvil cloud before becoming large enough to fall out. Particle 1, beginning near the front edge of the updraft, falls back into the updraft for another cycle of growth by accretion of cloud liquid water before it is carried over to the rear of the storm, where the largest hailstones fall at the front edge of the precipitation area (trajectory 3), while smaller particles are carried farther back into the precipitation region (dotted trajectory). This sorting of particles by size together with horizontal airflow normal to the plane of the cross section in Fig. 20 (further details in Section 3.3.5) accounts in a general way for the distribution of precipitation shown in Figs. 16 and 17. Further variations of hailstone structure, size, and trajectory can occur within this basic pattern, depending on such factors as whether the particles are initiated in the main updraft or in feeder clouds, hailstone density (Pflaum *et al.*, 1982), or inhomogeneity in the structure of the main updraft (Battan, 1980; Nelson and Knight, 1982).

The fallout of precipitation illustrated in Fig. 20a drives the downdraft of the supercell by precipitation drag and evaporation into and cooling of entrained midlevel environmental air. In Fig. 20, the downdraft occupies the region between 0 and 20 km on the horizontal axis. As in the multicell storm (cf. Fig. 14), the air from the storm-scale downdraft spreads out at low levels and sustains the storm-scale updraft. To understand the relationship between the updraft and downdraft of the supercell more fully, the storm's circulation pattern is examined in three dimensions and in time in the next subsection.

3.3.5. Storm Splitting; Left- and Right-Moving Storms. Supercell thunderstorms occur in environments in which the vertical shear of the horizontal wind is very strong. The shear is usually especially strong in one direction (e.g., back wall of Fig. 19), with lesser shear in the orthogonal direction (side wall of Fig. 19). Basic aspects of supercell formation and structure can be understood by considering first the direction in which the shear is particularly strong. Strong vertical shear of the horizontal wind is associated with vorticity about a horizontal axis normal to the shear. If an updraft is formed in this environment, the initially horizontal vortex tubes are bent upward (Fig. 21a). The updraft then contains two counterrotating

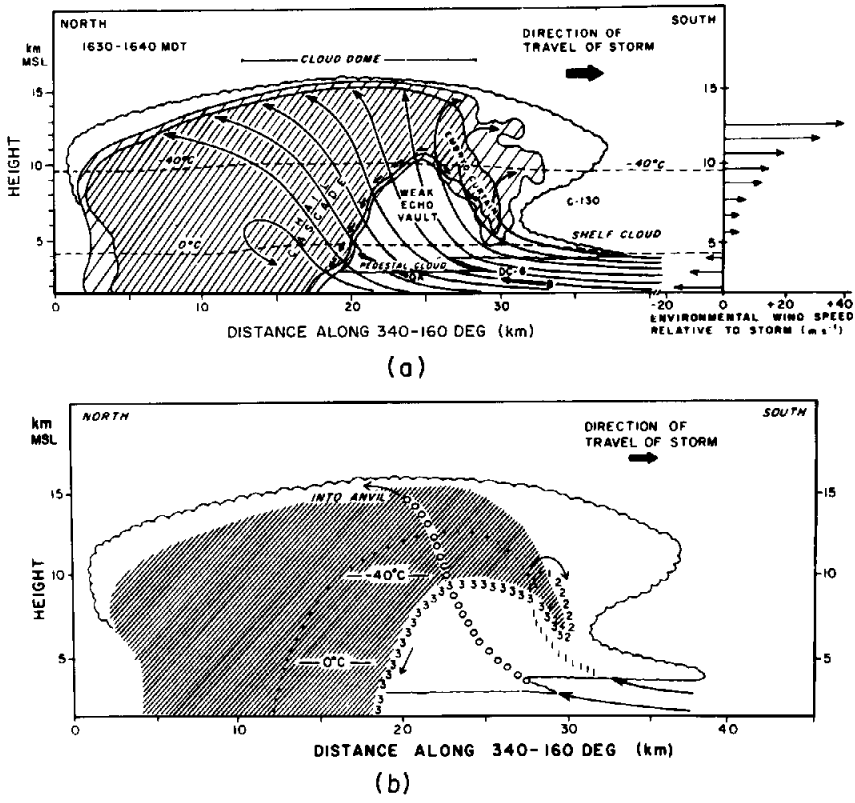

FIG. 20. (a) Vertical section showing features of the visual cloud boundaries superimposed on the radar echo pattern of a supercell thunderstorm in northeastern Colorado. The section is oriented along the direction of travel of the storm, through the center of the main updraft. Two levels of radar reflectivity are represented by different densities of hatched shading. The locations of four instrumented aircraft are indicated, namely, D-130, QA (Queen Air), DC-6, and B (Buffalo). Bold arrows denote wind vectors in the plane of the diagram as measured by two of the aircraft (scale is only half that of winds plotted on right side of diagram). Short thin arrows skirting the boundary of the vault represent a hailstone trajectory. The thin lines are streamlines of airflow relative to the storm drawn to be consistent with other observations. To the right of the diagram is a profile of the wind component along the storm's direction of travel, derived from a sounding 50 km south of the storm. (b) Vertical section corresponding to (a). The echo distribution and cloud boundaries are as before. Trajectories 1, 2, and 3 represent the three stages in the growth of large hailstones. The transition from stage 2 to stage 3 corresponds to the reentry of a hailstone embryo into the main updraft prior to a final up-and-down trajectory during which the hailstone may grow large, especially if it grows close to the boundary of the vault as in the case of the indicated trajectory 3. Other, less favored hailstones will grow a little farther from the edge of the vault and will follow the dotted trajectory. Cloud particles growing within the updraft core are carried rapidly up and out into the anvil along trajectory 0 before they can attain precipitation size. From Browning and Foote (1976).

centers of vorticity about a vertical axis. This vortex-couplet structure is seen in the results of three-dimensional numerical cloud models when an initial perturbation in a thermodynamically unstable environment is allowed to grow in an environment of wind shear similar to that indicated in Fig. 19 (Klemp and Wilhelmson, 1978a,b; Wilhelmson and Klemp, 1978,

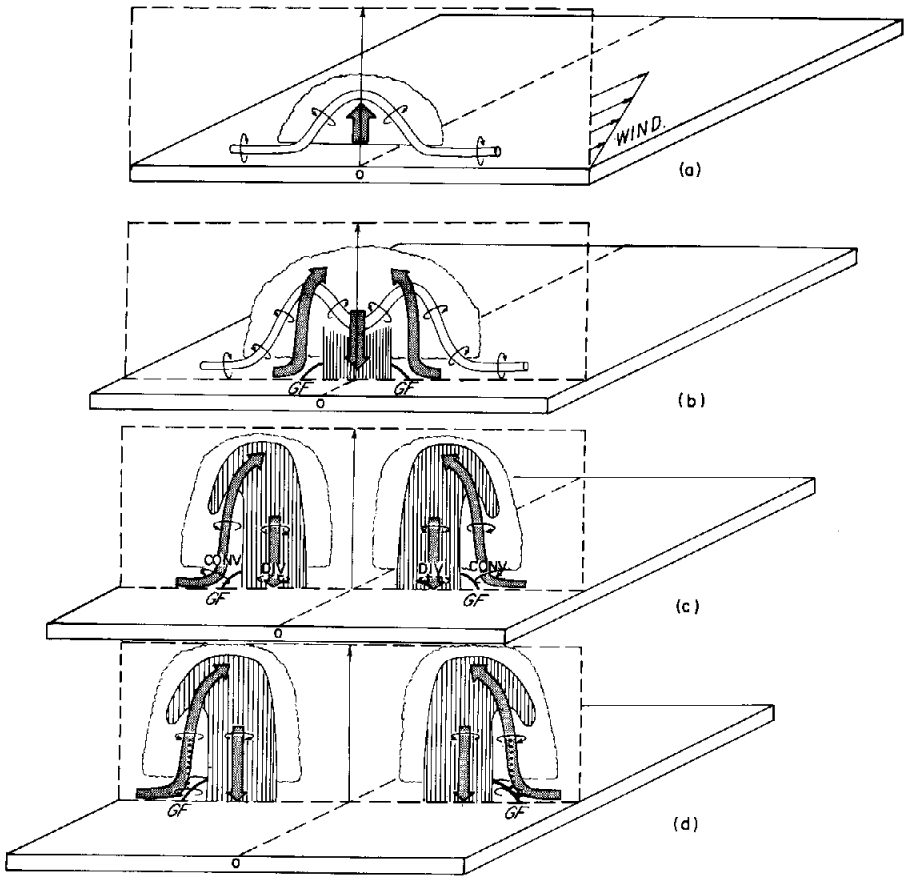

FIG. 21. Schematic of storm-splitting process leading to left- and right-moving supercell thunderstorms. Cloud boundary is sketched. Precipitation is hatched. White tube represents a vortex tube. Heavy arrows are updrafts and downdrafts. GF indicates gust front. Storms move over a horizontal surface shown in perspective. Point 0 is fixed to the surface and is directly under the center of the cloud in (a). Storms move away from 0 in time. Storm cross sections are in vertical planes outlined by dashed lines. In (b) the split occurs, and subsequently gust front propagation leads to a component of storm motion away from the center line of the horizontal plane in (c) and (d). In (c) divergence (DIV) and convergence (CONV) are indicated, and dashed vortices indicate their being weakened by divergence.

1981; Schlesinger, 1978, 1980, 1982a,b; Clark, 1979; Blechman, 1981). The counterrotating vortices entrain potentially cool midlevel air on the downwind side of the cloud. This introduction of cool air together with the downward drag of developing precipitation starts a downdraft in the center of the cloud, and the previously upward-bent vortex tube is bent downward in its middle (Fig. 21b). The downdraft then contains counterrotating vortices of its own, and the updraft is split into two parts, one on each side of the downdraft. The split of the original updraft by the downdraft is seen in the model simulations to be followed by one updraft–downdraft pair's moving to the left of the mean wind while the other moves to the right of the mean wind as a result of gust-front propagation. This motion makes the split complete, leading to two separate storms, which continue to propagate away from each other (Fig. 21c,d). The storm moving to the right in the figure is referred to as the "right-moving" storm. The other is referred to as the "left-moving" storm.

We shall temporarily focus attention on the right-moving storm. If Coriolis effects are ignored, the left-moving storm may be regarded as the mirror image of the right-moving storm. Rotunno (1981) has analyzed the development of rotation in the right-moving storm that forms in Wilhelmson and Klemp's (1978) model experiments. He shows that, at midlevels (more specifically, the level of nondivergence), the centers of cyclonic and anticyclonic rotation occur at first to the right of the updraft and downdraft cores, respectively, as shown in the right half of Fig. 21b. However, as the storms continue to move apart, the centers of rotation migrate to the draft cores, resulting in a cyclonically rotating updraft and an anticyclonically rotating downdraft (Fig. 21c). At low levels, Rotunno finds (in accordance with work of Brandes, 1978, 1981; Heymsfield, 1978; and Bluestein and Sohl, 1979) that the vorticity structure is strongly modified by convergence, which strengthens the rotation in the updraft, and divergence, which weakens the counterrotation in the downdraft (the weakened downdraft rotation is indicated by the dashed lines in Fig. 21c). Rotunno further finds that the center of cyclonic rotation at low levels migrates from its initial position to the right of the updraft core (Fig. 21b) past the center of updraft (Fig. 21c), finally coming to rest on the gust-front boundary separating the downdraft and updraft air (Fig. 21d).[4] At this stage, the center of cyclonic rotation extends vertically from the gust-front boundary at low levels to the updraft core at midlevels. This vertically continuous region of cyclonic rotation in the right-moving storm (dotted line in Fig. 21c) is referred to as the "mesocyclone" (Fujita, 1965; Burgess, 1976; Lemon *et al.*, 1978; Burgess *et al.*,

[4] How the downdraft air with its weakened anticyclonic rotation actually develops cyclonically curved streamlines near the gust front (as indicated in Fig. 16) is a question under active investigation. See comments by both Brandes (1981) and Rotunno (1981).

1982), and it is recognized as the likely origin of most tornadoes formation (see Section 3.3.7 for further details). The counterpart to the mesocyclone in the left-moving storm is referred to as the "mesoanticyclone"[5] (Burgess, 1981).

Examples of the three-dimensional structures of the left- and right-moving storms formed by splitting in unidirectional shear are shown in Fig. 22. We shall again restrict discussion to the right-moving storm, except where indicated otherwise. Qualitatively, the right-moving storm has the characteristics of the supercell storm described in preceding sections. At low levels (Fig. 22a), the precipitation field resembles that of a supercell, except for the absence of hail, which does not occur because the ice phase is excluded from these calculations. The horizontal rainfall pattern, however, exhibits a hook-echo configuration, with a notch at the core of maximum updraft intensity. South of this maximum, the updraft region is elongated along an apparent flanking line. Warm air streams in toward the flanking line and updraft core region from the east. Air is seen diverging from the downdraft, which is centered in the precipitation area. This downdraft air flows into the region behind the flanking line and forms a gust front, which meets the air flowing in from the east. At middle levels (Fig. 22b,c), the cyclonic rotation in the updraft core is clearly seen. The counterrotation in the downdraft core is not as evident in the plotted winds; however, it can be seen clearly in analyses of the vorticity field (e.g., Figs. 14 and 15 of Wilhelmson and Klemp, 1978). Midlevel ambient flow is deflected around the rotating updraft, especially around the south side, as though the updraft were an obstacle to the flow. After passing around the updraft, this air is entrained into the precipitation area on the east or forward side of the storm. The midlevel air is dry, and the precipitation particles readily evaporate into it. The cooling from the evaporation together with precipitation drag induces the air to subside after it is entrained. Passage of midlevel air around the updraft core prior to its entrainment into the precipitation region (Fig. 22b,c) and the exit of downdraft air and outflow at low levels, behind the flanking-line gust front (Fig. 22a) were postulated on the basis of indirect observational evidence by Browning (1964). Comparing the locations of the updraft centers at different levels in Fig. 22a–d, we see further that the updraft core slopes over the downdraft with height (also postulated by Browning) and that divergent anvil flow is centered on the updraft summit[6] (Fig. 22d).

[5] The mesoanticyclone in the left-moving storm should not be confused with the thunderstorm high-pressure area typically observed behind the gust front.

[6] Note that the cloud-top level in this model simulation is lower than that observed in nature as a result of modifying the ambient sounding to reduce the model domain for computational simplicity.

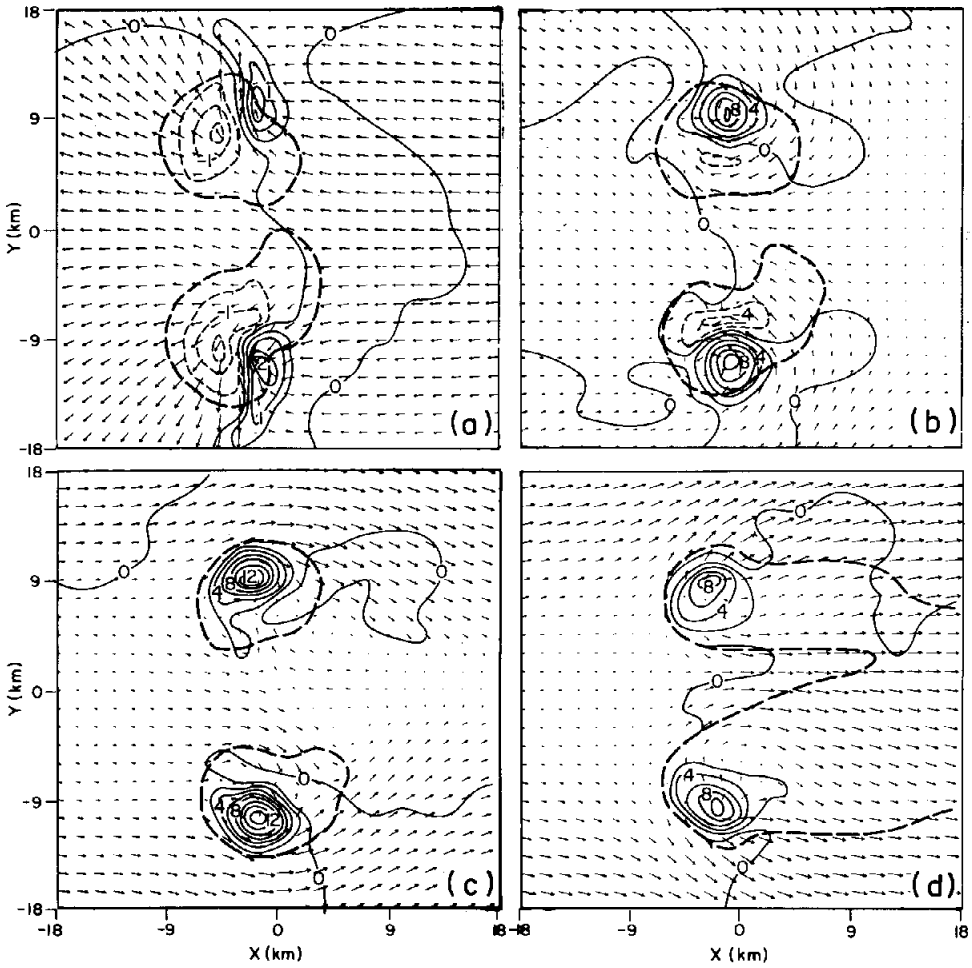

FIG. 22. Three-dimensional cloud model results showing three-dimensional structures of left-moving ($y > 0$) and right-moving ($y < 0$) thunderstorms formed by splitting in unidirectional shear. Horizontal relative wind vectors are shown with vertical velocity (m/sec) superimposed. (a) $z = 0.25$ km, max vector = 14 m/sec; (b) $z = 2.25$ km, max vector = 13.1 m/sec (c) $z = 3.75$ km, max vector = 13 m/sec; (d) $z = 5.75$ km, max vector = 13.0 m/sec. The heavy dashed line marks the outer boundary of the rainwater field, except in (d), where it encloses the cloud water field. From Klemp and Wilhelmson (1978b).

The left-moving storm in Fig. 22 is very nearly the mirror image of the right-moving storm. The slight departure from exact symmetry resulted from inclusion in the model of Coriolis terms, which had somewhat different effects on the left- and right-moving storms. The occurrence of storm splitting, in which both left- and right-moving storms are well defined, is ob-

served only infrequently in nature; however, it seems to occur, as expected, when the ambient shear is nearly unidirectional (e.g., see Charba and Sasaki 1971, and Wilhelmson and Klemp's, 1981, discussion of observed soundings and hodographs). Klemp and Wilhelmson (1978b) showed, however, that slight departures from unidirectional shear in the environment will favor either the left- or right-moving storm. For example, the shear depicted on the side wall of Fig. 19 modifies the unidirectional shear shown on the back wall to favor right-moving storm development. Hodographs favoring the development of symmetrically splitting, left-moving and right-moving model storms are shown in Fig. 23.

In model simulations with hodographs (b) and (c) in Fig. 23, the basic storm-splitting process seen in the case of unidirectional shear occurs, but

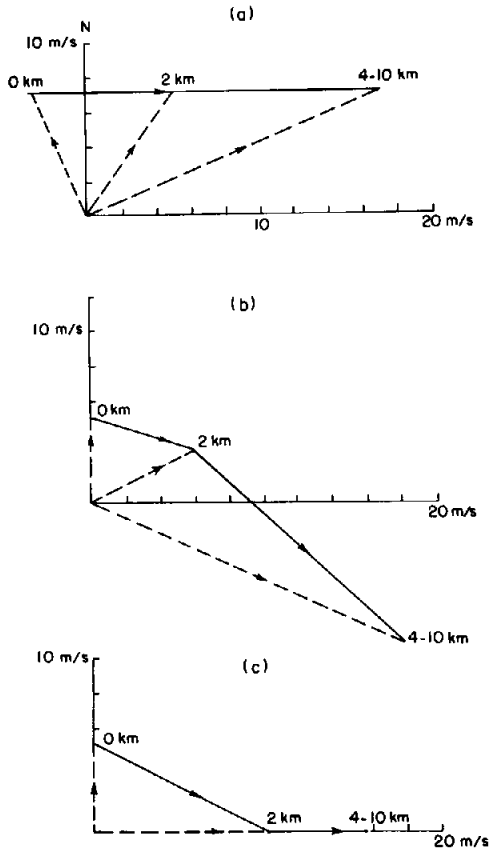

FIG. 23. Hodographs favoring (a) symmetrically splitting, (b) right-moving, and (c) left-moving supercell thunderstorms. From Klemp and Wilhelmson (1978b).

the disfavored storm is greatly weakened (Klemp and Wilhelmson, 1978b). If this process occurs in nature, the disfavored storm probably never develops sufficiently to be readily observable. Since severe storm situations in North America are usually characterized by the type of shear shown in hodograph (b) of Fig. 23, the right-moving storm is the type of supercell usually observed.

The low-level flow pattern of a supercell simulated using the wind and thermodynamic soundings for a specific case of right-moving supercell development (shear in the environment like that of Fig. 23c) is compared in Fig. 24 with the flow pattern observed at two times in the actual storm by

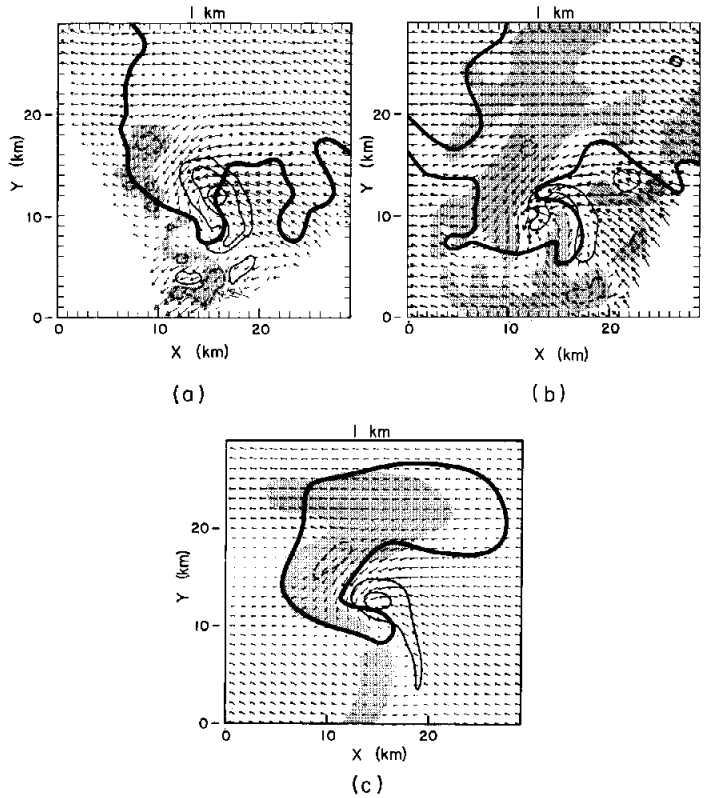

FIG. 24. Flow pattern and radar reflectivity at the 1-km level in the Del City, Oklahoma, tornadic thunderstorms observed by multicell Doppler radar at (a) 1833 LST and (b) 1847 LST and simulated by a three-dimensional numerical model (c). Updraft velocities (solid lines) and downdraft velocities (dashed lines) are contoured at 5 m/sec intervals in (a) and (c) and 10 m/sec in (b). Shaded regions designate areas of negative vertical velocity (< -1 m/sec). The heavy solid line outlines the rainwater field enclosed by the 0.5 g/kg contour in (c) and by the 30 dBZ contour in (a) and (b). Wind vectors are scaled such that one grid interval represents 20 m/sec. From Klemp *et al.* (1981).

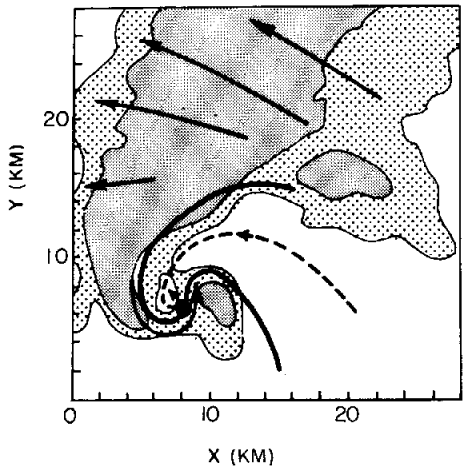

FIG. 25. Idealized version of radar reflectivity and dual-Doppler observed flow at the 0.4-km level in the Del City, Oklahoma, tornadic thunderstorm. Low- and high-density shading is for reflectivity thresholds of 30 and 40 dBZ, respectively. Solid (dashed) arrows show horizontal flow in downdraft (updraft) region. Heavy solid line is boundary between downdraft and updraft regions. Large dot shows tornado location. Adapted from Fig. 5 of Brandes (1981).

multiple-Doppler radar techniques. Several model and Doppler radar comparisons such as this one have now been made, and the similarity of major features is striking. The success of these comparisons lends confidence to both the modeling and radar methodologies.

3.3.6. Genesis of the Tornado. The Doppler radar observations depicted in Fig. 24a,b show a prominent center of cyclonic rotation, which is the low-level manifestation of the mesocyclone discussed in Section 3.3.5 and illustrated in Fig. 21d. The mesocyclone is the favored region for tornadogenesis, though, as we noted in Section 3.3.1, tornadoes may also occur along gust-front or "downburst" boundaries. These gust front and downburst tornadoes, though quite damaging, are not as severe or as well documented as the mesocyclonic tornado. We will restrict the present comments to the mesocyclonic tornado.

The vortex comprising the tornado is much more intense and occurs on a much smaller scale than the parent mesocyclone. The tornado vortex is in fact too small to resolve in multiple-Doppler radar analyses; however, it can often be detected in single-Doppler data as a location of extreme wind shear from one data sampling volume to the next (Brown *et al.*, 1978) or in the velocity spectrum for a single sampling volume (Zrnic *et al.*, 1977). This so-called tornado–vortex signature (TVS) is observed aloft, at the

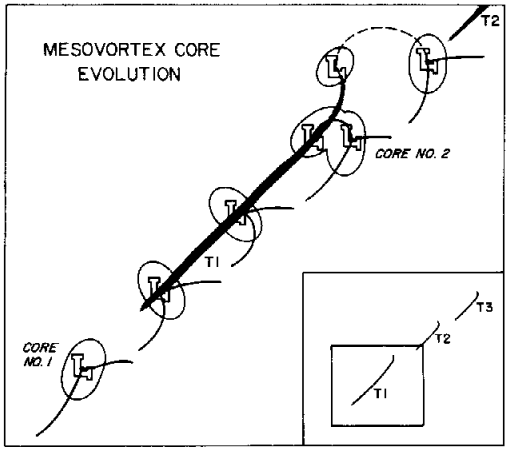

FIG. 26. Conceptual model of mesocyclone core evolution. Thick lines are low-level wind discontinuities. Tornado tracks are shaded. Inset shows the tracks of the tornado family, and the small square is the region expanded in the figure. From Burgess *et al.* (1982).

2–5-km level within the mesocyclone, some 20–30 min before it appears within the low-level mesocyclone and reaches the ground as a visible tornado funnel.

At low levels, the tornado appears after the mesocyclone center moves from the updraft core to the boundary between the downdraft and updraft (cf. Fig. 21c,d). In the Doppler radar data in Fig. 24, the circulation center was in the updraft at the earlier time (Fig. 24a), but by the later time (Fig. 24b) the updraft region had become distorted into the shape of a horseshoe by an intrusion of cyclonically rotating downdraft air. Klemp *et al.* (1981) have shown that this downdraft air began its sinking motion in the main precipitation region to the north of the mesocyclone and that it subsequently spiraled downward, around the mesocyclone center, where it split the updraft core as it sank to low levels. Brandes (1981) has related this intrusion to the formation of a tornado in the location indicated in Fig. 25. Brandes (1978; see his Fig. 18) and Golden and Purcell (1978a; see their Fig. 8) have shown similar downdraft intrusions in relation to the appearance of tornadoes at low levels. Brandes (1981) finds that once the downdraft intrusion has become established, both tilting and stretching of vortex tubes on a highly localized scale become active (stretching was of greater magnitude in this case) in forming the tornado at a location along the boundary of the updraft and downdraft air circulating around the mesocyclone (e.g., Fig. 25). Brandes argues further that, soon after the situation illustrated in Fig. 25, the updraft in the vicinity of the mesocyclone center was completely cut off from the inflow of warm air by the downdraft intrusion, and the

tornado and mesocyclone dissipated. A new supercell updraft and mesocyclone center then formed ahead of the rear-flank gust front.

Cutting off of the mesocyclone center in this way, while the rear-flank gust front propagates ahead and generates a new main updraft and mesocyclone, which in time spawns another tornado, accounts for the association of multiple tornado paths with a single supercell storm (Fig. 26). Lemon and Doswell (1979) noted that this sequence of secondary mesocyclone development bears an intriguing resemblance in miniature to synoptic-scale cyclone evolution. Burgess *et al.* (1982) have verified the sequence of events depicted in Fig. 26 statistically from Doppler radar observations. They note that, although long-track tornadoes have been observed, they are extremely rare and that "many tornadoes initially appearing long are in reality a family of segments, each associated with a different mesocyclone core." High-resolution three-dimensional model simulations confirm the tendency of the mesocyclone center to be cut off with new main updraft and vorticity centers developing along the gust front to the east (Klemp and Rotunno, 1982), and recent photographic documentation of multiple-tornado storms by tornado chase teams is consistent with the sequential mesocyclonic and tornadic evolution observed on radar (Rasmussen *et al.*, 1982; Marshall and Rasmussen, 1982).

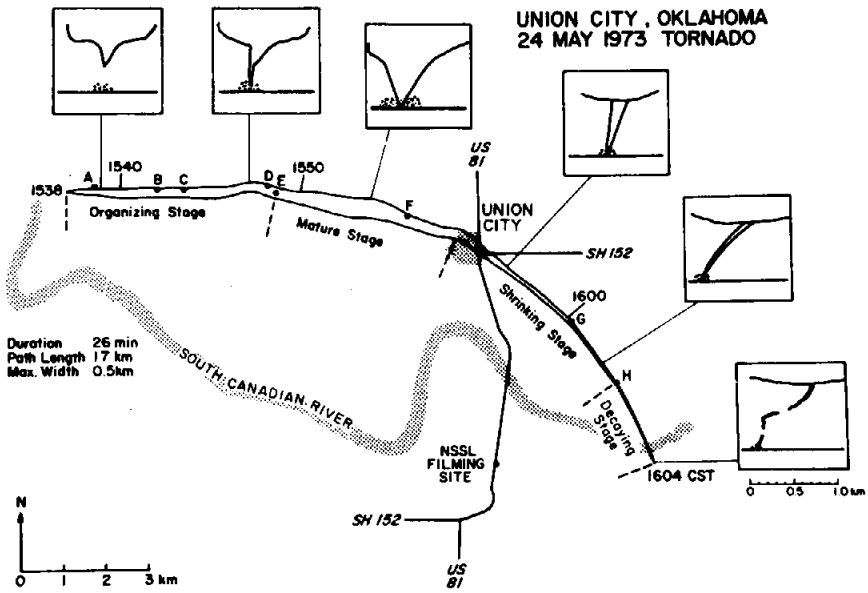

FIG. 27. Damage path of the Union City, Oklahoma, tornado with sketches of the funnel and associated debris cloud as seen from the south. Letters A–H indicate damaged farmsteads. From Golden and Purcell (1978a).

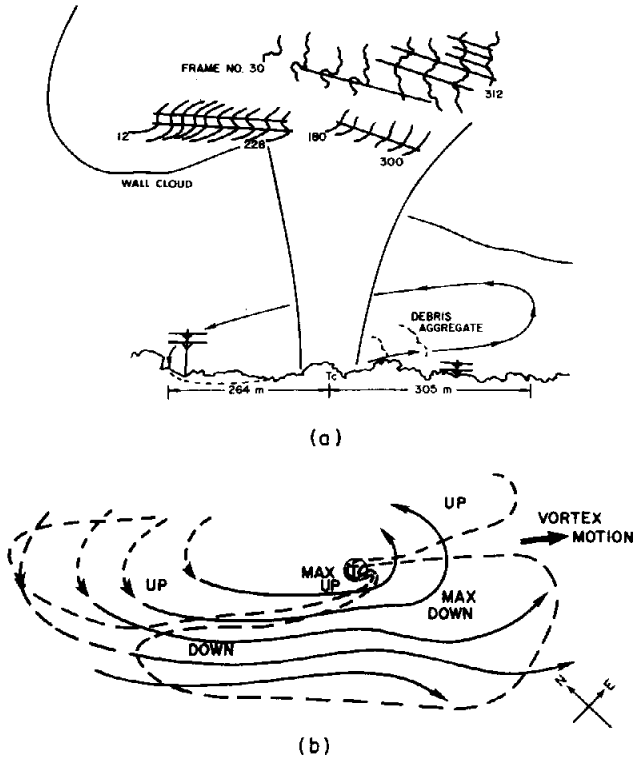

FIG. 28. Tornado structure from photogrammetry and damage surveys. (a) Outline of Union City, Oklahoma, tornado funnel and upper wall cloud showing features tracked on movie loops. Sequential outline of cloud tags and streamers in wall cloud and typical composited trajectory and displacement of debris aggregate are superimposed. (b) Schematic plan view of horizontal streamlines (solid lines) and low-level vertical motion patterns (dashed lines) around decaying tornado. From Golden and Purcell (1978b).

3.3.7. Life Cycle and Structure of the Tornado. An example of an individual tornado funnel that formed within a mesocyclone is described in detail by Golden and Purcell (1978a); for other examples, see Fujita (1960), Hoecker (1960), and Davies-Jones (1982a). The structure of the funnel observed by Golden and Purcell is illustrated schematically in Fig. 27 for several stages in its life cycle. The "organizing stage" was characterized by a visible funnel touching the ground intermittently, though the damage path was continuous. In the "mature stage," the tornado was largest. In the "shrinking stage," the entire funnel decreased to a thin column. The "decaying stage" was characterized by a fragmented and contorted but still destructive funnel. Air motions within and near the tornado (Fig. 28) were determined by tracing debris particles and identifiable cloud elements

("cloud tags") in motion pictures (Golden and Purcell, 1978b) and by surveying surface damage patterns (Davies-Jones *et al.*, 1978). In the mature stage, tangential velocities at a radius of 200 m and heights 60–120 m above ground were 50–80 m/sec, in agreement with deductions from various earlier but less intensively documented cases. The flow pattern was notably asymmetric. At the wall-cloud level, there was strong downward motion on the southwest side of the funnel with upward motion on the northeast side (Fig. 28b).

The tornado funnel is sometimes observed to contain one to six smaller subvortices, 0.5–50 m in diameter (Fujita, 1970, 1971, 1981; Fujita *et al.*, 1970; Agee *et al.*, 1975, 1976, 1977). These "suction vortices" may be stationary or orbit around the tornado center (Fig. 29). They contain some of the strongest winds of the tornado and leave a complex pattern of narrow trails of debris and extreme damage within the general path of the tornado. The observation of multiple funnel clouds [e.g., the 1965 Elkhart, Indiana, twin tornado (Fig. 46 of Fujita *et al.*, 1970) or the 1979 Wichita Falls, Texas, tornado, which exhibited six simultaneous vortices (Fig. 17 of Fujita, 1981)] is explained by the breakdown of the parent funnel into suction vortices.

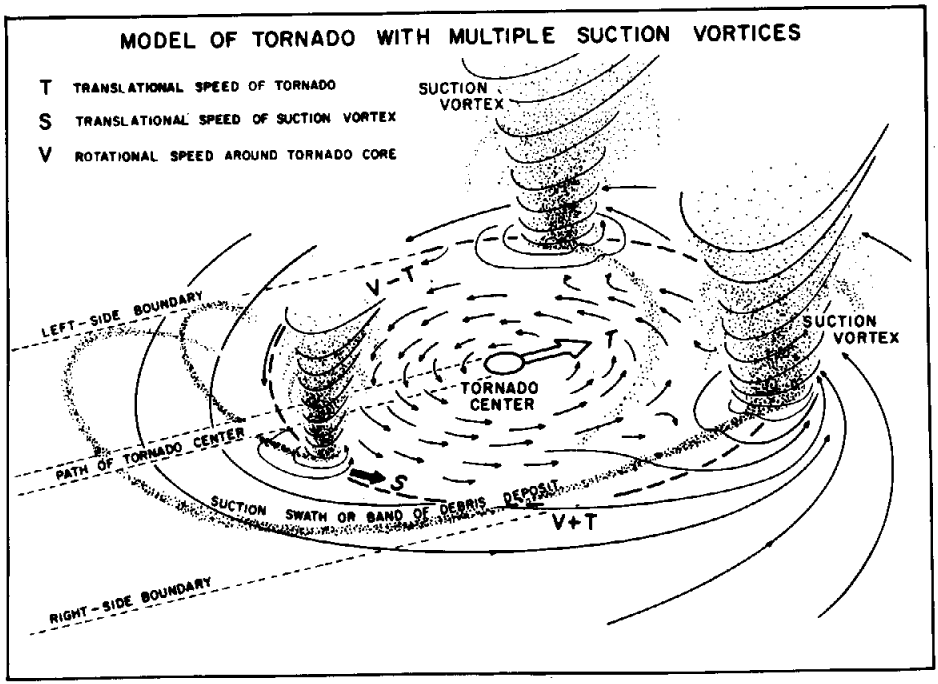

FIG. 29. A model of a tornado with multiple suction vortices proposed by Fujita in 1971. From Fujita (1981).

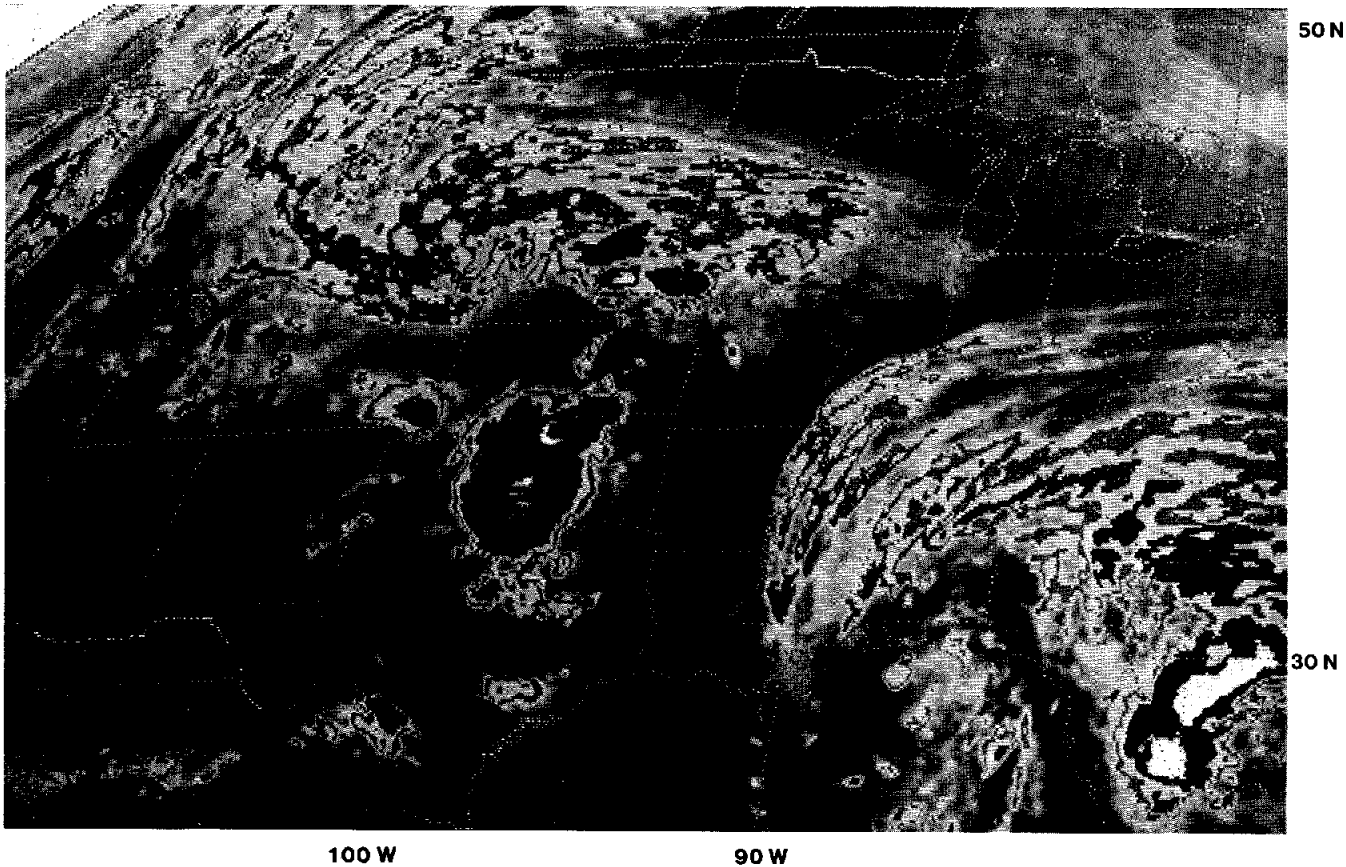

FIG. 30. Infrared satellite picture of a mesoscale convective complex over Oklahoma at 0330 GMT on 23 May 1976. Shading levels are for −32°C (medium gray), −42.2°C (light gray), −53.2°C (dark gray), −59.2°C (black), and −71.2°C (white).

This breakdown has been simulated in laboratory models (e.g., Ward, 1972; Leslie, 1977; Church *et al.*, 1977) and is related theoretically to the "swirl ratio," which is a nondimensional parameter expressing the relative strengths of circulation and forced convection in the parent vortex (Davies-Jones, 1976, 1982b). The breakdown of the mesocyclone into tornadoes, the tornadoes into suction vortices, and even the latter into twin suction vortices twisting around each other (Fujita, 1981) brings to mind the famous rhyme of L. F. Richardson:

> Big whirls have little whirls that feed upon their velocity
> And little whirls have lesser whirls and so on to viscosity.

3.4 Midlatitude Mesoscale Convective Complexes

It is quite common for several thunderstorms to be grouped together within a mesoscale complex, which covers an area one or more orders of magnitude greater than that covered by an individual thunderstorm. The storms comprising such a complex typically share a common upper-level cloud shield, which appears very prominently in satellite imagery when the system matures (e.g., the cloud centered over Oklahoma in Fig. 30). Maddox (1980b) has used this fact to define a midlatitude "mesoscale convective complex" (MCC) in terms of the time and space scales of its cirriform cloud top, as it appears in satellite data (Table I). Fritsch *et al.* (1981) have presented evidence that 50–60% of the summer rainfall in the Great Plains and midwestern United States is accounted for by MCCs identified by Maddox's criteria. Their work indicates, moreover, that the precipitation falling from an MCC at a given time typically covers a continuous area of mesoscale

TABLE I. CRITERIA USED TO IDENTIFY MIDLATITUDE MESOSCALE CONVECTIVE COMPLEXES IN INFRARED SATELLITE DATA[a]

	Physical characteristics
Size:	(A) Cloud shield with continuously low infrared temperature $\leq -32°C$ must have an area $\geq 100{,}000$ km^2
	(B) Interior cold cloud region with temperature $\leq -52°C$ must have an area $\geq 50{,}000$ km^2
Initiate:	Size definitions (A) and (B) are first satisfied
Duration:	Size definitions (A) and (B) must be met for a period ≥ 6 hr
Maximum extent:	Contiguous cold cloud shield (infrared temperature $\leq -32°C$) reaches maximum size
Shape:	Eccentricity (minor axis/major axis) ≥ 0.7 at time of maximum extent
Terminate:	Size definitions (A) and (B) no longer satisfied

[a] From Maddox (1980b).

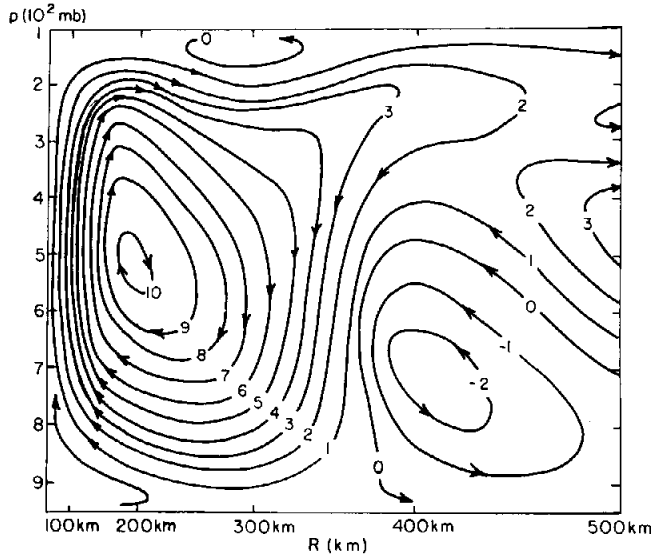

FIG. 31. "Mass-flow" stream function (at intervals of 10^7 mbar m^2 sec^{-1}) for the azimuthally averaged flow about an origin at the centroid ($R = 0$) of a rainstorm with the characteristics of a midlatitude MCC. The sense of the flow is indicated by the arrowheads. From Bosart and Sanders (1981).

dimensions; that is, the individual thunderstorms are embedded in a larger, mesoscale region of precipitation falling from the cloud shield.

The occurrence of a continuous area of precipitation on a scale greater than that of the individual thunderstorms indicates that an organized circulation occurs on the mesoscale in conjunction with the MCC. Bosart and Sanders (1981) deduced the circulation associated with an MCC that produced severe flooding in Johnstown, Pennsylvania, in 1977 (Fig. 31). Maddox (1981) has found a similar circulation to be characteristic of the mature midlatitude MCCs he has identified. This circulation should not be confused with the air motions of an individual thunderstorm. The MCC circulation is a much larger scale overturning in which the thunderstorms are embedded.

The mesoscale circulation of the mature MCC, shown in Fig. 31, was determined for a circularly symmetric region centered on the MCC. A radius–height cross section of the symmetric pattern is shown, with the origin of the graph corresponding to the center of the disturbance. The circulation was characterized by mean ascent over a region several hundred kilometers wide extending vertically through the entire troposphere, except for the boundary layer (below 950 mbar), where weak divergence and descent oc-

curred in the mean. This low-level net divergence reflects the influence of a mesohigh resulting from the spreading of convective downdraft issued by the various embedded thunderstorms. This mesohigh was of the type described in early work of Fujita (1955) and others. Although convergence and new thunderstorm development undoubtedly occurred along the edge of the mesohigh (or "cold dome"), the mesohigh dominated the boundary layer flow to an extent that the divergence and sinking prevailed in the mean pattern. The mean upward motion above the boundary layer connected a region of strong convergence at 900–700 mbar with a region of strong divergence centered at 200 mbar. The convergence was associated with a mesolow in the low to middle troposphere, while the divergence aloft was linked to a pronounced mesohigh. The upper-level mesohighs associated with MCCs have been described by Ninomiya (1971a,b), Maddox (1980a, 1981), Fritsch and Maddox (1981a,b), and Maddox *et al.* (1981).

The mesoscale circulation of the mature MCC develops by progressing through a life cycle described qualitatively by Maddox (1980b, 1981). In its early stages, the MCC is highly convective, being dominated by the individual thunderstorms it contains. As the system evolves, however, lifting on a larger scale becomes more pronounced. A stratiform upper cloud shield develops and precipitation becomes continuous, evidently consisting of a mixture of stratiform and convective components. This life cycle is similar to that typifying tropical cloud clusters (see Sections 4.2–4.5). Detailed radar studies of tropical cloud clusters have clearly distinguished convective and stratiform processes and hence have led to better understanding of the mesoscale organization and dynamics of the clusters. Similar work is needed to distinguish the convective and stratiform processes in midlatitude MCCs.

The dynamics of the development of the mesoscale circulation of the MCC (Fig. 31) are not yet well understood; however, some of their aspects may be surmised from existing observations, as well as from mesoscale models and by comparing MCCs to tropical cloud clusters. The initial development is apparently driven by convective heating (which is dominated by release of latent heat in the convective updrafts; Houze, 1982) associated with the embedded thunderstorms. Mesoscale models with parameterized (sub-grid-scale) convection (Brown, 1974, 1979; Kreitzberg and Perkey, 1977; Fritsch and Chappell, 1980; Fritsch and Maddox, 1981b; Maddox *et al.*, 1981) show that hydrostatic adjustment to the convective heating initiates a mid to low tropospheric mesolow and an upper tropospheric mesohigh of the sort evident at 900–700 mbar and 200 mbar in Fig. 31. Ninomiya (1971a,b) arrived at a similar conclusion from observational evidence. As the mesolow and mesohigh intensify, mesoscale lifting strengthens and widespread cloud and precipitation develop. At this stage, condensation, evaporation, melting, and radiative transfer can become important in the

stratiform cloud and precipitation areas and combine with the heat release by the embedded thunderstorms to provide the total thermal driving force for the mesoscale circulation. If the convection embedded in the MCC weakens or dies out after this stage, the MCC should be able to continue to exist since the mean circulation can continue, driven by the stratiform and/or radiative processes. Thus, the MCC becomes less convective and more stratiform as it ages. This sequence of thermodynamical and dynamical events is consistent with Maddox's (1980b, 1981) descriptive life-cycle observations and with tropical cloud clusters. Houze (1982) has examined the relative magnitudes of convective, stratiform, and radiative heating in tropical cloud clusters and has found them all to be significant, with the stratiform and radiative processes becoming more prominent in the later stages of a cluster. Further work is needed to distinguish these processes more clearly in midlatitude MCCs.

3.5. Midlatitude Squall Lines

A type of mesoscale convective system that has been recognized for a long time is the midlatitude squall line. Some confusion exists, however, regarding the definition of a squall line. The "Glossary of Meteorology" (Huschke, 1959) defines a squall line as "any non-frontal line or narrow band of active thunderstorms." This definition appears to be inadequate in at least two respects: The nonfrontal requirement is too restrictive, since thunderstorms associated with a front (or even frontal rainbands without thunderstorms) can occasionally take on squall-line characteristics (e.g., Fujita, 1955; Sanders and Paine, 1975; Sanders and Emanuel, 1977; Hobbs and Persson, 1982), whereas to say that "any" line of thunderstorms qualifies as a squall line is too general, since most observers recognize a squall line as a special class of convective line characterized by rapid propagation and certain mesoscale pressure, wind, and precipitation patterns. Fujita (1955) clearly identified these features. He showed that a squall line starting from a point, probably as one or two individual thunderstorms, successively expands its area of influence (Fig. 32). The leading edge of the system, commonly called the gust front (but referred to by Fujita as the "pressure-surge line"), has the characteristics of an intense cold front. As it propagates, it continually lengthens, and an expanding pool of downdraft air is left in its wake (Fig. 33). A narrow band of intense thunderstorms is found along the leading edge, with a broader region of light precipitation falling from an extensive cloud region to the rear. A mesohigh is found at the surface in the trailing region of lighter precipitation. A "wake-depression," or mesolow, induced by subsidence warming, is found in dry air to the rear of the precipitation zone. The horizontal extent of the system (~400 km), its widespread area of precipitation, and its oval shape make it comparable in

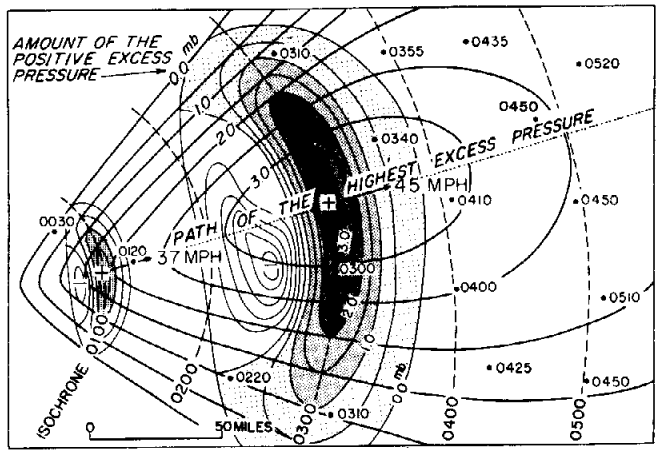

FIG. 32. Spread of area influenced by an advancing squall line. Isobars of excess pressure are drawn for two times (0100 and 0300) with hourly isochrones and envelopes of the various pressure values. From Fujita (1955).

size and shape to an MCC. A single squall-line system of this type develops an upper-cloud shield, which can attain the characteristics that qualify it as an MCC according to Maddox's (1980b) criteria (e.g., Fig. 30). Thus, Fujita's ideal midlatitude squall-line system can be considered as a special case of an MCC.

However, the midlatitude squall line is identified as an MCC by Maddox's criteria (Table I) only when it occurs in isolation. When several squall-line systems break out along a larger scale front or windshift line, leading edges may intersect and form a long chain of squall systems (e.g., see Figs. 37–43 of Fujita, 1955; or cf. Figs. 13.8 and 13.9 of Palmén and Newton, 1969). In this situation, upper cloud shields merge and the individual squall systems become impossible to distinguish as separate MCCs by strict application of Maddox's criteria, since his rules are designed to identify only isolated (i.e., round or oval) cloud shields. Therefore, while the isolated squall-line system in Fig. 30 is readily identified as an MCC, a squall-line system that is one of several along or ahead of a front cannot be separately identified in satellite data unless the time continuity of the cloud pattern is closely followed and subjective allowance is made for mergers. As shown by Fujita's (1955) work, radar and other detailed surface observations are needed to distinguish unambiguously the separate mesoscale squall systems forming parallel to a front. Such a distinction seems necessary, however, to understand both the isolated squall system and families of squall systems occurring parallel to fronts.

Squall lines occur in a variety of large-scale environments. Palmén and

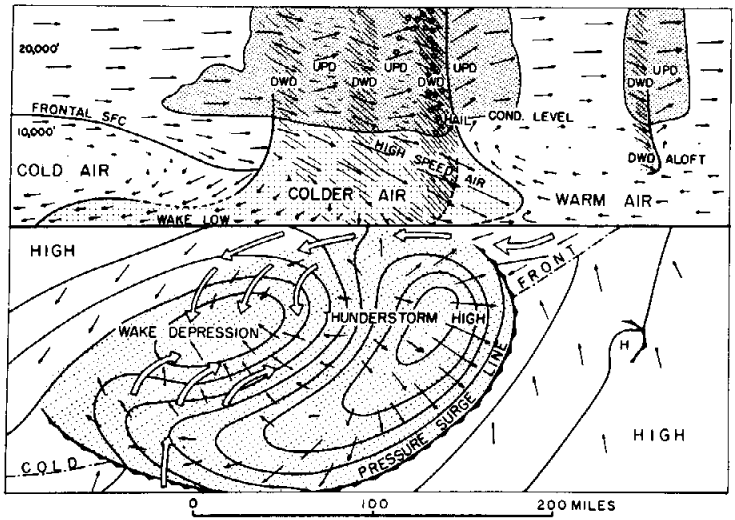

FIG. 33. Fujita's model of a squall line, in vertical cross section (upper) and in surface plan view (lower). Lines on surface map are isobars. Wind vectors are indicated by small arrows; the motion of the system at upper levels relative to the moving system is represented by the large open arrows on the surface map. UPD and DWD indicate updrafts and downdrafts, respectively. From Fujita (1955).

Newton (1969) note that, "Although squall lines most commonly occur in the warm sectors of cyclones (or in tropical air well removed from frontal systems), they often extend far north of warm fronts and occasionally form some distance behind cold fronts: in both cases the thunderstorms are in the warm air above the front." Thus, squall lines form in different situations of environmental wind shear, and, not surprisingly, squall lines take on various configurations. Often the winds in the environment are strongly veering, usually ahead of an approaching upper trough (Fig. 2 of Newton, 1963), and a line of severe organized multicell or supercell storms develops and may exhibit characteristics of the squall-line model of Fujita (1955) (Figs. 32 and 33). Newton and Fankhauser (1964) and Newton (1966) investigated severe convective lines of this type (Fig. 34). They consist of aligned thunderstorms, with wind shear favoring new development on the southern ends of individual squall lines. By this process, the southern end of a line to the north may join the northern end of a line to the south, thus forming a longer squall line. The ambient shear favors anvil blowoff to the north-northeast, along and ahead of the line. The older thunderstorms on the northern ends of lines evolve into "extensive stratified cloud masses";

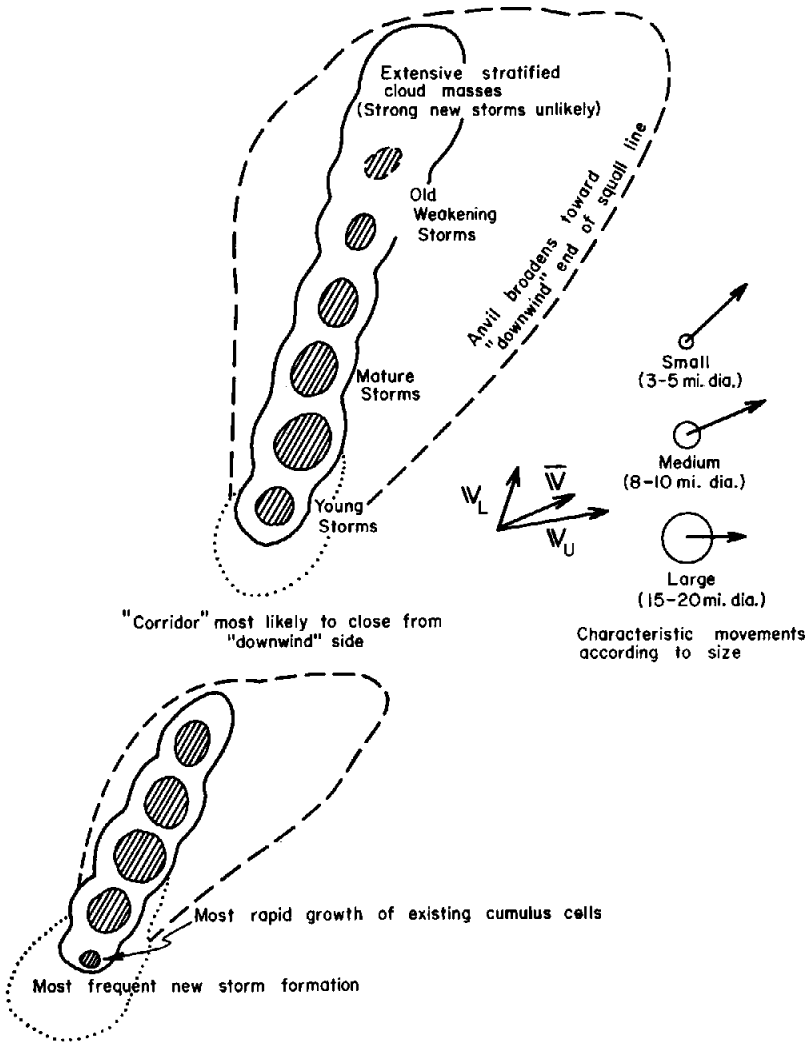

FIG. 34. Simplified horizontal map of principal features of one type of midlatitude squall line (north at top of page). Solid lines show precipitating cloud (regions of heavier rain cores hatched); dashed lines, the general anvil outline (which may be smaller or more extensive depending on the age of the squall line). New cell formation is most likely inside dotted boundaries, but may occur elsewhere. Inset shows most typical environmental winds, veering between lower (V_L) and upper (V_U) levels, and characteristic movements of storms of different sizes relatives to vector mean wind ($\bar{V}$). From Newton and Fankhauser (1964).

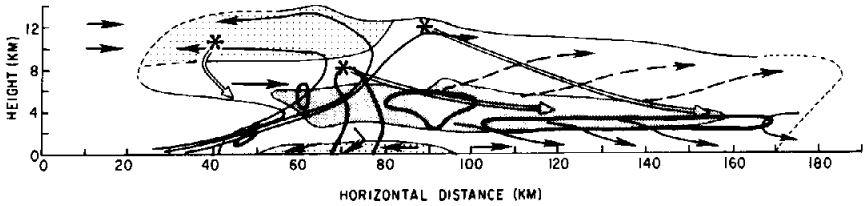

FIG. 35. Conceptual model of the 22 May 1976 Oklahoma squall-line system. Outside contour outlines radar echo. Heavy lines denote regions of more intense echo. Light shading indicates regions of system-relative horizontal wind component directed from right to left relative to the system. Heavy shading shows jet of maximum horizontal wind from left to right. System was propagating from right to left. These streamlines show two-dimensional relative flow consistent with observed wind and echo structure. Hypothesized ice particle trajectories are denoted by asterisks and broad white arrows. Environmental wind relative to the system is indicated just ahead of the leading anvil echo. From Houze and Smull (1982).

however, an extensive stratiform precipitation area is not typically found in this type of squall line.

In other situations, when the environment is characterized by a different type of wind shear, midlatitude squall lines exhibit an extended region of cloud and lighter precipitation behind the leading line of deep convection (Newton, 1950; Fujita, 1955; Chisholm, 1973; Sanders and Paine, 1975; Sanders and Emanuel, 1977; Ogura and Liou, 1980; Matejka and Srivastava 1981; Zipser and Matejka, 1982; Houze and Smull, 1982). This extended trailing precipitation enlarges the overall precipitation area of the system and gives it a continuous character of the type Fritsch *et al.* (1981) have associated with MCCs (cf. Section 3.4). Radar analyses of the trailing precipitation (Matejka and Srivastava, 1981; Zipser and Matejka, 1982; Houze and Smull, 1982) reveal that this trailing precipitation is similar to that which occurs to the rear of tropical squall lines (Houze, 1977; Leary and Houze, 1979b) in that it is highly stratiform, with an echo bright band in the melting layer.

The isolated squall-line system, whose upper cloud is shown in Fig. 30, was of the type that exhibited trailing stratiform precipitation. Its structure is illustrated schematically in Fig. 35 in a vertical cross section along the direction of propagation of the system. The structure depicted is inferred from studies of composited sounding data (Ogura and Liou, 1980) and detailed radar reflectivity and single-Doppler radar air motion fields (Houze and Smull, 1982).

The airflow into the front of the system is depicted as rising first above a gust front associated with downdraft outflow and then progressing into a region of convective cells. A new cell, identified by a first echo aloft, is shown at 60 km above the core of rising air, which was directed primarily

into a weak-echo indentation on the leading side of a mature cell echo at 70 km. As the core of rising air approached the mature cell, it developed a strong front-to-rear component of horizontal motion between 2 and 5 km. The core of the updraft was thus tilted substantially. Upon reaching the tops of convective cells, the updraft air split into distinct components directed to the front and rear of the system. The part directed forward carried ice particles into the leading anvil. As the particles fell into the inflow stream in mid levels, they were either evaporated or swept back into the region of active cells.

Mature cells, such as the one at 70 km in Fig. 35, were followed by dissipating cells, such as the one at 90 km, which is shown as having lost its core of updraft air. The horizontal outflow of downdraft air was strongest under mature cells, but was also seen under the dissipating cells. Consequently, the forward-rushing downdraft air was seen at low levels throughout the region of forming, mature, and dying cells (between 50 and 100 km in Fig. 35).

The sequence of forming, mature, and dissipating cells at the leading edge of the system is rather similar to that of the forward-propagating multicell thunderstorm depicted in Fig. 14. The thunderstorm structure along the leading edge of the squall system may vary. Occasionally—particularly, early in the lifetime of a squall system—individual storms along the line may develop rotation and take on the character of a supercell storm rather than a multicell storm.

In the case illustrated in Fig. 35, Doppler observations showed that the relative airflow in the stratiform region was everywhere directed from front to rear, except at the very back edge of the system, where some inflow from the rear occurred. The airflow through the squall system was particularly interesting at mid levels, where a jet of maximum front-to-rear flow occurred (heavily shaded region). Houze and Smull (1982) found that the largest front-to-rear velocity components within this jet occurred near the front of the system at the locations of the convective cells. The jet extended through the trailing stratiform region, with magnitudes of velocity tapering off toward the back edge of the system, where the jet met the midlevel inflow from the rear. A rather similar horizontal velocity component field was reported by Sanders and Paine (1975) and Sanders and Emanuel (1977). The latter authors attributed the generation of the maximum horizontal velocities primarily to horizontal pressure-gradient accelerations directed into a mid-tropospheric mesolow, apparently of the type known to be characteristic of MCCs. Houze and Smull (1982) noted that this jet was located just above the melting layer and appears to have played a role in spreading the trailing precipitation region out into a stratiform pattern. Houze (1981) pointed out that a melting layer $\sim$100-km wide, to the rear of a convective

line that is propagating by the successive development of new cells at its leading edge (as in the Oklahoma squall system depicted in Fig. 35), can be explained by the relative horizontal motions of ice particles falling from the tops of cells. The particles move in a relative sense toward the rear of the system as a result of the continuing redefinition of the position of the leading edge of the system by the formation of new cells. This effect was exaggerated in the Oklahoma squall line by the jet of particularly strong relative wind just above the melting layer. Hypothesized particle trajectories are indicated in Fig. 35.

The stratiform precipitation occasionally seen trailing midlatitude squall lines thus appears to develop partly by the successive incorporation of old cells into the trailing region (as noted by Sanders and Emanuel 1977) and partly by rearward spreading of ice particles by the midlevel jet. In addition, mesoscale lifting above the melting layer, indicated by Ogura and Liou's (1980) results and depicted schematically in Fig. 35, may contribute to the development of the stratiform precipitation. Ogura and Liou's results also indicate that the air below the melting layer subsides in a mesoscale downdraft. Matejka and Srivastava (1981) have confirmed this mesoscale updraft–downdraft structure with Doppler radar data obtained in the trailing stratiform region of an Illinois squall line.

The mid- to upper-tropospheric mesoscale updraft and mid- to lower-tropospheric mesoscale downdraft associated with a broad continuous area of precipitation are consistent with the divergence and vertical motion profiles obtained for MCCs by Bosart and Sanders (1981) and Maddox (1981). Distinguishing between the stratiform and convective portions of the squall systems, however, has helped resolve and distinguish the different roles of convective (cellular) and mesoscale components of motions. Further radar studies should improve the understanding of this type of squall line and of MCCs in general.

3.6. Effects of Downdraft Spreading

The downdrafts from a single thunderstorm, or from a group of thunderstorms occurring in an MCC or squall line, spread horizontally in the boundary layer. In Sections 3.2 and 3.3.5, it was seen that downdraft spreading serves as a mechanism for the discrete regeneration of multicell storms, where downdrafts from older cells trigger new cells, and as a mechanism of continuous regeneration for left- and right-moving supercell storms in which the downdraft air continually spreads under the inflowing updraft air. Below MCCs and squall-line systems, larger regions of cold air are formed by the merger of the various downdrafts emanating from the nu-

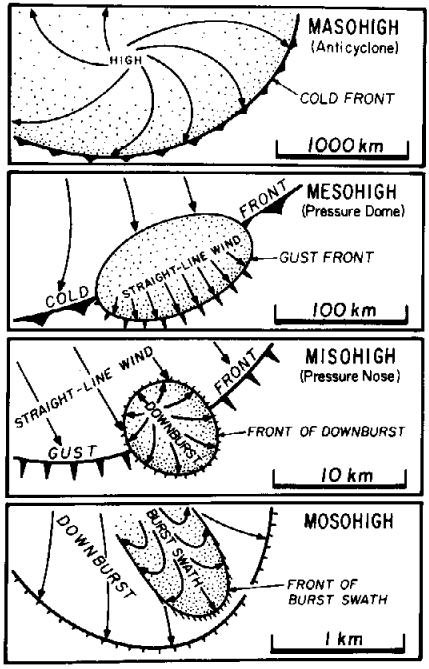

FIG. 36. Schematic drawings showing the airflow patterns associated with cold front, gust front, downburst, and burst swath. From Fujita (1981).

merous thunderstorms embedded in these systems. These large pools of cool air in the boundary layer account for the low-level mesohighs characterizing these systems. Some effects of spreading downdrafts are discussed in the following subsections. First, violent downdraft outflows characterized by severe low-level winds are discussed in Section 3.6.1. Then the role of old downdraft outflow boundaries from past or decaying storm systems in triggering new storms is described in Section 3.6.2.

3.6.1. Nontornadic Severe Winds. As noted in Section 3.1, strong winds that can classify a thunderstorm as "severe" can be associated with downdrafts as well as tornadoes. Fujita (1981) has classified downdraft winds according to horizontal scale (Fig. 36b–d). His classification has been determined largely from studying patterns of surface damage. Debris and fall patterns of certain flora left on the ground by downdraft winds are distinguishable from those left by tornadoes since the downdraft patterns reflect divergent flow, while tornadic damage reflects convergent flow.

The largest thunderstorm wind pattern is the "straight-line wind" asso-

ciated with the gust front marking the leading edge of the mesohigh of a squall-line system (cf. Figs. 32 and 36). Fujita (1981) reports, however, that "against our expectations, the damage by straight-line winds behind these gust fronts turned out to be minimal." Instead, damage is concentrated in "downbursts" (referred to earlier as "pressure noses" by Byers and Braham, 1949) which are $\sim$10 km or less in horizontal dimension and occur sporadically at points along the gust front. Smaller scale downbursts are referred to as "microbursts." Emanuel (1981) has suggested that downbursts are a manifestation of unsaturated downdraft instability of the type that he has described theoretically. Within a downburst, a concentrated "burst swath," $<$1 km in dimension, can occur. Fujita (1981) notes further that a downburst can occur along a supercell gust front as well as along a squall-line and that downbursts along supercell gust fronts, by virtue of the rotational flow of the supercell, have a "twisting airflow" at the surface rather than the purely divergent flow depicted in Fig. 36. Further damage can occur when tornadoes are generated at the lateral boundaries of downbursts (Fig. 9a).

When a downburst occurs along a squall-line gust front, as in Fig. 36, the radar echo of the leading line of thunderstorms juts out ahead of the main squall line to form a "bow echo." The relationship of the bow echo and downburst airflow is discussed by Fujita (1981). As pointed out in Section 2.6, the bow echoes associated with downbursts appears to have a counterpart in the "boomerang echoes" associated with strong cold fronts (Fig. 9b).

3.6.2. Arc Cloud Lines and Triggering of New Storms. Satellite studies (Purdom, 1973, 1979; Purdom and Marcus, 1982) show that the boundaries of downdraft outflows from thunderstorms or thunderstorm complexes can maintain their identities as arc-shaped lines of cumulus clouds for several hours after the storms that produced the downdrafts have dissipated. These lines can trigger new deep convective development up to 200 km from the location of the original storm. A great proportion of new deep convective developments occur where propagating arc lines intersect each other or where an arc line encounters preexisting convection (Purdom and Marcus, 1982). Aircraft data show that the arc lines contain some lightly precipitating cumulus (Sinclair and Purdom, 1982). However, these lines are mostly invisible to radar. Thus new deep convection triggered by an arc line may seem to appear at a random location on radar. However, in satellite data the location of development can often be anticipated by observing the history of the arc lines. Perhaps some of the simultaneous cell-formation events in the Thunderstorm Project, noted by Byers (1959) to be unexplainable in terms of locally preexisting cells (see Section 3.2), were occurring along outflow boundaries from previous, distant thunderstorms.

The ability of the arc lines to maintain themselves for several hours, while

traveling great distances from the sites of their originating storms, is not readily explained. Sinclair and Purdom (1982) suggest that subcloud evaporation of the light rain from some of the cumulus along the line plays a role. Observations of arc cloud lines emanating from cumulonimbus, possibly being perpetuated by precipitation showers along the line, and contributing to the development of new storms, have also been made in the tropics (Warner *et al.*, 1979; see also review of Houze and Betts, 1981).

4. Tropical Cloud Systems

4.1. The Spectrum of Clouds in the Tropics

Clouds in the tropics occur in a spectrum of sizes ranging from small isolated cumulus to large "cloud clusters." The cloud clusters are identified in satellite pictures by their mesoscale cirrus shields, each shield being ~100–1000 km in dimension (Fig. 37). Statistical studies indicate that the tropical cloud spectrum, whether measured in terms of heights, areas, durations, or rainfall rates, tends to be distributed log-normally (see review of Houze and Betts, 1981). That is, smaller, isolated cumulus and cumulonimbus greatly outnumber cloud clusters. Nevertheless, the cloud clusters, owing to their size, dominate the mean cloudiness and total precipitation of the tropics.

The cloud clusters resemble midlatitude MCCs in being identified by their large cirrus canopies. They contain continuous rain areas covering up to 5×10^4 km^2. The cirrus shields of cloud clusters are typically not as cold as required by Maddox's (1980b) criteria for midlatitude MCCs (Table I)[7]; however, they are of the same scale and qualitatively rather similar. The tropical systems could be called tropical MCCs. However, the term "cloud cluster," which emerged from early satellite studies of tropical cloudiness (e.g., Frank, 1970; Martin and Suomi, 1972), has become traditional, and for the present we retain its usage.

Cloud clusters generally have lifetimes of a day or less (Martin, 1975; Martin and Schreiner, 1981) and are confined to a very low latitudes. Occasionally, however, a cluster evolves into a longer lived tropical storm or hurricane,[8] which can move out of the tropics into midlatitudes. Since large,

[7] The somewhat weaker cloud shields in the tropics are probably a result of the convection over tropical oceans being generally weaker than extratropical continental convection (see comments of Zipser and LeMone, 1980; Simpson and van Helvoirt, 1980; and Simpson *et al.*, 1982).

[8] According to the "Glossary of Meteorology" (Huschke, 1959, p. 593), a "hurricane" (in the Atlantic, Caribbean, and Gulf of Mexico) or "typhoon" (in the Pacific) is a cyclone that originates over tropical oceans and attains a maximum wind of 65 knots or higher. In extreme cases such storms attain maximum winds of 175 knots or more. In this paper, we use the term hurricane to include the typhoon and other local names for the same phenomenon.

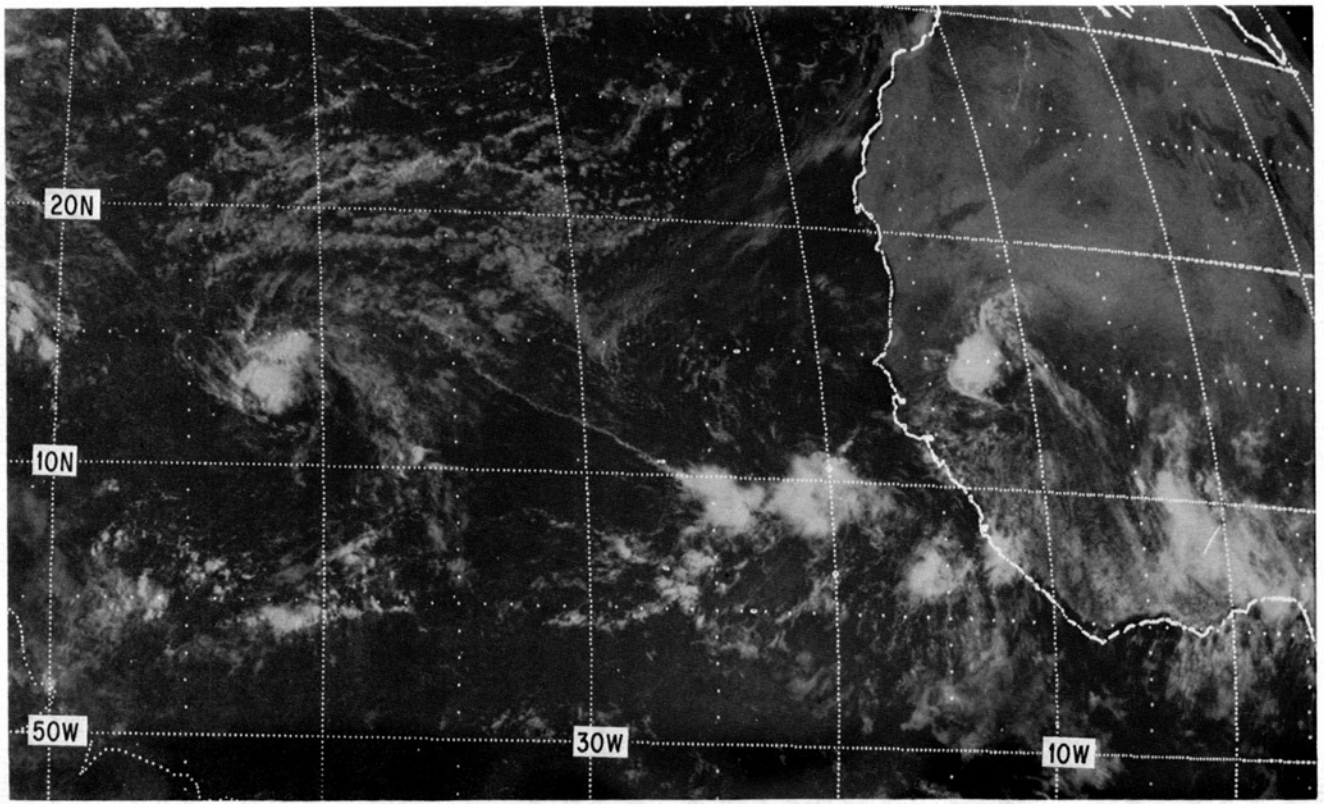

FIG. 37. Visible satellite photograph showing tropical clouds ranging in size from small cumulus to large cloud clusters. Cloud clusters are evident by the large cirrus shields at 17°N 42°W, 9°N 24°W, 9°N 21°W, 7°N 16°W, 8°N 12°W, 7°N 2°W, and 14°N 13°W. The last one mentioned was a squall cluster with a well-defined arc cloud line on its leading (southwest) side. Photograph from the SMS-1 satellite is for 1130 GMT, 5 September 1974.

precipitating cloud systems are the subject of the present article, we shall concentrate the remainder of our discussion on cloud clusters and hurricanes.

Knowledge of cloud clusters has expanded greatly during the past decade as an outcome of international field experiments conducted during the 1960s and 1970s. The most ambitious of these were the Global Atmospheric Research Program's Atlantic Tropical (GATE) and Monsoon (MONEX) experiments. GATE was carried out over the eastern tropical Atlantic in the summer of 1974, and MONEX was held over the South China Sea near Malaysia and Indonesia in the winter of 1978–1979 and in the regions of the Arabian Sea and Bay of Bengal in the summer of 1979. In addition to this work, the U.S. National Oceanic and Atmospheric Administration (NOAA) conducts ongoing research on hurricanes. Their studies involve both storm modeling and observations obtained by extensive aircraft penetration of hurricanes. In the last several years, the instrumentation on NOAA research aircraft has improved sufficiently to have produced a new generation of hurricane data that promises to revolutionize the understanding of these storms.

Characteristics of clouds observed in GATE have been reviewed in detail by Houze and Betts (1981). Cloud clusters have been further examined by Houze (1982). To avoid redundancy with these papers as much as possible, we shall concentrate here on GATE, MONEX, and hurricane studies that have been completed since 1980.

4.2. Types of Cloud Clusters

Two types of cloud clusters are generally recognized. Squall clusters are associated with tropical squall lines of the type identified by Hamilton and Archbold (1945) and Zipser (1969). They are notable in geosynchronous satellite imagery by their rapid propagation (15 m/sec), explosive growth, high brightness, and distinct convex leading edge (Martin, 1975; Aspliden *et al.*, 1976; Payne and McGarry, 1977; Martin and Schreiner, 1981). Nonsquall clusters travel more slowly than squall clusters (typically only a few meters per second) and do not possess the distinctive oval cirrus shield or arc-shaped leading edge of squall systems. A squall cluster is seen over Africa at lat 15° N, long 17° W in Fig. 37. The other clusters seen in the figure are nonsquall clusters. The importance of nonsquall clusters lies in their sheer number. They are the predominant type of cloud cluster in the tropics. The more dramatic squall clusters are relatively rare. However, the well-defined structure and motion they possess make them more amenable to study, and much attention has been devoted to squall clusters in the literature. Despite

differences in motion and appearance in satellite data, squall and nonsquall clusters exhibit strong similarities in other aspects of their structure—both to each other and to midlatitude convective complexes. Thus, much of the understanding gained in studies of both types of clusters is consequently applicable to a general understanding of mesoscale convective systems. In Sections 4.3 and 4.4 below, the structures of squall and nonsquall clusters are described in turn, and their similarities to each other and to midlatitude systems are pointed out in Section 4.5. Hurricanes are treated in Section 4.6.

4.3. Squall-Line Cloud Clusters

The tropical squall line (or "disturbance line") was first described as a distinct meteorological phenomenon by Hamilton and Archbold (1945). The first documentation of a tropical squall line observed during an organized field experiment was presented by Zipser (1969). More recent field experiments have revealed further details of these systems (Betts *et al.*, 1976; Zipser, 1977; Houze, 1977; Leary and Houze, 1979b; Fortune, 1980). Houze and Betts (1981) summarized knowledge accumulated from this past work. The squall line is found to be part of a propagating mesoscale disturbance, namely, the "squall-line cloud cluster" or simply the "squall cluster." As in the midlatitude squall system (Section 3.5, Fig. 35), the squall line is the leading portion of the disturbance and consists of cumulonimbus line elements (or cells), while an extensive, precipitating mid- to upper-level stratiform cloud shield, or "anvil cloud" (as defined by Brown, 1979), trails the squall line (Fig. 38).

The convective elements composing the squall line contain buoyant updrafts that carry air of high moist static energy from the boundary layer to the upper troposphere. As in the midlatitude squall line, the tropical squall line tends to travel by a combination of translation and discrete propagation, wherein new cells systematically form on the leading edge of the system. As the cells mature, they become the main cells of the squall line. Dissipating cells occur to the rear of the mature cells.

Although similar in spatial arrangement and propagation, the cells of the tropical squall line are typically weaker than those of midlatitude squall lines. The cells in the midlatitude case described in Fig. 34 appeared with a first echo well aloft, exhibited weak-echo regions in zones between the first echoes and mature cells, and contained peak reflectivities centered aloft. The cells in the tropical squall line, on the other hand, exhibit peak echo intensities at low levels as a result of their weaker updrafts (Caracena *et al.*, 1979; Zipser and LeMone, 1980; Szoke and Zipser, 1981; Cheng, 1981).

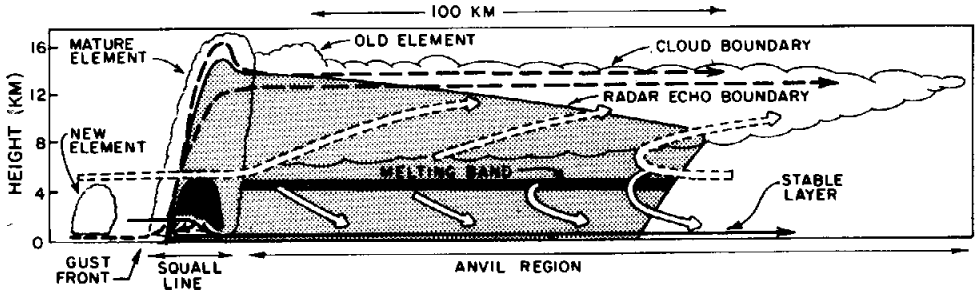

FIG. 38. Schematic of a typical cross section through a tropical squall system. Dashed streamlines show convective-scale updraft and downdraft motions associated with the mature squall-line element. Wide solid arrows show mesoscale downdraft circulation. Wide dashed arrows show mesoscale updraft circulation. Dark shading shows strong radar echo in the melting band and in the heavy precipitation zone of the mature squall-line element. Light shading shows weaker radar echoes. Scalloped line indicates visible cloud boundary. Adapted from Houze (1977).

Negatively buoyant downdrafts associated with the convective towers of the tropical squall line carry air of low moist static energy downward from the low to middle troposphere into the boundary layer. A portion of this convective downdraft air spreads forward and produces a gust front at the leading edge of the mesoscale system, similar to the gust front at the leading edge of the midlatitude squall system (Figs. 33, 35, and 36). Another portion of this convective downdraft air spreads rearward, leaving an extensive wake of cool, stable air in the boundary layer.

The trailing anvil region of the squall cluster, in contrast to the leading line of convective cells, has a predominantly stratiform structure. As noted in Fig. 38, the cloud and precipitation in this region tend to be horizontally uniform, with distinct vertical layering. Precipitation particles in the upper portions of the anvil cloud are initially in the form of ice particles, which grow as they drift downward until they melt in a shallow layer and then evaporate partially while falling as rain through unsaturated air below the base of the anvil. Most of the ice particles are probably generated in the tops of convective cells located along the leading squall line. These particles then move, in a relative sense, toward the rear of the system as a result of the continuing redefinition of the position of the leading edge of the system by the formation of new cells (as suggested by Houze, 1981). The airflow at anvil levels apparently aids in this process. Chen and Zipser (1982) have shown the existence of a midlevel jet of front-to-rear flow emanating from the cells just above the height of the melting level in a tropical squall system in a position somewhat similar to the jet shown by Houze and Smull (1982) and Zipser and Matejka (1982) to be spreading ice particles back into the

stratiform region of a midlatitude squall system (Fig. 35). The layer in which the ice particles melt after they are spread rearward into the anvil region appears on radar as a bright band of the type normally associated with stratiform precipitation. The bright-band region behind tropical squall lines appears to be wider than that behind midlatitude squall lines. Bright-band regions behind tropical squall lines can be 200 km across (Houze, 1977; Rappaport, 1982), while those behind midlatitude squall lines appear to be ~100 km in most cases. The reason for this difference is not yet understood.

The vertical air motions in the trailing anvil region of the squall cluster are widespread, generally nonconvective, and on the order of tens of centimeters per second. Downward motion occurs below the base of the anvil, while rising motion occurs within the anvil cloud itself (Fig. 38). Widespread subsidence below the anvil was first shown to exist from observed penetration of low moist static energy to low levels throughout the anvil region (Zipser, 1969). Its magnitude was determined from observed low-level divergence (Zipser, 1977), and Brown (1979) successfully simulated the downdraft below the anvil in a mesoscale model.

The existence of the mesoscale updraft in the tropical squall-line anvil has been more difficult to establish firmly, although its existence has been indicated indirectly by a variety of evidence (see discussion by Houze and Betts, 1981). Recently, however, Gamache and Houze (1982) have demonstrated the existence of the mesoscale updraft and computed its magnitude by using time-to-space conversion to group wind soundings in relation to the radar echo pattern of a squall line observed in GATE. The ability of the radar to identify the horizontally uniform precipitation falling from the anvil and distinguish it from the intense vertical cells that characterize the squall line made it possible to locate wind observations with respect to the squall-line (i.e., convective) and anvil (i.e., stratiform) regions separately. From the wind pattern in the radar-delineated anvil area, the vertical profiles of divergence within and below the anvil were obtained, and from these profiles the vertical velocities in the mesoscale anvil updrafts and downdrafts were determined (solid curve in Fig. 39). The mesoscale updraft above the base of the anvil cloud (~650 mbar) and the downdraft below are both clearly shown. The vertical velocity profile determined from the winds in the squall-line region is also shown (dashed cuve in Fig. 39a). It was the result of convective updrafts and downdrafts as shown in Fig. 39b. The squall-line region was characterized by boundary-layer convergence feeding the deep convective updrafts. The convective downdrafts spreading out in the boundary layer intensified the low-level convergence feeding the convective updrafts. The circulation in the anvil region, on the other hand, was characterized by midlevel convergence supporting both the mesoscale updraft within the anvil cloud and the mesoscale downdraft below. This

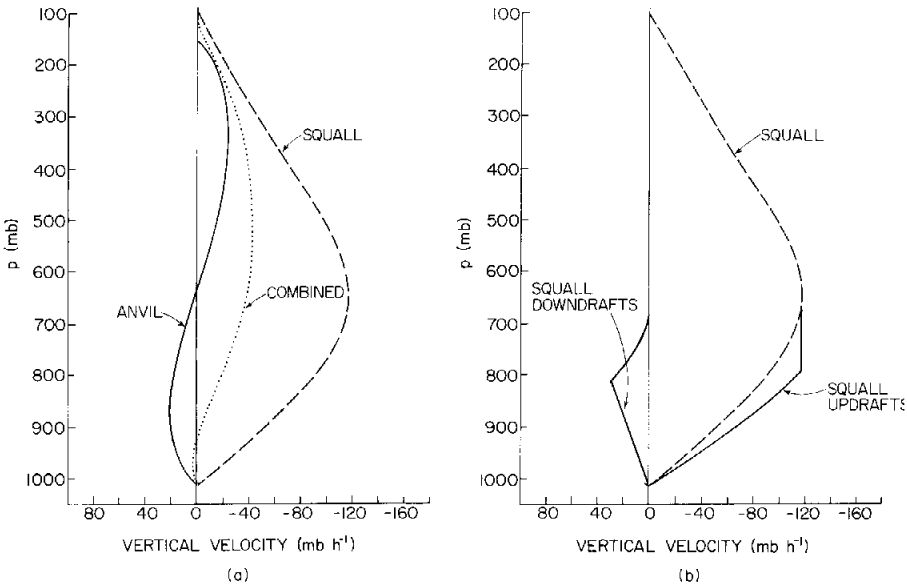

FIG. 39. Average vertical velocity ω for: (a) the squall-line (dashed), anvil (solid), and combined (dotted) regions of a tropical squall cluster; (b) the squall-line updrafts and downdrafts (dotted). From Gamache and Houze (1982).

midlevel convergence is probably akin to that associated with midlatitude MCCs (Section 3.4). However, the mesoscale divergence and vertical velocity pattern determined for the MCCs was not decomposed into separate convective and stratiform components and is therefore probably a mixture of convective and stratiform motion (as is the combined squall-line plus anvil region curve shown for the tropical system by the dotted line in Fig. 39a). Further work using radar observations to delineate the stratiform and convective components of the midlatitude MCCs might shed light on the dynamics of the midlatitude complexes and their similarities to tropical systems.

4.4. Nonsquall Cloud Clusters

Beneath the large cirrus shield that identifies a cloud cluster in a satellite picture, there is typically found one or more mesoscale rain areas, each attaining a maximum horizontal dimension $\sim$100–500 km. Leary and Houze (1979a) extended the conceptual model of a tropical squall-line system (Fig. 38) to describe the structure and behavior of these rain areas. They

arrived at the more general concept of a "mesoscale precipitation feature" (MPF), of which the rain area of a squall cluster is an example, but which also applies to the rain areas of nonsquall clusters. This model has been elaborated on by Zipser (1980), Houze and Betts (1981), and Houze (1982).

Squall clusters and some nonsquall clusters contain just one MPF, while other clusters contain several MPFs interconnected by a common mid- to upper-level cloud shield. Intersections and mergers of the MPFs can add complexity to the precipitation pattern of the cluster. However, Leary and Houze (1979a) found that when the individual MPFs making up the pattern are identified and followed closely in time, they each exhibit a life cycle similar to that of a squall-line MPF.

To illustrate this life cycle, we use as an example nonsquall clusters that were observed over the South China Sea during winter MONEX (Houze *et al.*, 1981a; Johnson and Priegnitz, 1981; Johnson, 1982; Churchill, 1982). These clusters formed diurnally off the northern coast of Borneo and typically contained one MPF (Fig. 40), which progressed through the stages of the life cycle identified by Leary and Houze (1979a).

The *formative stage* of an MPF is initiated with an imposed mesoscale convergence at low levels (Zipser, 1980). This convergence may be associated with a downdraft outflow boundary from a previous cloud cluster (e.g., Houze, 1977; Fortune, 1980), a confluence line in a larger scale flow (e.g., Zipser and Gautier, 1978), or some other feature that intensifies convergence locally. The winter monsoon clusters used as an example here are triggered by the convergence of the nocturnal land breeze from Borneo with the large-scale northeasterly monsoon flow over the South China Sea (Fig. 40a). The triggering of convection by low-level convergence is followed by the growth of several discrete cumulonimbus elements, which may be randomly distributed in a group or arranged in a line. This initial spatial arrangement probably depends on the form of the initiating convergence.

The *intensifying stage* of the MPF is not shown explicitly in Fig. 40. It corresponds to the period of transition between Figs. 40a and b. During this stage, older convective elements grow and merge while newer elements continue to form. Gradually, this process leads to a large continuous rain area composed of convective cells interconnected by stratiform precipitation of moderate intensity falling from a spreading mid- to upper-level stratiform cloud shield.

The *mature stage* of the MPF is reached when the stratiform precipitation between cells becomes quite extensive, covering areas 100–200 km in horizontal dimension (region between cells in Fig. 40b). This stratiform precipitation resembles that associated with the anvil clouds of squall clusters. Associated with the stratiform precipitation region of a nonsquall MPF, moreover, are a mesoscale downdraft below the melting level and a me-

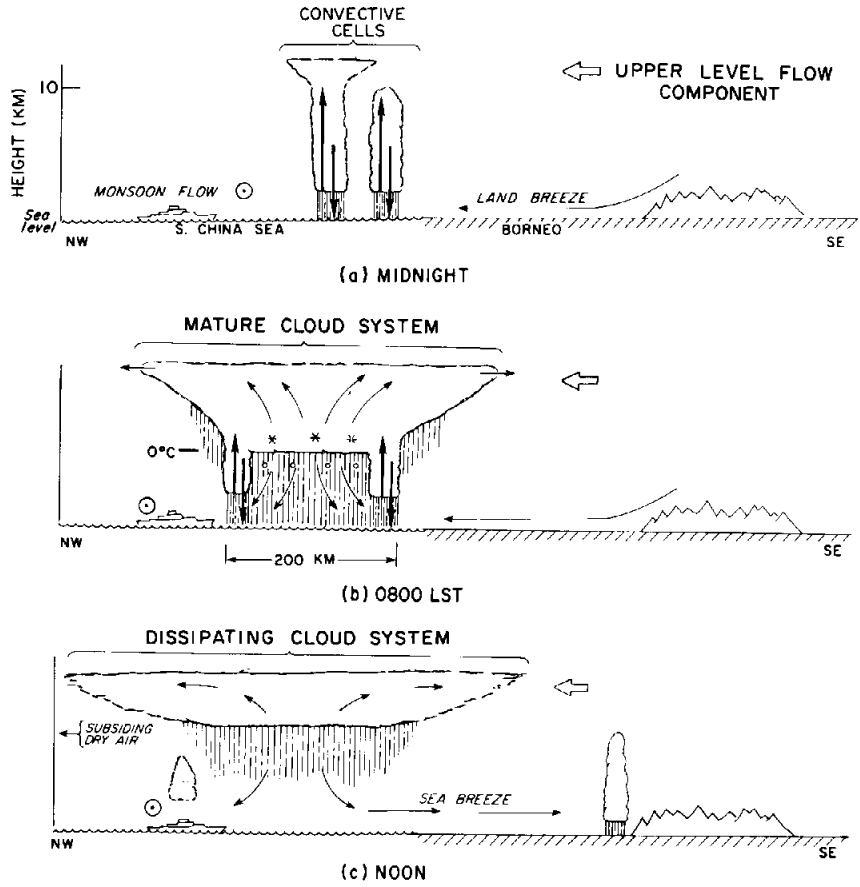

FIG. 40. Schematic of the development of diurnally generated nonsquall cloud cluster off the coast of Borneo. Various arrows indicate airflow. Circumscribed dot indicates northeasterly monsoon flow out of page. Wide open arrow indicates the component of the typical east-southeasterly upper-level flow in the plane of the cross section. Heavy vertical arrows in (a) and (b) indicate cumulus-scale updrafts and downdrafts. Thin arrows in (b) and (c) show a mesoscale updraft developing in a mid- to upper-level stratiform cloud with a mesoscale downdraft in the rain below the middle-level base of the stratiform cloud. Asterisks and small circles indicate ice above the 0°C level melting to form raindrops just below this level. From Houze *et al.* (1981a).

soscale updraft above, similar to those of squall-line anvils. For evidence of these mesoscale motions in the stratiform regions of nonsquall clusters, see Zipser and Gautier (1978), Leary and Houze (1979a), Zipser *et al.* (1981), Houze and Betts (1981), Johnson and Priegnitz (1981), Johnson (1982), and Churchill (1982).

In the *dissipating stage* of a cluster's MPF, the formation of new convective cells diminishes. However, the feature can persist for several hours as a region of mostly mid- to upper-level cloud, with continuing light precipitation or virga (Fig. 40c).

4.5. Generalized Cloud Cluster Structure

The ability of the Leary–Houze conceptual model to describe the evolution of both squall and nonsquall mesoscale precipitation features is supported by studies of the development of precipitation in both types of clusters (Fig. 41). In each case, the rainfall is dominated in the formative stage of the MPF by convective cells. However, as the upper cloud shield develops (during the intensifying stage) the stratiform precipitation begins to account for a large proportion of the total precipitation from the MPF. By the mature stage, the stratiform component can equal or surpass the convective component. The stratiform component continues to be strong into the dissipating stage, although both the convective and stratiform components gradually weaken. In the squall case shown in Fig. 41a, the integrated stratiform component accounted for 40% of the total rain, whereas in the nonsquall cases in Fig. 41b,c the stratiform rain accounted for 30% and 50% of the totals, respectively. Similar results have been obtained for other squall clusters by Gamache and Houze (1981) and Rappaport (1982). They found stratiform totals of 57% and 42%, respectively. Zipser *et al.* (1981) found essentially similar results for a nonsquall cluster.

The quantitative similarity of the squall and nonsquall precipitation curves, together with the descriptive similarities of squall and nonsquall MPFs noted by Leary and Houze (1979a), allows certain generalizations to be made about the mesoscale structure of tropical cloud clusters. To the extent that midlatitude MCCs are similar to tropical cloud clusters, these generalizations also apply to those systems as well.

Consider a cluster containing a single MPF in its mature stage. Whether a squall cluster (Fig. 38) or a nonsquall cluster (Fig. 40b), the MPF consists partly of convective cells and partly of stratiform precipitation falling from a mid- to upper-level cloud shield. The mature midlatitude squall system (Fig. 35) also exhibits this structure, and it is likely that nonsquall midlatitude MCCs do also. However, this latter possibility awaits confirmation by detailed radar studies to distinguish the convective and stratiform components of midlatitude MCCs.

From the observed structures of mature MPFs in tropical cloud clusters, Houze (1982) has computed the net sensible heating in a large-scale area (2×10^5 km^2) containing an idealized cluster (Fig. 42). The heating associated with the convective cells is dominated by the latent-heat release in

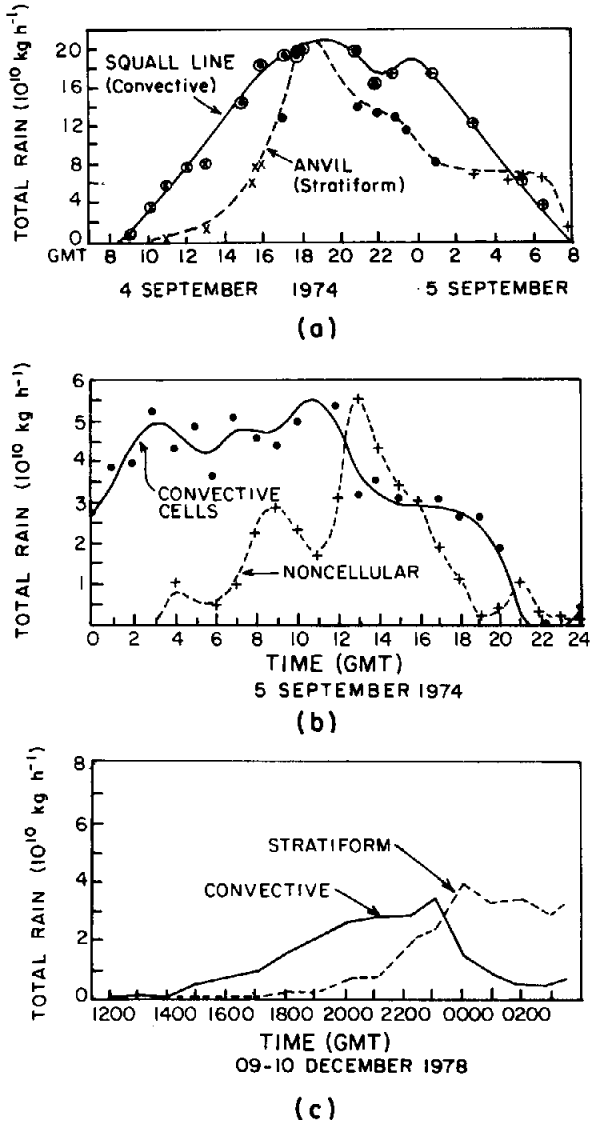

FIG. 41. Time variation of total rain integrated over areas covered by the convective and nonconvective regions of (a) a squall cluster and (b) and (c) two nonsquall clusters. The squall-line case is from Houze (1977). The nonsquall cases are from Leary (1981) and Churchill (1982).

the deep convective updrafts. This convective heating is distributed through the full depth of the troposphere (dashed curve in Fig. 42). To this heating is added the heating and cooling associated with the stratiform regions of

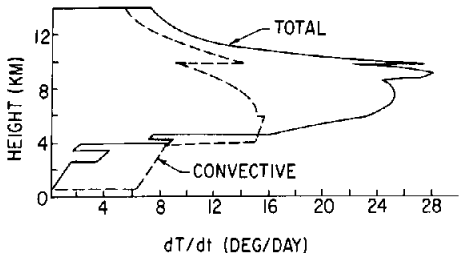

FIG. 42. Total heating of large-scale region (2×10^5 km^2 in area) by a mature cloud cluster (solid curve). The total heating by the convective towers in the cluster (dashed curve) is shown for comparison. From Houze (1982).

the cluster. Latent heat released by condensation in the mesoscale updraft in the mid- to upper-tropospheric cloud shield (e.g., Fig. 40b) together with net radiative absorption in the cloud shield (daytime conditions were assumed) increases the total heating aloft (upper part of solid curve in Fig. 42). Cooling associated with melting and evaporation in the mesoscale downdraft region of the stratiform precipitation area (e.g., Fig. 40b) decreased the total heating in the lower troposphere (lower part of solid curve in Fig. 42).

From these calculations, it is apparent that in considering the effects of mesoscale convective systems on their environments, the structure of the mesoscale stratiform clouds and precipitation that develop in association with these systems must be considered. Moreover, when they are considered, results such as those indicated by the solid curve in Fig. 42 are obtained, indicating that the net effect of a mature cluster (or MCC) on its environment should be felt most strongly in the mid to upper troposphere, where the convective, stratiform and radiative processes reinforce to produce strong heating. Large-scale vertical velocity profiles (Houze, 1982) and horizontal wind fields (Esbensen *et al.*, 1982) in the vicinities of GATE cloud clusters conform to this expectation. Strong responses also have been noted in the upper-level wind fields around mature midlatitude MCCs (Nimomiya, 1971a,b; Maddox, 1980a, 1981; Fritsch and Maddox, 1981a; Maddox *et al.*, 1981; cf. Section 3.4).

In generalizing about the structure of cloud clusters and midlatitude MCCs, we have emphasized the development of mesoscale stratiform structures, which accompany the development of deep convection in these systems. While making these generalizations, we must, at the same time, recognize and try to understand the fundamental *differences* between squall and nonsquall systems and tropical and midlatitude systems. For example, why do squall systems propagate while nonsquall systems do not? For some discussion of this problem, see Houze and Betts (1981). Such differences

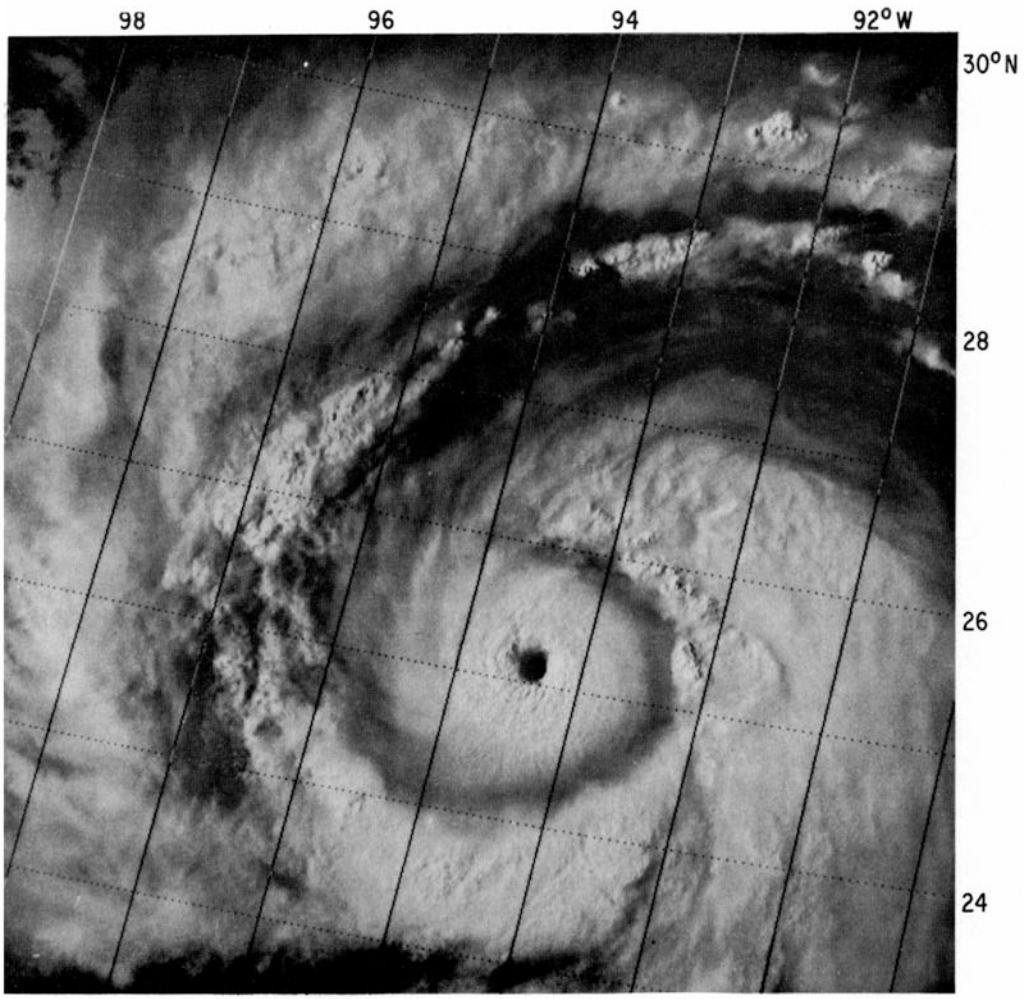

FIG. 43. Visible satellite image of Hurricane Allen, 2123 GMT, 8 August 1980. Photograph provided by the National Hurricane Research Laboratory.

appear to be more than incidental. For example, Zipser (1971) has pointed out that tropical squall-line clusters may be relatively ineffective at influencing large-scale development, whereas nonsquall clusters tend to produce positive feedbacks. His speculation, moreover, appears to be borne out by mesoscale hurricane modeling results (Rosenthal, 1980). Clearly, much work lies ahead to sort out the various similarities and differences among these mesoscale systems and their effects on larger scales of motion.

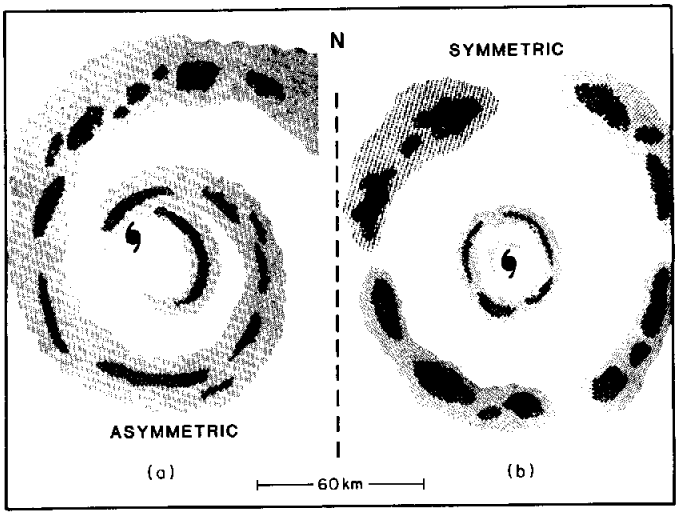

FIG. 45. Schematic horizontal radar echo pattern in asymmetric and symmetric hurricanes. Shading thresholds are for echo intensities of 30 and 40 dBZ. Hurricane symbol is located at the center of the wind circulation. Symmetric storm is patterned after hurricanes Anita (1977), David (1979), and Allen (1980). Asymmetric storm is patterned after hurricanes Frederick (1979), Floyd (1981), Gert (1981), and Irene (1981). From Jorgensen (1982a).

4.6. Hurricanes

A small fraction of tropical cloud clusters are associated with disturbances that develop into hurricanes (Frank, 1970). When hurricane development occurs, upper-level winds take on a high degree of anticyclonic rotation, and the upper cloud shield of the initial cluster becomes circular. In well-defined storms, a clear spot or "eye" is found near the center of the cloud shield (e.g., Fig. 43). The precipitation falling from the hurricane cloud shield is generally concentrated in a mesoscale "eyewall rainband," which surrounds the eye of the storm, and in several mesoscale "outer rainbands." Examples of rainbands in several mature hurricanes are shown in Fig. 44. Lighter precipitation occurs throughout much of the area between rainbands. Early papers on rainbands in hurricanes include Maynard (1945), Wexler (1947), Kessler and Atlas (1956), Senn and Hiser (1959), Atlas *et al.* (1963), Fujita *et al.* (1967), and Gentry *et al.* (1970).

FIG. 44. Radar reflectivity patterns showing structure of precipitation in four mature hurricanes. Data obtained with radars aboard National Oceanic and Atmospheric Administration research aircraft on (a) 12 September 1979 in Hurricane Frederick, (b) 30 August 1979 in Hurricane David, (c) 5 August 1980 in Hurricane Allen, and (d) 8 August 1980 in Hurricane Allen. Photographs provided by the National Research Laboratory.

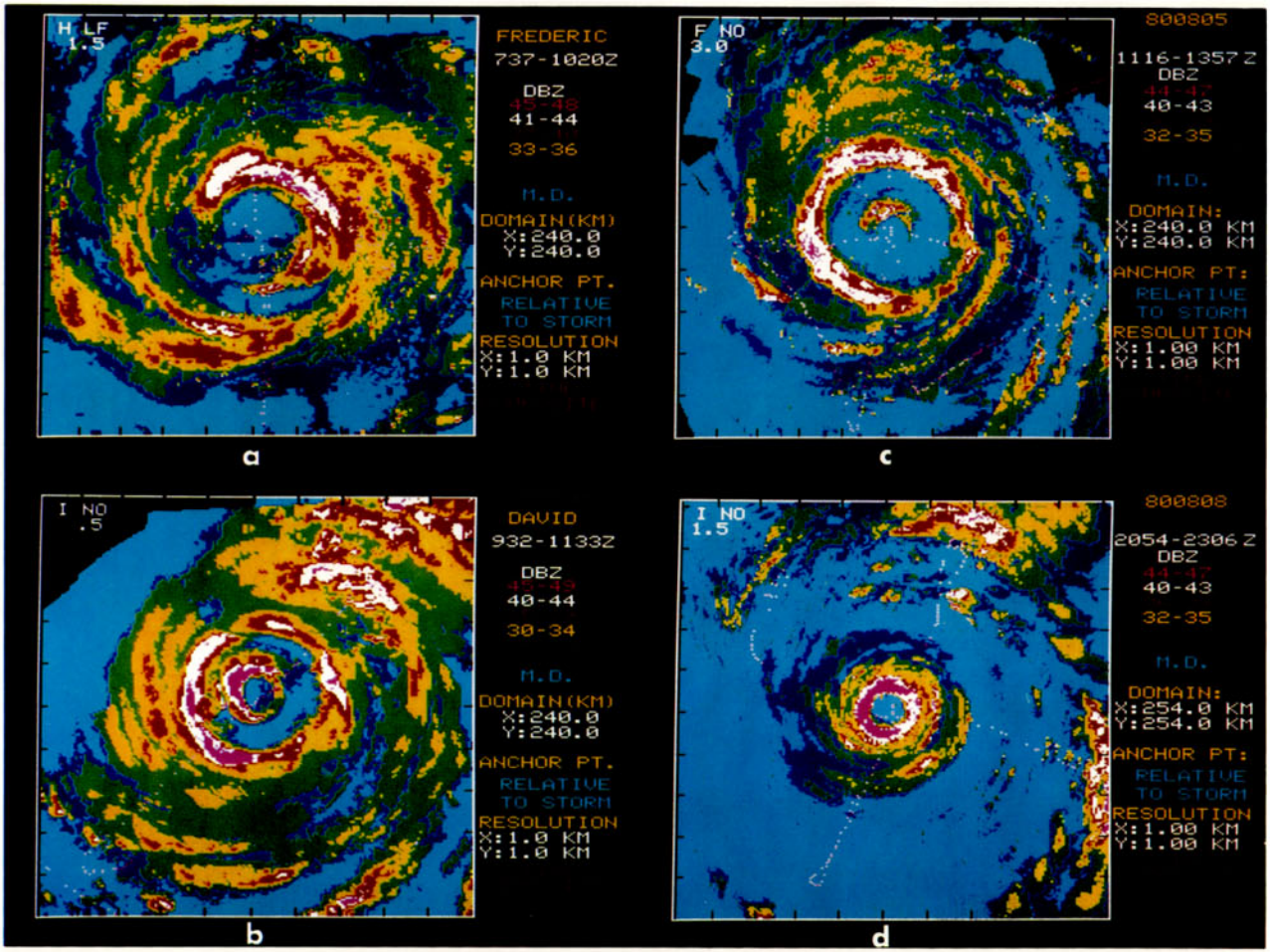
H LF
1.5
FREDERIC
737-1020Z
DBZ
41-44
33-36
M.D.
DOMAIN(KM)
X:240.0
Y:240.0
ANCHOR PT.
RELATIVE
TO STORM
RESOLUTION
X:1.0 KM
Y:1.0 KM
a
F NO
3.0
800805
1116-1357Z
DBZ
40-43
32-35
M.D.
DOMAIN:
X:240.0 KM
Y:240.0 KM
ANCHOR PT:
RELATIVE
TO STORM
RESOLUTION
X:1.00 KM
Y:1.00 KM
c
I NO
.5
DAVID
932-1133Z
DBZ
40-44
30-34
M.D.
DOMAIN(KM)
X:240.0
Y:240.0
ANCHOR PT.
RELATIVE
TO STORM
RESOLUTION
X:1.0 KM
Y:1.0 KM
b
I NO
1.5
800808
2054-2306Z
DBZ
40-43
32-35
M.D.
DOMAIN:
X:254.0 KM
Y:254.0 KM
ANCHOR PT:
RELATIVE
TO STORM
RESOLUTION
X:1.00 KM
Y:1.00 KM
d

That deep convection is important to the development of the hurricane through cooperative interaction between the convection and larger scale flow is well known from the classic work of Ooyama (1964) and Charney and Eliassen (1964).[9] Accordingly, the precipitation in the rainbands exhibits a high degree of convective character. However, the precipitation can also be partly stratiform, with well-defined melting layers (as evidenced by radar bright bands) occurring over considerable portions of the storm (Atlas *et al.*, 1963; Black *et al.*, 1972; Hawkins and Imbembo, 1976). The latter two studies did not indicate specifically whether the observed bright bands were within rainbands or in the regions of lighter rain between bands. The observations of Atlas *et al.* (1963), however, were obtained in outer rainbands. These bands were composed of convective cells at one end, with their remaining portions being stratiform. The presence of mesoscale rainbands, partly stratiform in character, suggests similarity between hurricane precipitation processes and those of cloud clusters (Sections 4.1–4.5).

Current study of hurricanes is being directed toward better understanding of both the eyewall and outer rainbands, particularly regarding their convective versus stratiform structure, their similarities to cloud-cluster precipitation features, and their dynamics. Radar observations indicate two apparent modes of rainband organization (Jorgensen, 1982a,b). "Symmetric" hurricanes (Fig. 45b) are characterized by a closed circular eyewall rainband. The center of the wind circulation is located in the center of the circle defined by the eyewall rainband, while the outer rainbands take on various forms (convective, stratiform, spiral, concentric). "Asymmetric" hurricanes (Fig. 45a) have an eyewall rainband that is not closed. Outer rainbands in these storms tend to be more spiral than concentric, and the center of the wind circulation is not coincident with the geometric center of curvature of the eyewall but is displaced toward the eyewall. An example of asymmetric hurricane structure is shown in Fig. 44a, while symmetric structures may be seen in Fig. 44b–d.

The eyewall rainband in a symmetric storm is often observed to contract; that is, it propagates toward the center of the storm and thus shrinks (Marks, 1981; Willoughby *et al.*, 1982). As the eyewall rainband contracts, the central pressure of the storm lowers. After 1–2 days, the radius of the eyewall band reaches its minimum size, and as the band disappears, it is replaced by a new eyewall rainband at a radius of about 50–150 km and the central pressure of the storm rises (note the old eyewall band near the storm center and the new one farther out shown schematically in Fig. 45b and by actual examples in Fig. 45b,c). The life cycle of the eyewall band is then repeated. Thus, a symmetric storm is often characterized by a succession of shrinking eyewall rainbands and a pulsating central pressure.

[9] For a comprehensive review of hurricane dynamics, see Anthes (1974, 1982).

A theoretical explanation for the propagation of the symmetric eyewall rainbands inward has been suggested by Shapiro and Willoughby (1982). In earlier work, Shea and Gray (1973) showed that the maximum vertical motion (and hence the maximum cloud and precipitation development) associated with eyewalls is consistently located close to the radius of maximum wind. The rising motion in the eyewall region is associated with the convergence at low levels of radial inflow and outwardly directed components of supergradient flow within the eye. Shapiro and Willoughby explain the inward propagation of this eyewall structure in symmetric storms as a secondary-circulation response to a point source of heat placed near the radius of maximum wind in a hurricane-like vortex. In that idealized situation, temporal increases in tangential wind are greatest just inside the radius of maximum wind. This effect leads to contraction of the zone of maximum wind as the vortex intensifies. Willoughby *et al.* (1982) find observational support for this theory in data from recent hurricane flights. The eyewall rainbands of asymmetric storms do not appear to shrink and undergo the life cycle exhibited by the symmetric eyewall rainbands. A satisfactory explanation for this difference between symmetric and asymmetric storms has not yet been obtained.

Jorgensen (1981, 1982a,b) has compiled radar, wind, thermodynamic, and cloud-physics measurements from flights through eyewall and outer rainbands. A schematic cross section through the eyewall region of a symmetric storm (Fig. 46) summarizes his findings. Air flowing radially inward

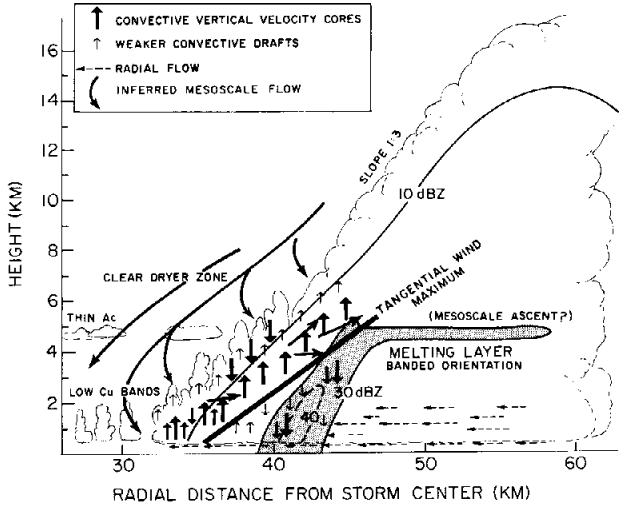

FIG. 46. Schematic vertical cross section through north-northwestern section of hurricane Allen (1980). See. Figs. 42 and 43c for horizontal views. From Jorgensen (1982b).

meets radial outflow from the eye (between 30 and 35 km radius) and rises along an outward-sloping mean streamline pattern. Superimposed on the mean upslope motion are intense convective updraft cores. The sloping tangential wind maximum also shown is accounted for by conservation of absolute angular momentum of the low-level inflow, which turns upward in the eyewall convergent zone. Fallout of precipitation initiated in the upward flow above the tangential wind maximum accounts for the sloping radar echo core below the wind maximum. Convective downdraft cores occur in the core of heavy rain. The maximum echo intensity occurs at low levels, as in the convective echoes of tropical cloud clusters (Houze, 1977; Leary and Houze, 1979a; Caracena *et al.*, 1979; Zipser and LeMone, 1980; Szoke and Zipser, 1981; Cheng, 1981). A region of stratiform precipitation characterized by a well-defined melting layer occurs adjacent to and just outside the convective eyewall zone. Similarities in the patterns of circulation, cloud and precipitation in Fig. 46 to those of the squall-line cloud cluster (Fig. 38) and the midlatitude squall system (Fig. 35) are striking. Jorgensen (1981, 1982a,b) finds the structure depicted in Fig. 46 to be characteristic of the eyewall rainbands of both symmetric and asymmetric storms. Less is known about outer rainbands. Jorgensen (1982a,b) finds that some outer bands resemble eyewall rainbands. However, a variety of structures occur: some are purely stratiform, others convective; whereas some, such as those reported by Atlas *et al.* (1963) are a mixture of convective and stratiform structure.

5. Conclusions

In this article, we have surveyed the major types of cloud systems that contribute to precipitation over the earth. A common attribute of these systems is their tendency to become organized on the mesoscale. In extratropical cyclones, this organization is manifested in mesoscale rainbands. In deep convective cloud systems, mesoscale organization is apparent in the tendency for cumulonimbus elements to occur in groups, which in turn drive mesoscale circulations, with which are associated mid- to upper-level cloud shields, stratiform precipitation, melting layers, mesohighs and -lows, gust fronts, and arc lines. Mesoscale systems driven by deep convection include midlatitude mesoscale convective complexes and squall lines, tropical squall and nonsquall cloud clusters, and hurricane rainbands.

In the case of frontal rainbands, progress has been made in classifying the various types of bands that occur and in documenting their basic air motions and cloud microphysical processes. In the case of deep convective phenomena, progress has been made in understanding the basic modes of cumulonimbus structure and dynamics, particularly in the identification of

the splitting mechanism and subsequent development of rotation that occurs in the evolution of supercell thunderstorms, and in describing the evolution of groups of deep convective thunderstorms into mesoscale systems. In these descriptions, intriguing similarities are seen among midlatitude and tropical systems—compare, for example, the midlatitude squall-line system (Fig. 35), the tropical squall cluster (Fig. 38), and the hurricane eyewall rainband (Fig. 46).

Further progress can be made in nearly all aspects of the mesoscale organization of frontal and deep convective cloud systems. Certain outstanding problems, however, seem to be particularly wanting, and in closing we take special note of these.

The question of the origin of frontal rainbands remains unresolved. That is, the basic reasons for precipitation to become enhanced in mesoscale bands have not yet been identified. As was pointed out in Section 2, several dynamical instability mechanisms can act on the scale of the rainbands; however, the association of specific instabilities with specific types of rainbands has not been satisfactorily accomplished.

In the case of mesoscale systems associated with deep convection, problems remain in comparing midlatitude and tropical systems. In the tropics, radar observations have been used to distinguish between convective and stratiform regions of mesoscale systems, and as a result the deep convective and mesoscale stratiform components of the air motions in these systems have been identified. Similar radar work with midlatitude mesoscale convective complexes and squall lines should be carried out to improve the understanding of the midlatitude systems and make possible their comparison with tropical systems. For both the tropical and midlatitude mesoscale convective systems, a better understanding of their life cycles should be sought. Mesoscale models, such as those of Brown (1974, 1979), Kreitzberg and Perkey (1977), Fritsch and Chappell (1980), and Fritsch and Maddox (1981b), together with the presently available descriptive studies, give glimpses of understanding; but further work, both observational and theoretical, is needed to understand fully the chain of events involved in the development of the mesoscale mid- to upper-level cloud and stratiform precipitation that accompanies deep mesoscale convective systems in their mature stages.

We look forward to intensive research on mesoscale cloud systems in upcoming years. Better understanding of the mesoscale phenomena we have described in this article will contribute to the basic understanding of precipitation processes in the atmosphere, and will have benefits to society ranging from improved detailed weather forecasting to better general-circulation models and improved management of water resources on local, regional, and global scales.

ACKNOWLEDGMENTS

The authors' studies in this subject are supported by the National Science Foundation under grants ATM-8017327 and ATM-8009203 and by the National Oceanic and Atmospheric Administration under grant NA80RAD00025. Helpful comments of J. C. Fankhauser, B. F. Smull, and E. J. Zipser greatly enhanced the quality of Sections 3 and 4. This article is Contribution No. 627, Department of Atmospheric Sciences, University of Washington.

REFERENCES

Abercromby. R. (1887). "Weather." Appleton, London.

Agee, E. M., Church, C. R., Morris, C., and Snow, J. T. (1975). Some synoptic aspects and dynamic features of vortices associated with the tornado outbreak of 3 April 1974. *Mon. Weather Rev.* **103,** 318–333.

Agee, E. M., Snow, J. T., and Clare, P. R. (1976). Multiple vortex features in the tornado cyclone and the occurrence of tornado families. *Mon. Weather Rev.* **104,** 552–563.

Agee, E. M., Nickerson, F. S., Clare, P. R., Church, C. R., and Schaal, I. A. (1977). An observational study of the West Lafayette, Indiana, tornado of 20 March 1976. *Mon. Weather Rev.* **105,** 893–907.

Anthes, R. A. (1974). The dynamics and energetics of mature tropical cyclones. *Rev. Geophys. Space Phys.* **12,** 495–522.

Anthes, R. A. (1982). Tropical cyclones: Their evolution, structure and effects. *Meteorol. Monogr.* **19,** No. 41.

Atlas, D., Hardy, K. R., Wexler, R., and Boucher, R. J. (1963). On the origin of hurricane spiral bands. *Geofis. Int.* **3,** 123–132.

Aspliden, C. I., Tourre, Y., and Sabine, J. C. (1976). Some climatological aspects of West African disturbance lines during GATE. *Mon. Weather Rev.* **104,** 1029–1035.

Austin, P. M., and Houze, R. A., Jr. (1972). Analysis of the structure of precipitation patterns in New England. *J. Appl. Meteorol.* **11,** 926–935.

Bader, M. J., and Roach, W. T. (1977). Orographic rainfall in warm sectors of depressions. *Q. J. R. Meteorol. Soc.* **103,** 269–280.

Barge, B. L., Bergwall, F., and Goyer, G. G. (1976). "Fine Scale Structure of Convective Storms—Implications for Cloud Seeding in Alberta," Atmos. Sci. Rep. 76-3. Alberta Research Council, Edmonton, Alberta, Canada.

Barnes, S. L. (1970). Some aspects of a severe, right-moving thunderstorm deduced from mesonetwork rawinsonde observations. *J. Atmos. Sci.* **27,** 634–648.

Bates, F. C. (1968). A theory and model of the tornado. *Proc. Int. Conf. Cloud Phys. 1968* pp. 559–563.

Battan, L. J. (1975). Doppler radar observations of a hailstorm. *J. Appl. Meteorol.* **14,** 98–108.

Battan, L. J. (1980). Observations of two Colorado thunderstorms by means of a zenith-pointing Doppler radar. *J. Appl. Meteorol.* **17,** 580–592.

Benjamin, T. B. (1968). Gravity currents and related phenomena. *J. Fluid Mech.* **32,** 209–248.

Bennetts, D. A., and Hoskins, B. J. (1979). Conditional symmetric instability—a possible explanation for frontal rainbands. *Q. J. R. Meteorol. Soc.* **105,** 945–962.

Bergeron, T. (1935). On the physics of cloud and precipitation. *Proc. Assembly, Int. Union Geodesy Geophys., 5th, 1933* Vol. 2, pp. 156–161.

Betts, A. K., Grover, R. W., and Moncrieff, M. W. (1976). Structure and motion of tropical squall lines over Venezuela. *Q. J. R. Meteorol. Soc.* **102,** 395–404.

Black, P. G., Senn, H. V., and Courtright, C. L. (1972). Airborne radar observations of eye

configuration changes, bright band distribution, and precipitation tilt during the 1969 multiple seeding experiments in Hurricane Debbie. *Mon. Weather Rev.* **100,** 208–217.

Blechman, J. B. (1981). Vortex generation in a numerical thunderstorm model. *Mon. Weather Rev.* **109,** 1061–1071.

Bluestein, H. B., and Sohl, C. J. (1979). Some observations of a splitting severe thunderstorm. *Mon. Weather Rev.* **107,** 861–873.

Bosart, L. F., and Sanders, F. (1981). The Johnstown flood of July 1977: A long-lived convective system. *J. Atmos. Sci.* **38,** 1616–1642.

Boucher, R. J. (1959). Synoptic-physical implications of 1.25 cm vertical beam radar echoes. *J. Meteorol.* **16,** 312–326.

Brandes, E. A. (1978). Mesocyclone evolution and tornadogenesis: Some observations. *Mon. Weather Rev.* **106,** 995–1011.

Brandes, E. A. (1981). Finestructure of the Del City–Edmond tornadic mesocirculation. *Mon. Weather Rev.* **109,** 635–647.

Brooks, H. B. (1946). A summary of some radar thunderstorm observations. *Bull. Am. Meteorol. Soc.* **27,** 557–563.

Brown, J. M. (1974). Mesoscale motions induced by cumulus convection: A numerical study. Ph.D. Thesis, Massachusetts Institute of Technology, Cambridge.

Brown, J. M. (1979). Mesoscale unsaturated downdrafts driven by rainfall evaporation: A numerical study. *J. Atmos. Sci.* **36,** 313–338.

Brown, R. A., Lemon, L. R., and Burgess, D. A. (1978). Tornado detection by pulsed Doppler radar. *Mon. Weather Rev.* **106,** 29–38.

Browning, K. A. (1962). Cellular structure of convective storms. *Meteorol. Mag.* **91,** 341–350.

Browning, K. A. (1964). Airflow and precipitation trajectories with severe storms which travel to the right of the winds. *J. Atmos. Sci.* **21,** 634–639.

Browning, K. A., and Foote, G. B. (1976). Airflow and hail growth in supercell storms and some implications for hail suppression. *Q. J. R. Meteorol. Soc.* **102,** 499–533.

Browning, K. A., and Harrold, T. W. (1969). Air motion and precipitation growth in a wave depression. *Q. J. R. Meteorol. Soc.* **95,** 288–309.

Browning, K. A., and Harrold, T. W. (1970). Air motion and precipitation growth at a cold front. *Q. J. R. Meteorol. Soc.* **96,** 369–389.

Browning, K. A., and Pardoe, C. W. (1973). Structure of low-level jet streams ahead of mid-latitude cold fronts. *Q. J. R. Meteorol. Soc.* **99,** 619–668.

Browning, K. A., Hardman, M. E., Harrold, T. W., and Pardoe, C. W. (1973). The structure of rainbands within a mid-latitude depression. *Q. J. R. Meteorol. Soc.* **99,** 215–231.

Browning, K. A., Hill, F. F., and Pardoe, C. W. (1974). Structure and mechanism of precipitation and effect of orography in a wintertime warm-sector. *Q. J. R. Meteorol. Soc.* **100,** 309–330.

Browning, K. A., Fankhauser, J. C., Chalon, F. P., Eccles, P. J., Strauch, R. C., Merrem, F. H., Musil, D. J., May, E. L., and Sand, W. R. (1976). Structure of an evolving hailstorm. Part V. Synthesis and implications for hail growth and hail suppression. *Mon. Weather Rev.* **104,** 603–610.

Burgess, D. W. (1976). Single Doppler radar vortex recognition. Part I. Mesocyclone signatures. *Prepr., Conf. Radar Meteorol., 17th, 1976* pp. 97–103.

Burgess, D. W. (1981). Evidence for anticyclonic rotation in left-moving thunderstorms. *Prepr., Conf. Radar Meteorol., 20th, 1981* pp. 52–54.

Burgess, D. W., Wood, V. T., and Brown, R. A. (1982). Mesocyclone evolution statistics. *Prepr., Conf. Severe Local Storms, 12th, 1982* pp. 422–424.

Byers, H. R. (1959). "General Meteorology." McGraw-Hill, New York.

Byers, H. R., and Braham, R. R., Jr. (1949). "The Thunderstorm." U.S. Govt. Printing Office, Washington, D. C.

Caracena, R., Maddox, R. A., Hoxit, L. R., and Chappell, C. F. (1979). Mesoanalysis of the Big Thompson Storm. *Mon. Weather Rev.* **107,** 1–17.

Carbone, R. E. (1982). A severe winter squall line storm. I. Hydrodynamic structure. *J. Atmos. Sci.* **39,** 258–279.

Chalon, J.-P., Fankhauser, J. C., and Eccles, P. J. (1976). Structure of an evolving hailstorm. Part I. General characteristic and cellular structure. *Mon. Weather Rev.* **104,** 564–575.

Charba, J. (1974). Application of gravity current model to analysis of squall-line gust front. *Mon. Weather Rev.* **102,** 140–156.

Charba, J., and Sasaki, Y. (1971). Structure and movement of the severe thunderstorm of 3 April 1964 as revealed from radar and surface mesonetwork data analysis. *J. Meteorol. Sci.* **49,** 191–213.

Charney, J. G., and Eliassen, A. (1964). On the growth of the hurricane depression. *J. Atmos. Sci.* **21,** 68–75.

Chen, Y.-L., and Zipser, E. J. (1982). The role of horizontal advection of hydrometeors in the water budget of a large squall line system. *Prepr., Conf. Severe Local Storms, 12th, 1982* pp. 335–358.

Cheng. C.-P. (1981). Numerical simulation of the dynamics, cloud microphysics and radar echo structures of tropical and mid-latitude convection. Ph.D. Dissertation, University of Washington, Seattle.

Chisholm, A. J. (1973). Alberta hailstorms. Part I. Radar case studies and airflow models. *Meteorol. Monogr.* **14, 36,** 1–36.

Chisholm, A. J., and Renick, J. H. (1972). The kinematics of multicell and supercell Alberta hailstorms. *In* "Alberta Hail Studies 1972," Hail Stud. Rep. 72–2, pp. 27–31. Alberta, Research Council, Edmonton, Alberta, Canada.

Church, C. R., Snow, J. T., and Agee, E. M. (1977). Tornado vortex simulation at Purdue University. *Bull. Am. Meteorol. Soc.* **58,** 1070–1096.

Churchill, D. D. (1982). Development and structure of winter monsoon cloud clusters. M.S. Thesis, University of Washington, Seattle.

Clark, T. L. (1979). Numerical simulations with a three-dimensional cloud model: Lateral boundary condition experiments and multicellular severe storm simulations. *J. Atmos. Sci.* **36,** 2191–2215.

Cunningham, R. M. (1951). Some observations of natural precipitation processes. *Bull. Am. Meteorol. Soc.* **32,** 334–343.

Davies-Jones, R. P. (1974). Discussion of measurements inside high-speed thunderstorm updrafts. *J. Appl. Meteorol.* **13,** 710–717.

Davies-Jones, R. P. (1976). Laboratory simulations of tornadoes. *Proc. Symp. Tornadoes: Assessment Knowledge Implications Man, 1976* pp. 151–171.

Davies-Jones, R. P. (1982a). Tornado interception with mobile teams. *In* "Thunderstorms: A Social, Scientific and Technological Documentary" (E. Kessler, ed.), Vol. III, Chapter II. U.S. Govt. Printing Office, Washington, D. C. (in press).

Davies-Jones, R. P. (1982b). Tornado dynamics. *In* "Thunderstorms: A Social, Scientific and Technological Documentary" (E. Kessler, ed.), Vol. II, Chapter X. U.S. Govt. Printing Office, Washington, D. C. (in press).

Davies-Jones, R. P., and Kessler, E. (1974). Tornadoes. *In* "Weather and Climate Modification" (W. N. Hess, ed.), pp. 552–595. Wiley, New York.

Davies-Jones, R. P., Burgess, D. W., Lemon, L. R., and Purcell, D. (1978). Interpretation of surface marks and debris patterns from the 24 May 1973 Union City, Oklahoma, tornado. *Mon. Weather Rev.* **106,** 12–21.

Dye, J. E., Knight, C. A., Toutenhoofd, V., and Cannon, L. W. (1974). The mechanism of precipitation formation in northeastern Colorado cumulus. III. Coordinated microphysical and radar observations and summary. *J. Atmos. Sci.* **31,** 2152–2159.

Elliott, R. D., and Hovind, E. L. (1964). On convection bands within Pacific Coast storms and their relation to storm structure. *J. Appl. Meteorol.* **3,** 143–154.

Elliott, R. D., and Hovind, E. L. (1965). Heat, water, and vorticity balance in frontal zones. *J. Appl. Meteorol.* **4,** 196–211.

Emanuel, K. A. (1981). A similarity theory for unsaturated downdrafts within clouds. *J. Atmos. Sci.* **38,** 1541–1557.

English, M., Cheng, L., and Knight, N. C. (1982). Hail embryo type in Alberta storms. *Prepr., Conf. Severe Local Storms, 12th, 1982* pp. 9–12.

Esbensen, S. K., Tollerud, E. I., and Chu, J.-H. (1982). Cloud cluster circulations and the vorticity budget of synoptic scale waves over the eastern Atlantic Intertropical Convergence Zone. *Mon. Weather Rev.* (submitted for publication).

Forbes, G., and Wakimoto, R. (1982). A concentrated outbreak of tornadoes, down-bursts and microbursts on 6 August 1977. *Mon. Weather Rev.* **110** (in press.)

Fortune, M. (1980). Properties of African disturbance lines inferred from time-lapse satellite imagery. *Mon. Weather Rev.* **108,** 153–168.

Frank, N. L. (1970). Atlantic tropical systems of 1969. *Mon. Weather Rev.* **98,** 307–314.

Fraser, A. B., Easter, R. C., and Hobbs, P. V. (1973). A theoretical study of the flow of air and fallout of precipitation over mountainous terrain. Part I. Airflow model. *J. Atmos. Sci.* **30,** 801–812.

Fritsch, J. M., and Chappell, C. G. (1980). Numerical prediction of convectively driven mesoscale pressure systems. II. Mesoscale model. *J. Atmos. Sci.* **37,** 1734–1762.

Fritsch, J. M., and Maddox, R. A. (1981a). Convectively driven mesoscale weather systems aloft. Part I. Observations. *J. Appl. Meteorol.* **20,** 9–19.

Fritsch, J. M., and Maddox, R. A. (1981b). Convectively driven mesoscale weather systems aloft. Part II. Numerical simulations. *J. Appl. Meteorol.* **20,** 20–26.

Fritsch, J. M., Maddox, R. A., and Barnston, A. G. (1981). The character of mesoscale convective complex precipitation and its contribution to warm season rainfall in the U.S. *Prepr. Conf. Hydrometeorol., 4th, 1981* pp. 94–99.

Fujita, T. T. (1955). Results of detailed synoptic studies of squall lines. *Tellus* **7,** 405–436.

Fujita, T. T. (1960). "A Detailed Analysis of the Fargo Tornadoes of June 20, 1957," Res. Pap. No. 42. U.S. Weather Bureau, Washington, D. C.

Fujita, T. T. (1965). Formation and steering mechanisms of tornado cyclones and associated echoes. *Mon. Weather Rev.* **93,** 67–78.

Fujita, T. T. (1970). Lubbock tornadoes: A study of suction spots. *Weatherwise* **23,** 160–173.

Fujita, T. T. (1971). Proposed mechanism of suction spots accompanied by tornadoes. *Prepr., Conf. Severe Local Storms, 7th, 1971* pp. 208–213.

Fujita, T. T. (1981). Tornadoes and downbursts in the context of generalized planetary scales. *J. Atmos. Sci.* **38,** 1511–1534.

Fujita, T. T., Izawa, T., Watanabe, K., and Imai, I. (1967). A model of typhoons accompanied by inner and outer rainbands. *J. Appl. Meteorol.* **6,** 3–19.

Fujita, T. T., Bradbury, D. L., and von Thullenar, C. F. (1970). Palm Sunday tornadoes of April 11, 1965. *Mon. Weather Rev.* **98,** 29–69.

Gamache, J. F., and Houze, R. A., Jr. (1981). The water budget of a tropical squall-line system. *Prepr., Conf. Radar Meteorol., 20th, 1981* pp. 346–351.

Gamache, J. F., and Houze, R. A., Jr. (1982). Mesoscale air motions associated with a tropical squall line. *Mon. Weather Rev.* **110,** 118–135.

Gentry, R. C., Fujita, T. T., and Sheets, R. C. (1970). Aircraft, spacecraft, satellite and radar observations of Hurricane Gladys, 1968. *J. Appl. Meteorol.* **9,** 837–850.

Gocho, Y. (1978). Numerical experiment of orographic heavy rainfall due to a stratiform cloud. *J. Meteorol. Soc. Jpn.* **56,** 405–422.

Godske, C. L., Bergeron, T., Bjerknes, J., and Bundage, R. C. (1957). "Dynamic Meteorology and Weather Forecasting." Am. Meteorol. Soc., Boston, Massachusetts.

Golden, J. H., and Purcell, D. (1978a). Life cycle of the Union City, Oklahoma, tornado and comparison with waterspouts. *Mon. Weather Rev.* **106,** 3–11.

Golden, J. H., and Purcell, D. (1978b). Airflow characteristics around the Union City Tornado. *Mon. Weather Rev.* **106,** 22–28.

Goyer, G. G. (1977). Response to "The Climatology of Hail in North America." *Meteorol. Monogr.* **16,** No. 38, 129–133.

Hamilton, R. A., and Archbold, J. N. (1945). Meteorology of Nigeria and adjacent territory. *Q. J. R. Meteorol. Soc.* **71,** 231–262.

Hammond, G. R. (1967). "Study of a Left-moving Thunderstorm of 23 April 1964," Tech. Memo, IERTM-NSSL 31. National Severe Storms Laboratory, Norman, Oklahoma.

Harrold, T. W. (1973). Mechanisms influencing the distribution of precipitation within baroclinic disturbances. *Q. J. R. Meteorol. Soc.* **99,** 232–251.

Harrold, T. W., and Austin, P. M. (1974). The structure of precipitation systems—A review. *J. Rech. Atmos.* **8,** 41–57.

Hawkins, H. F., and Imbembo, S. M. (1976). The structure of a small, intense hurricane—Inez, 1966. *Mon. Weather Rev.* **104,** 418–442.

Herzegh, P. H., and Hobbs, P. V. (1980). The mesoscale and microscale structure and organization of clouds and precipitation in midlatitude cyclones. II. Warm-frontal clouds. *J. Atmos. Sci.* **37,** 597–611.

Heymsfield, A. J., Jameson, A. R., and Frank, H. W. (1980). Hail growth in a Colorado storm. Part II. Hail formation processes. *J. Atmos. Sci.* **37,** 1779–1807.

Heymsfield, G. M. (1978). Kinematic and dynamic aspects of the Harrah tornadic storm from dual-Doppler radar data. *Mon. Weather Rev.* **106,** 233–254.

Hobbs, P. V. (1978). Organization and structure of clouds and precipitation on the mesoscale and microscale in cyclonic storms. *Rev. Geophys. Space Phys.* **16,** 741–755.

Hobbs, P. V. (1981a). The Seattle workshop on extratropical cyclones: A call for a National Cyclone Project. *Bull. Am. Meteorol. Soc.* **62,** 244–254.

Hobbs, P. V. (1981b). Mesoscale structure in midlatitude frontal systems. *Proc. IAMAP Symp. Nowcasting: Mesoscale Observations and Short-Range Prediction, 1981* Eur. Space Agency Publ. SP-165, pp. 29–36.

Hobbs, P. V., and Biswas, K. R. (1979). The cellular structure of narrow cold-frontal rainbands. *Q. J. R. Meteorol. Soc.* **105,** 723–727.

Hobbs, P. V., and Locatelli, J. D. (1978). Rainbands, precipitation cores and generating cells in a cyclonic storm. *J. Atmos. Sci.* **35,** 230–241.

Hobbs, P. V., and Matejka, T. J. (1980). Precipitation efficiencies and the potential for artificially modifying extratropical cyclones. *Proc. WMO Sci. Conf. Weather Modification, 3rd, 1980* pp. 9–15.

Hobbs, P. V., and Persson, O. P. G. (1982). The mesoscale and microscale structure and organization of clouds and precipitation in midlatitude cyclones. V. The substructure of narrow cold-frontal rainbands. *J. Atmos. Sci.* **39,** 280–295.

Hobbs, P. V., Houze, R. A., Jr., and Matejka, T. J. (1975). The dynamical and microphysical structure of an occluded front and its modification by orography. *J. Atmos. Sci.* **32,** 1542–1562.

Hobbs, P. V., Matejka, T. J., Herzegh, P. H., Locatelli, J. D., and Houze, R. A., Jr. (1980). The mesoscale and microscale structure and organization of clouds and precipitation in midlatitude cyclones. I. A case study of a cold front. *J. Atmos. Sci.* **37,** 568–596.

Hoecker, W. K. (1960). Windspeed and airflow patterns in the Dallas tornado of April 2, 1957. *Mon. Weather Rev.* **88,** 167–180.

Houze, R. A., Jr. (1977). Structure and dynamics of a tropical squall-line system. *Mon. Weather Rev.* **105,** 1540–1567.

Houze, R. A., Jr. (1981). Structure of atmospheric precipitation systems—A global survey. *Radio Sci.* **16,** 671–689.

Houze, R. A., Jr. (1982). Cloud clusters and large-scale vertical motions in the tropics. *J. Meteorol. Soc. Jpn.* **60,** 396–410.

Houze, R. A., Jr., and Betts, A. K. (1981). Convection in GATE. *Rev. Geophys. Space Phys.* **16,** 541–576.

Houze, R. A., Jr., and Smull, B. F. (1982). Comparison of an Oklahoma squall line to mesoscale convective systems in the tropics. *Prepr., Conf. Severe Local Storms, 12th, 1982* pp. 338–341.

Houze, R. A., Jr., Locatelli, J. D., and Hobbs, P. V. (1976a). Dynamics and cloud microphysics of the rainbands in an occluded frontal system. *J. Atmos. Sci.* **33,** 1921–1936.

Houze, R. A., Jr., Hobbs, P. V., Biswas, K. R., and Davis, W. M. (1976b). Mesoscale rainbands in extratropical cyclones. *Mon. Weather Rev.* **104,** 868–878.

Houze, R. A., Jr., Geotis, S. G., Marks, F. D., Jr., and West, A. K. (1981a). Winter monsoon convection in the vicinity of North Borneo. Part I. Structure and time variation of the clouds and precipitation. *Mon. Weather Rev.* **109,** 1595–1614.

Houze, R. A., Jr., Rutledge, S. A., Matejka, T. J., and Hobbs, P. V. (1981b). The mesoscale and microscale structure and organization of clouds and precipitation in extratropical cyclones. III. Air motions and precipitation growth in a warm-frontal rainband. *J. Atmos. Sci.* **38,** 639–649.

Huschke, R. E. (1959). "Glossary of Meteorology." Am. Meteorol. Soc., Boston, Massachusetts.

James, P. K., and Browning, K. A. (1979). Mesoscale structure of line convection at surface cold fronts. *Q. J. R. Meteorol. Soc.* **105,** 371–382.

Johnson, R. H. (1982). Vertical motion of near-equatorial winter monsoon convection. *J. Meteorol. Soc. Jpn.* **60,** 682–690.

Johnson, R. H., and Priegnitz, D. L. (1981). Winter monsoon convection in the vicinity of North Borneo. Part II. Effects on large-scale fields. *Mon. Weather Rev.* **109,** 1619–1632.

Jorgensen, D. P. (1981). Meso- and convective-scale characteristics common to several mature hurricanes. *Prepr., Conf. Radar Meteorol., 20th, 1981* pp. 726–733.

Jorgensen, D. P. (1982a). Meso- and convective-scale characteristics common to several mature hurricanes. Part I. General observations by research aircraft. *J. Atmos. Sci.* (to be submitted for publication).

Jorgensen, D. P. (1982b). Meso- and convective-scale characteristics common to several mature hurricanes. Part II. Inner core structure. *J. Atmos. Sci.* (to be submitted for publication.)

Kessler, E., and Atlas, D. (1956). Radar-synoptic analysis of hurricane Edna (1954). *Geophys. Res. Pap.* **50,** 1–113.

Klemp, J. B., and Rotunno, R. (1982). High resolution numerical simulations of the tornadic region within a mature thunderstorm. *Prepr., Conf. Severe Local Storms, 12th, 1982*, pp. 532–535.

Klemp, J. B., and Wilhelmson, R. (1978a). The simulation of three-dimensional convective storm dynamics. *J. Atmos. Sci.* **35,** 1070–1096.

Klemp, J. B., and Wilhelmson, R. (1978b). Simulations of right and left-moving storms through storm splitting. *J. Atmos. Sci.* **35,** 1097–1110.

Klemp, J. B., Wilhelmson, R. B., and Ray, P. S. (1981). Observed and numerically simulated structure of a mature supercell thunderstorm. *J. Atmos. Sci.* **38,** 1558–1580.

Kreitzberg, C. W. (1964). The structure of occlusions, as determined from serial ascents and vertically directed radars. *Air Force Cambridge Res. Lab. Rep.* **64-20,** 1–121.

Kreitzberg, C. W., and Brown, H. A. (1970). Mesoscale weather systems within an occlusion. *J. Appl. Meteorol.* **9,** 419–432.

Kreitzberg, C. W., and Perkey, D. J. (1976). Release of potential instability. Part I. A sequential plume model within a hydrostatic primitive equation model. *J. Atmos. Sci.* **33,** 456–475.

Kreitzberg, C. W., and Perkey, D. J. (1977). Release of potential instability. Part II. The mechanism of convective/mesoscale interactions. *J. Atmos. Sci.* **34,** 1569–1595.

Krishnamurti, R. (1975a). On cellular cloud patterns. Part I. Mathematical model. *J. Atmos. Sci.* **32,** 1353–1363.

Krishnamurti, R. (1975b). On cellular cloud patterns. Part II. Laboratory model. *J. Atmos. Sci.* **32,** 1364–1372.

Krishnamurti, R. (1975c). On cellular cloud patterns. Part III. Applicability of the mathematical and laboratory models. *J. Atmos. Sci.* **38,** 1373–1383.

Leary, C. A. (1981). The precipitation spectrum of a mesoscale feature in a tropical cloud cluster. *Prepr., Conf. Radar Meteorol. 20th, 1981* pp. 358–363.

Leary, C. A., and Houze, R. A., Jr. (1979a). The structure and evolution of convection in a tropical cloud cluster. *J. Atmos. Sci.* **36,** 437–457.

Leary, C. A., and Houze, R. A., Jr. (1979b). Melting and evaporation of hydrometeors in precipitation from the anvil clouds of deep tropical convection. *J. Atmos. Sci.* **36,** 669–679.

Lemon, L. R. (1976). The flanking line, a severe thunderstorm intensification source. *J. Atmos. Sci.* **33,** 686–694.

Lemon, L. R., and Doswell, C. A., III (1979). Severe thunderstorm evolution and meso-cyclone structure as related to tornadogenesis. *Mon. Weather Rev.* **107,** 1184–1197.

Lemon, L. R., Burgess, D. W., and Brown, R. A. (1978). Tornadic storm airflow and morphology derived from single-Doppler radar measurements. *Mon. Weather Rev.* **106,** 48–61.

Leslie, F. W. (1977). Surface roughness effects on suction vortex formation: A laboratory simulation. *J. Atmos. Sci.* **34,** 1022–1027.

Ley, B. E., and Peltier, W. R. (1978). Wave generation and frontal collapse. *J. Atmos. Sci.* **35,** 3–17.

Lindzen, R. S. (1974). Wave-CISK in the tropics. *J. Atmos. Sci.* **37,** 166–179.

Lindzen, R. S., and Tung, K. K. (1976). Banded convective activity and ducted gravity waves. *Mon. Weather Rev.* **104,** 1602–1617.

Locatelli, J. D., Hobbs, P. V., and Werth, J. A. (1982). Mesoscale structures of vortices in polar air streams. *Mon. Weather Rev.* (in press).

López, R. E. (1978). Internal structure and development processes of C-scale aggregates of cumulus clouds. *Mon. Weather Rev.* **106,** 1488–1494.

Maddox, R. A. (1980a). An objective technique for separating macroscale and mesoscale features in meteorological data. *Mon. Weather Rev.* **108,** 1108–1121.

Maddox, R. A. (1980b). Mesoscale convective complexes. *Bull. Am. Meteorol. Soc.* **61,** 1374–1387.

Maddox, R. A. (1981). "The Structure and Life Cycle of Mid-latitude Mesoscale Convective Complexes," Atmos. Sci. Pap. No. 336. Colorado State University, Ft. Collins.

Maddox, R. A., Perkey, D. J., and Fritsch, J. M. (1981). Evolution of upper tropospheric features during the development of a mesoscale convective complex. *J. Atmos. Sci.* **38,** 1664–1674.

Marks, F. D., Jr. (1981). Evolution of the structure of precipitating convection in Hurricane Allen. *Prepr., Conf. Radar Meteorol., 20th, 1981* pp. 720–725.

Marshall, J. S., and Gordon, W. E. (1957). Radiometeorology. *Meteorol. Monogr.* **3,** 73–113.

Marshall, T. P., and Rasmussen, E. N. (1982). The mesocyclone evolution of the Warren, Oklahoma, tornadoes. *Prepr., Conf. Severe Local Storms, 12th, 1982* pp. 375–378.

Martin, D. W. (1975). "Characteristics of West African and Atlantic Cloud Clusters," GATE Rep. 14, Vol. I, pp. 182–192. Int. Counc. Sci. Unions/World Meteorol. Organ., Geneva.

Martin, D. W., and Schreiner, A. J. (1981). Characteristics of West African and East Atlantic cloud clusters: A survey from GATE. *Mon. Weather Rev.* **109,** 1671–1688.

Martin, D. W., and Suomi, V. E. (1972). A satellite study of cloud clusters over the tropical North Atlantic Ocean. *Bull. Am. Meteorol. Soc.* **53,** 135–156.

Marwitz, J. D. (1972). The structure and motion of severe hailstorms. Part I. Supercell storms. *J. Appl. Meteorol.* **11,** 166–179.

Matejka, T. J. (1980). Mesoscale organization of cloud processes in extratropical cyclones. Ph.D. Thesis, University of Washington, Seattle.

Matejka, T. J., and Srivastava, R. C. (1981). Doppler radar study of a region of widespread precipitation trailing a mid-latitude squall line. *Prepr., Conf. Radar Meteorol., 20th, 1981* pp. 353–357.

Matejka, T. J., Houze, R. A., Jr., and Hobbs, P. V. (1980). Microphysics and dynamics of clouds associated with mesoscale rainbands in extratropical cyclones. *Q. J. R. Meteorol. Soc.* **106,** 29–56.

Maynard, R. H. (1945). Radar and weather. *J. Meteorol.* **2,** 214–226.

Monteverdi, J. P. (1976). The single air mass disturbance and precipitation characteristics at San Francisco. *Mon. Weather Rev.* **104,** 1289–1296.

Nagle, R. E., and Serebreny, S. M. (1962). Radar precipitation echo and satellite observations of a maritime cyclone. *J. Appl. Meteorol.* **1,** 279–295.

Nelson, S. P., and Knight, N. C. (1982). Variations in hailstone growth characteristics in a supercell storm. *Prepr., Conf. Severe Local Storms, 12th, 1982* pp. 5–11.

Newton, C. W. (1950). Structure and mechanism of the prefrontal squall line. *J. Meteorol.* **7,** 210–222.

Newton, C. W. (1963). Dynamics of severe convective storms. *Meteorol. Monogr.* **5,** No. 27, 33–58.

Newton, C. W. (1966). Circulations in large sheared cumulonimbus. *Tellus* **18,** 699–713.

Newton, C. W., and Fankhauser, J. C. (1964). On the movements of convective storms, with emphasis on size discrimination in relation to water-budget requirements. *J. Appl. Meteorol.* **3,** 651–688.

Newton, C. W., and Fankhauser, J. C. (1975). Movement and propagation of multi-cellular convective storms. *Pure Appl. Geophys.* **113,** 747–763.

Ninomiya, K. (1971a). Dynamical analysis of outflow from tornado producing thunderstorms as revealed by ATS III pictures. *J. Appl. Meteorol.* **10,** 275–294.

Ninomiya, K. (1971b). Mesoscale modification of synoptic situations from thunderstorm development as revealed by ATS III and aerological data. *J. Appl. Meteorol.* **10,** 1103–1121.

Nozumi, Y., and Arakawa, H. (1968). Prefrontal rainbands located in the warm sector of subtropical cyclones over the ocean. *J. Geophys. Res.* **73,** 487–492.

Ogura, Y., and Liou, M. T. (1980). The structure of a mid-latitude squall line: A case study. *J. Atmos. Sci.* **37,** 553–567.

Ogura, Y., and Takahashi, T. (1971). Numerical simulation of the life cycle of a thunderstorm cell. *Mon. Weather Rev.* **99,** 895–911.

Ooyama, K. (1964). A dynamical model for the study of hurricane development. *Geofis. Int.* **4,** 187–198.

Orlanski, I. (1975). A rational subdivision of scales for atmospheric processes. *Bull. Am. Meteorol. Soc.* **56,** 529–530.

Palmén, E., and Newton, C. W. (1969). "Atmospheric Circulation Systems: Their Structure and Physical Interpretations." Academic Press, New York.

Parsons, D. B., and Hobbs, P. V. (1981). Origins, behaviors, and interactions of mesoscale

rainbands in extratropical cyclones. *Prepr., Conf. Radar Meteorol., 20th, 1981* pp. 623–628.

Parsons, D. B., and Hobbs, P. V. (1982a). The mesoscale and microscale structure and organization of clouds and precipitation in midlatitude cyclones. VII. Effects of orography on rainbands. *J. Atmos. Sci.* (in press).

Parsons, D. B., and Hobbs, P. V. (1982b). The mesoscale and microscale structure and organization of clouds and precipitation in midlatitude cyclones. X. Comparisons between observational and theoretical aspects of mesoscale rainbands. *J. Atmos. Sci.* (submitted for publication).

Payne, S. W., and McGarry, M. M. (1977). The relationship of satellite inferred convective activity to easterly waves over West Africa and the adjacent ocean during Phase III of GATE. *Mon. Weather Rev.* **105,** 413–420.

Pflaum, J. C., Nelson, S. P., and Foster, M. P. (1982). Hail growth studies within a Doppler-radar reconstructed supercell. *Prepr., Conf. Severe Local Storms, 12th, 1982* pp. 9–12.

Plank, V. G., Atlas, D., and Paulsen, W. H. (1955). The nature and detectability of clouds and precipitation as determined by 1.23 centimeter radar. *J. Meteorol.* **12,** 358–377.

Purdom, J. F. W. (1973). Meso-highs and satellite imagery. *Mon. Weather Rev.* **101,** 180–181.

Purdom, J. F. W. (1979). The development and evolution of deep convection. *Prepr., Conf. Severe Local Storms, 11th, 1979* pp. 143–150.

Purdom, J. F. W., and Marcus, K. (1982). Thunderstorm trigger mechanisms over the southeast United States. *Prepr., Conf. Severe Local Storms, 12th, 1982* pp. 487–488.

Rappaport, E. N. (1982). Structure and dynamics of an atypical tropical squall-line system. M.S. Thesis, University of Washington, Seattle.

Rasmussen, E. N., Peterson, R. E., Minor, J. E., and Campbell, B. D. (1982). Evolutionary characteristics and photogrammetric determination of wind speeds within the Tulia outbreak tornadoes 28 May 1980. *Prepr., Conf. Severe Local Storms, 12th, 1982* pp. 301–304.

Raymond, D. G. (1975). A model for predicting the movement of continuously propagating convective storms. *J. Atmos. Sci.* **32,** 1308–1317.

Reed, R. J. (1979). Cyclogenesis in polar air streams. *Mon. Weather Rev.* **107,** 38–52.

Rosenthal, S. L. (1980). "Numerical Simulation of Tropical Cyclone Development with Latent Heat Release by the Resolvable Scales. II. Propagating Small-scale Features Observed in the Pre-hurricane Phase," Tech. Rep. ERL413-AOML29. NOAA Environ. Res. Lab., Boulder, Colorado.

Ross, B. B., and Orlanski, I. (1978). The circulations associated with a cold front. Part II. Moist case. *J. Atmos. Sci.* **35,** 445–465.

Rotunno, R. (1981). On the evolution of thunderstorm rotation. *Mon. Weather Rev.* **109,** 577–586.

Rutledge, S. A., and Hobbs, P. V. (1982). The mesoscale and microscale structure and organization of clouds and precipitation in midlatitude cyclones. VI. A model for the "seeder-feeder" process in warm-frontal rainbands. *J. Atmos. Sci.* (submitted for publication).

Sanders, F., and Emanuel, K. A. (1977). The momentum budget and temporal evolution of a mesoscale convective system. *J. Atmos. Sci.* **34,** 322–330.

Sanders, F., and Paine, R. J. (1975). The structure and thermodynamics of an intense mesoscale storm in Oklahoma. *J. Atmos. Sci.* **32,** 1563–1579.

Schlesinger, R. E. (1978). A three-dimensional numerical model of an isolated thunderstorm. Part I. Comparative experiments for variable ambient wind shear. *J. Atmos. Sci.* **35,** 690–713.

Schlesinger, R. E. (1980). A three-dimensional numerical model of an isolated thunderstorm: Dynamics of updraft splitting and mesovortex evolution. *J. Atmos. Sci.* **37,** 395–420.

Schlesinger, R. E. (1982a). Three-dimensional numerical modeling of convective storms: A review of milestones and challenges. *Prepr., Conf. Severe Local Storms, 12th, 1982* pp. 506–515.

Schlesinger, R. E. (1982b). Effects of mesoscale lifting, precipitation and boundary-layer shear on severe storm dynamics in a three-dimensional numerical modeling study. *Prepr., Conf. Severe Local Storms, 12th, 1982* pp. 536–541.

Scorer, R. S. (1972). "Clouds of the World." Stackpole Books, Harrisburg, Pennsylvania.

Sellers, W. D. (1965). "Physical Climatology." Univ. of Chicago Press, Chicago, Illinois.

Senn, H. V., and Hiser, H. W. (1959). On the origin of hurricane spiral rainbands. *J. Meteorol.* **16,** 419–426.

Shapiro, L. J., and Willoughby, H. E. (1982). The response of balanced hurricanes to local sources of heat and momentum. *J. Atmos. Sci.* **39,** 378–394.

Shea, D. J., and Gray, W. M. (1973). The hurricane's inner core region. I. Symmetric and asymmetric structure. *J. Atmos. Sci.* **30,** 1544–1564.

Simpson, J. E. (1972). Effects of the lower boundary on the head of a gravity current. *J. Fluid Mech.* **53,** 759–768.

Simpson, J. S., and van Helvoirt, G. (1980). GATE cloud–sub cloud layer interactions examined using a three-dimensional cumulus model. *Beitr. Phys. Atmos.* **53,** 106–134.

Simpson, J. S., van Helvoirt, G., and McCumber, M. (1982). Three-dimensional simulations of cumulus congestus clouds on GATE Day 261. *J. Atmos. Sci.* **39,** 126–145.

Simpson, J. S., Wescott, N. E., Clerman, R. J., and Pielke, R. A. (1980). On cumulus mergers. *Arch. Meteorol. Geophys., Bioklimatol., Ser. A* **29,** 1–40.

Sinclair, P. C., and Purdom, J. F. W. (1982). Integration of research aircraft data and 3 min interval GOES data to study the genesis and development of deep convective storms. *Prepr., Conf. Severe Local Storms, 12th, 1982* pp. 269–271.

Storebø, P. B. (1976). Small scale topographical influences on precipitation. *Tellus* **28,** 45–59.

Szoke, E. J., and Zipser, E. J. (1981). Life cycles of convective cells in organized mesoscale systems in GATE. *Prepr., Conf. Radar Meteorol., 20th, 1981* pp. 338–345.

Thorpe, A. J., and Miller, M. J. (1978). Numerical simulations showing the role of the downdraught in cumulonimbus motion and splitting. *Q. J. R. Meteorol. Soc.* **104,** 873–893.

Ward, N. B. (1972). The exploration of certain features of tornado dynamics using a laboratory model. *J. Atmos. Sci.* **29,** 1194–1204.

Warner, C., Simpson, J., Martin, D. W., Suchman, D., Mosher, F. R., and Reinking, R. F. (1979). Shallow convection on day 261 of GATE: Mesoscale arcs. *Mon. Weather Rev.* **107,** 1617–1635.

Weickmann, H. K. (1953). Observational data on the formation of precipitation in cumulonimbus clouds. *In* "Thunderstorm Electricity," pp. 66–138. Univ. of Chicago Press, Chicago, Illinois.

Weisman, M. L., and Klemp, J. B. (1981). The dependence of storm structure on vertical wind shear and buoyancy. *Prepr., Conf. Radar Meteorol., 20th, 1981* pp. 155–162.

Weisman, M. L., and Klemp, J. B. (1982). The effects of directional turning of the low level wind shear vector on modeled multicell and supercell storms. *Prepr., Conf. Severe Local Storms, 12th, 1982* pp. 528–531.

Wexler, H. (1947). Structure of hurricanes as determined by radar. *Ann. N. Y. Acad. Sci.* **48,** 821–844.

Wexler, R., and Atlas, D. (1959). Precipitation generating cells. *J. Meteorol.* **16,** 327–332.

Wilhelmson, R. B., and Chen, C.-S. (1982). Cell development along cold outflow boundaries. *Prepr., Conf. Severe Local Storms, 12th, 1982* pp. 127–130.

Wilhelmson, R. B., and Klemp, J. B. (1978). A numerical study of storm splitting that leads to long-lived storms. *J. Atmos. Sci.* **35,** 1975–1986.

Wilhelmson, R. B., and Klemp, J. B. (1981). A three-dimensional numerical simulation of splitting severe storms on 3 April 1964. *J. Atmos. Sci.* **38,** 1558–1580.

Willoughby, H. E., Clos, J. A., and Shoreibah, M. G. (1982). Concentric eye walls, secondary wind maxima, and the evolution of the hurricane vortex. *J. Atmos. Sci.* **39,** 395–411.

Zipser, E. J. (1969). The role of organized unsaturated convective downdrafts in the structure and rapid decay of an equatorial disturbance. *J. Appl. Meteorol.* **8,** 799–814.

Zipser, E. J. (1971). Internal structure of cloud clusters. GATE Experiment Design Proposal, Vol. 2, Annex VII. World Meteorol. Organ., Geneva.

Zipser, E. J. (1977). Mesoscale and convective-scale downdrafts as distinct components of squall-line circulation. *Mon. Weather Rev.* **105,** 1568–1589.

Zipser, E. J. (1980). Kinematic and thermodynamic structure of mesoscale systems in GATE. *In* "Proceedings of the Seminar on the Impact of GATE on Large-Scale Numerical Modeling of the Atmosphere and Ocean," pp. 91–99. Natl. Acad. Sci., Washington, D. C.

Zipser, E. J., and Gautier, C. (1978). Mesoscale events within a GATE tropical depression. *Mon. Weather Rev.* **106,** 789–805.

Zipser, E. J., and LeMone, M. A. (1980). Cumulonimbus vertical velocity events in GATE. II. Synthesis and model core structure. *J. Atmos. Sci.* **37,** 2458–2469.

Zipser, E. J., and Matejka, T. J. (1982). Comparison of radar and wind cross-sections through a tropical and midwestern squall line. *Prepr., Conf. Severe Local Storms, 12th, 1982* pp. 342–345.

Zipser, E. J., Meitin, R. J., and LeMone, M. A. (1981). Mesoscale motion fields associated with slowly moving GATE convective band. *J. Atmos. Sci.* **38,** 1725–1750.

Zrnic, D. S., Doviak, R. J., and Burgess, D. W. (1977). Probing tornadoes with a pulse Doppler radar. *Q. J. R. Meteorol. Soc.* **103,** 707–720.